SOIL-SPRING MODEL FOR FATIGUE EVALUATION OF CYCLIC-LOADED OFFSHORE CONDUCTORS

A Thesis

by

OLUSOLA AYANDIRE ILUPEJU

Submitted to the Office of Graduate and Professional Studies of
Texas A&M University
in partial fulfillment of the requirements for the degree of

MASTER OF SCIENCE

Chair of Committee,	Charles Aubeny
Co-Chair of Committee,	Giovanna Biscontin
Committee Member,	Jerome J. Schubert
Head of Department,	Robin Autenrieth

May 2014

Major Subject: Civil Engineering

ABSTRACT

As oil exploration projects move further into deep and ultra-deep waters, where severe environmental conditions persist, having safe and functional structures, at optimal cost, by optimizing designs of offshore structures and foundations becomes more important. Design considerations and methodology for dealing with conductors and piles subjected to cyclic lateral loads, have been based on modifications to formulations for monotonic loads. Soil-structure interaction problems involving offshore conductors are nonlinear. A convenient and computationally efficient approach to modeling this behavior uses lateral transfer curves (P-y curves) from which deflections resulting from applied loads can be estimated. P-y curves can be back-calculated from instrumented laterally loaded test piles, either full-scale field tests or small-scale laboratory model tests. Centrifuge tests, which permit small scale model tests at stress levels representative of those occurring in situ, are particularly useful for this purpose. This research involves the back-analysis of centrifuge test data on piles subjected to cyclic lateral loads to obtain P-y curves applicable to soft to medium clays. The tests were conducted in a kaolin test bed in an overconsolidated stress state. Instrumentation data included strain gage measurements along the length of the pile, and displacement, force, and tilt measurements at the pile head.

The test interpretation involved deducing equivalent soil resistance (P) and pile deflection (y) measurements from the strain gage data. The former is particularly challenging, because it requires obtaining numerical second derivatives from a spatial array of strain gages. For this purpose a local least squares regression analysis was developed. For convenient implementation into an analytical model the resulting P-y curves were fitted to two alternative model forms: power law and Ramberg-Osgood. A 0.91m conductor was subjected to small lateral displacements (0.01D to 0.02D), for

which simplified expressions for secant stiffness and equivalent damping ratio has been presented. The back calculated moments from the Power law and Ramberg-Osgood equations, compared very well with measured bending moments.

This study has provided a framework for interpreting and generating P-y curves for cyclic load on offshore conductors. It has also provided design parameters, the stiffness modulus, and damping ratio that can be used as input for pile deflection and fatigue analysis of cyclic loaded offshore conductors. The results of this study will contribute towards understanding the behavior of offshore conductors installed below the ocean floor in harsh environmental conditions.

DEDICATION

I will like to dedicate this thesis to God almighty, my parents Mr. and Mrs Gbadegesin Ilupeju, and my two lovely brothers, Adedayo Ilupeju and Ayodeji Ilupeju; a great friend Peter Akopkodje; my beloved cousin, Comfort Adeboje; without them, my education leading to this thesis would not have materialized.

ACKNOWLEDGEMENTS

I am exceptionally grateful to God, who gave me the opportunity to pursue my studies at Texas A&M University, for strength, good health, and wisdom needed to complete my studies.

I would like to thank my wonderful committee chair, Dr. Aubeny, who provided financial assistance and a conducive academic environment for me. I am sincerely grateful for his patience, time, valuable suggestions, and guidance with getting my education and research completed. Thank you so much. I will also like to thank my committee members, Dr. Biscontin and Dr. Schubert, for their help, patience, and input. Thank you.

I exceptionally want to thank Dr. Arash Zakeri, for his guidance and valuable contribution during the entire period of this research study. I am really grateful, and I say thank you.

Thanks also go to my friends and colleagues, the department faculty and staff for making my time at Texas A&M University a great experience. I also want to extend my gratitude to everyone who was a part of my academic life, and contributed immensely to the commencement and completion of this research study.

Finally, many thanks to my mother and father for their encouragement, parental guide, love, support, and prayers; my father especially for his patience, love, and financial assistance, and also my fiancé Osasuvben Aiyudu, I say thank you for your love, care, and prayers.

TABLE OF CONTENTS

LIST OF FIGURES

LIST OF TABLES

CHAPTER I

INTRODUCTION

1.1 Overview

The quest for more crude oil reserves due to increasing demand for power globally, pushes the limits of oil exploration into deeper waters with harsh environmental conditions. The trend in **Fig. 1.1** depicts that more future oil production in the United States (U.S.) will come from offshore units**.** In deep and ultra-deep water, floating exploration and production structures moored or tethered to the sea bed via anchors or deep foundations are utilized. These structures are continuously subjected to loads (wind, currents, wave actions, and ship impacts) that are transmitted to adjoining and supporting structures. Such offshore structures includes, Tension Leg Platforms (TLP), Spars, Semi submersibles, and Floating Production Storage Offloading units (FPSO). Optimized designs which can deliver safe and functional structures, at optimal cost are required for these offshore facilities in such adverse environmental conditions. Amongst the design issues for offshore structures are the loads supported by the foundation systems and behavior of such systems, which the well conductor as a supporting structure falls under. The design of such supporting structures must be functional, cost effective, and reliable.

This thesis will contribute additional knowledge to design methods for cyclically loaded offshore conductors and piles, by creating a Soil-Spring Model, using existing relationships (Power law and Ramberg-Osgood). It will provide secant stiffness and equivalent damping ratio parameters, obtained from numerical analysis of centrifuge test data from a cyclically loaded conductor.

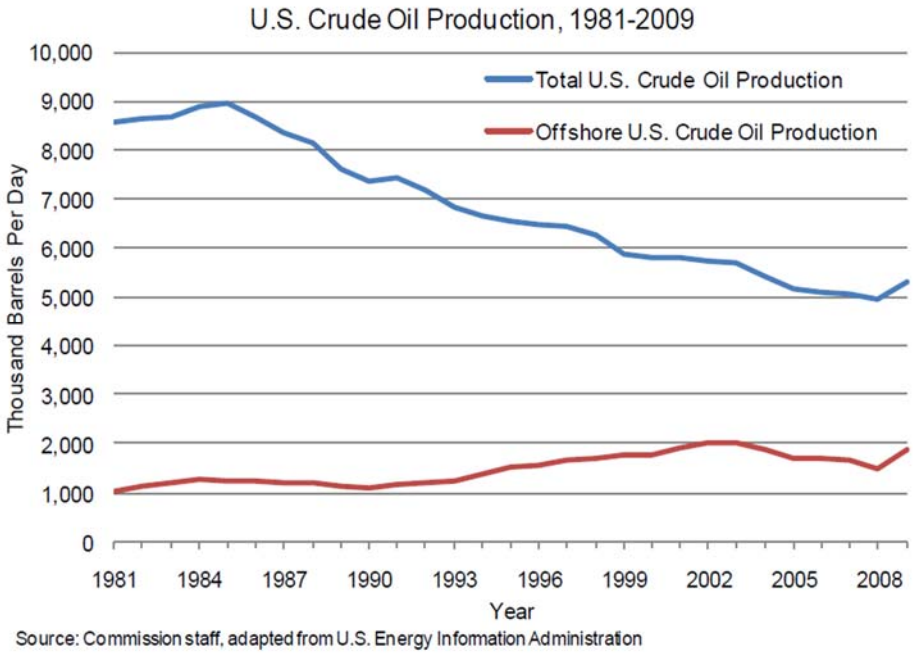

Fig. 1.1: The Margin Between the Total U.S Crude Oil Production and Offshore U.S. Closing Up as We Progress into the Future (Retrieved from the Encyclopedia of Earth, 2013).

1.2 Offshore Conductors

Offshore conductors are the widest diameter casings used for offshore wells and the key structural foundation for the subsea wellhead, as shown in Fig. 1.2. Offshore conductors also serve the purpose of protecting the wellstream from outside contaminant, as well as preventing oil and gas from contaminating any fresh water reservoir. They are usually connected to the floating moored structures through a top-tensioned or catenary riser, which links the conductor wellhead to the platform. The response of the risers to platform motions, sea currents and waves induces cyclic horizontal loads on the wellhead and the conductor system which can potentially cause fatigue damage to the conductor. The conductor transmits these lateral loads to the surrounding soil below the

sea bed in a complex non-linear manner. A good understanding of the interactions between the conductor and surrounding soil is very important for a functional, cost effective and reasonably conservative design. To ensure adequate conductor-soil resistance in an extreme loading event, the offshore conductor should be designed to adequately support both static and cyclic loads. A challenging aspect to having a unified design or rule that works in all conditions is the variability of the soil type and conditions across different locations. A better understanding of the behavior these offshore structures in relation to the soil supporting them, will add to the existing body of knowledge in soil/structure interaction (SSI) of offshore conductors. SSI of monotonic and cyclic loaded conductors can be modeled by assuming that the soil around the conductor acts as a series of closely spaced independent elastic springs, which will mobilize resistance to the motions of the conductor and experience some deformation during this process, as shown in Fig. 1.3.

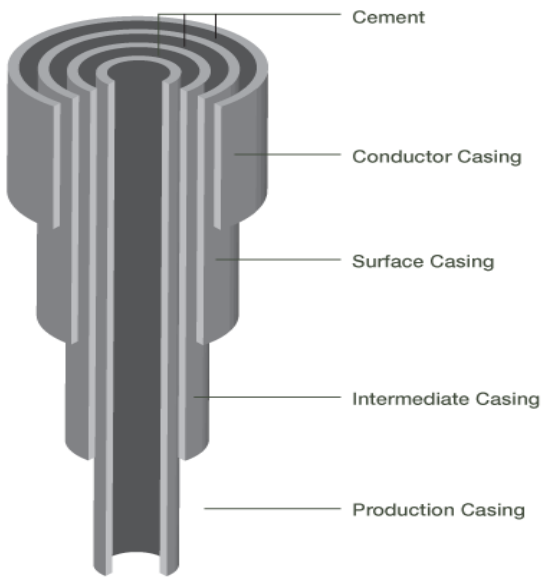

Fig. 1.2: The Offshore Conductor Shown as the First and Widest Casing in the Offshore Well (Steve Everley, 2013, Stated to Have been Originally Obtained from Http://www.Encana.Com/Images/Environment/Well-Casing.Gif).

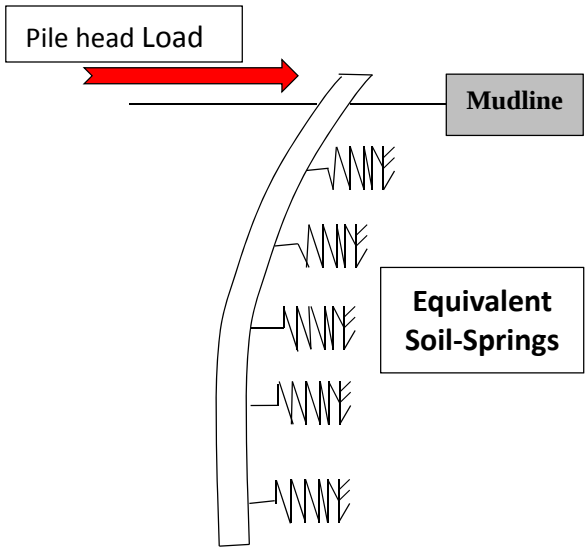

Fig. 1.3: Equivalent Soil Springs Used to Model Mobilized Soil Resistance When the Offshore Conductor is Subjected to Lateral Load.

1.3 P-y Relationship

Laterally loaded conductors mobilizes soil resistance which varies with depth along the conductor. P-y curves are generally used to show the relationship between the mobilized resistance in the soil (P), and the deflection (y) that occurs. P-y curves are usually normalized to make them dimensionless to help eliminate site dependency and conductor dimensions effects, thereby improving generality of obtained results. "The P-y curves, widely used by designers, were proposed by Matlock (1970), the Strain-Hardening clay criteria for soft clays and Reese et al. (1975), the Strain-Softening criteria for stiff clays.

In this thesis, the P-y model of interest is to be generated for conductor in soft overconsolidated to slightly overconsolidated clay at depth. Matlock (1970) developed a procedure for construction of P-y curves from field and laboratory tests. The cyclic P-y curves developed were modifications from the static P-y curves to match observed field

data. The soil resistance was normalized by an ultimate soil pressure calculated from a soil bearing pressure factor of 9. The recommended curves by Matlock (1970) have been the adopted practice for cyclic P-y curves for several years now. Stevens and Audibert (1979) showed a series of case histories where the bearing pressure constants had been reported higher than the value of 9, and also concluded that the use of the previously formulated P-y curves in predicting the behavior of laterally loaded pile over-estimates the pile deflection at the mudline and underestimates the maximum bending moment. Randolph and Houlsby (1984); Murff and Hamilton (1993, 1995), have presented formulations for obtaining the ultimate pressure on a laterally loaded pile in cohesive soils, and values higher than 9 for the soil bearing pressure factor was reported. The recommendations in the API RP2A (2010), is based on the recommendations of Matlock (1970), with difference in the formulations for the unit lateral bearing capacity at depths in soft clays.

In more recent studies, Templeton (2009) and Jeanjean (2009) have shown that the conventional methods for assessing lateral performance of conductor, using P-y curves as formulated by API RP2A manual in year 2000 for soft clays are too conservative. These methods may produce soil springs that are too soft, predicting larger cyclic lateral displacements and bending stresses for a given load range than the P-y curves obtained from the centrifuge test and Finite Element Analysis (FEA). The predicted cyclic stresses and lateral displacements will affect the predictions of the fatigue life of the structure, which is dependent on the P-y curves used in the analysis. Therefore, the use of P-y relations that reliably simulate the actual soil-conductor interaction is essential to safe and cost-effective design of conductors. .

Non-linear lateral soil springs called P-y curves and vertical soil springs called stress/displacement (T-z) curves throughout the depth of conductor can be developed with, the soil data approach or empirical approach. The availability of soil data from either a field test or laboratory test will determine which approach is possible. In

designing conductors, the P-y curves representing the equivalent lateral soil reactions on the conductor significantly controlling its response more than the T-z curve, Pilisi et al. (2012). For the offshore conductors, the significant loads of interest are the horizontal loads that these pipes are subjected to, so P-y curve formulation is the focus of this study.

1.4 Objective of Thesis

The purpose of this thesis is to develop and verify an equivalent linear soil/spring (P-y) model that characterizes the interaction between the soil and the conductor during cyclic lateral loading. The analysis will be considered for relatively small displacement levels, which are representative of most fatigue analysis conditions. The spring model is intended for use in analysis of fatigue life of a conductor pipe; the main focus will be on the steady state response of the soil mass around the conductor, neglecting the transient response.

From the P-y curve of subsea-conductor interaction, we could successfully characterize the stiffness (k) of the soil, which is an integral input for the design of the offshore conductors and simulation of soil-conductor interaction problems. This P-y model is capable of simplifying the complex behavior of the soil-conductor, load-deflection relationship under cyclic loading. With the P-y curves, it should be possible to determine the maximum bending moment and the depth at which it occurs along the conductor, in addition to the shear force, deflection and rotation of the conductor wellhead.

The centrifuge tests involved cyclic loads applied on a model offshore conductor, for various loading condition and sequences. In this experimental sequence, 4 tests were carried out on model conductors, and a description of these test procedures and relevance can be found in Jeanjean (2009). The current study described in this thesis was based on data obtained from Test 4 as described in Chapter 3 of this thesis. The objective

of the tests was to understand the effect of lateral riser motions generated by hull vortex induced vibration (VIV) on the lateral response of the soil. A series of schematics of applied pile head displacements for Test 4 are shown in Fig. 1.4.

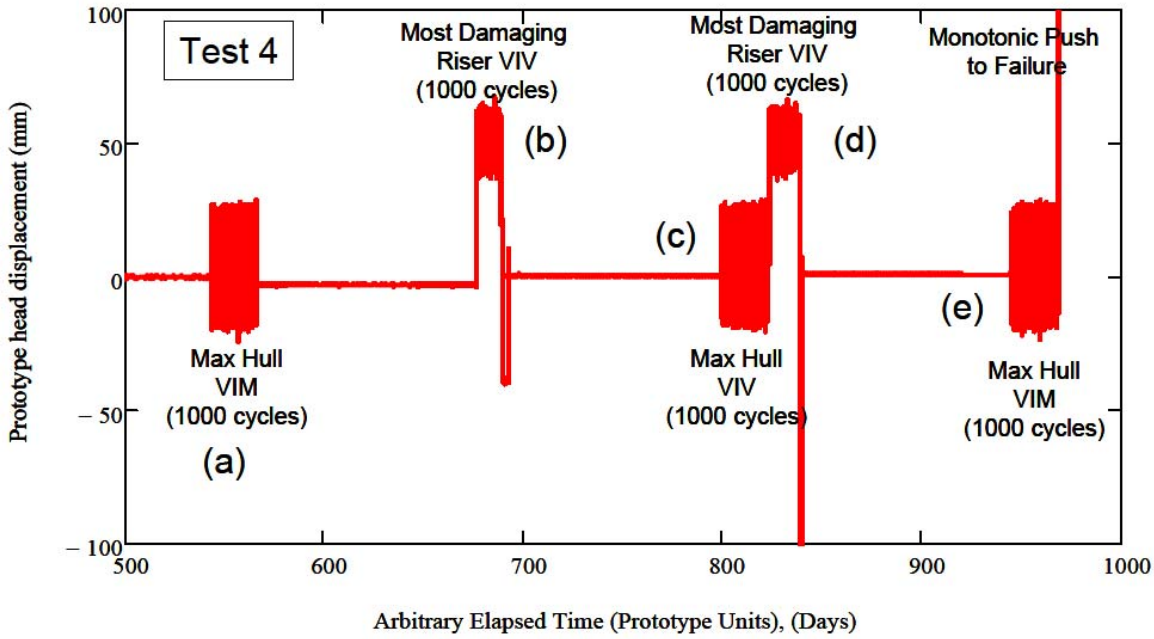

Fig. 1.4: Pile Head Displacement vs Time for Test 4 (Retrieved from Jeanjean, 2009).

The testing program as described by Jeanjean (2009) consisted of 5 sets of 1000 cycles of lateral load applied some distance from the pile head, until very large lateral displacements were achieved at the pile head. The conductor model was instrumented with 13 strain gages to measure strains at discrete points along the conductor; measurement of load, inclination, and lateral movement of the well head were also made. Each set of the 1000 loading cycles were separated by different waiting periods which progressed in the sequence enumerated below:

1) Initial consolidation of the soil.
2) 1000 cycles of loading about a mean displacement position, with amplitude corresponding to wellhead displacement, equal to the maximum hull VIV case at a frequency of 1.2 Hz.
3) A rest period in which dissipation of excess pore pressures induced by cyclic loads and soil consolidation occurs.
4) 1000 cycles of loading at an offset from the mean displacement position, with amplitude corresponding to wellhead displacement, equal to the most damaging riser VIV case at a frequency of 2.2 Hz.
5) A rest period in which dissipation of excess pore pressures induced by cyclic loads and soil consolidation occurs.
6) 1000 cycles of loading about a mean displacement position, with amplitude corresponding to wellhead displacement, equal to the maximum hull VIV case at a frequency of 1.2 Hz.
7) 1000 cycles of loading at an offset from the mean displacement position, with amplitude corresponding to wellhead displacement, equal to the most damaging riser VIV case at a frequency of 2.0 Hz.
8) A rest period in which dissipation of excess pore pressures induced by cyclic loads and soil consolidation occurs.
9) 1000 cycles of loading about a mean displacement position, with amplitude corresponding to wellhead displacement, equal to the maximum hull VIV case at a frequency of 1.2 Hz.
10) Monotonic push of the conductor to failure after cyclic loading.

The data from 5 sets of the 1000 cyclic load sequence in test 4 will be used in the analysis considered in this thesis; the first corresponding to the loading about a mean displacement position and the second with an offset from the mean position. Fig. 1.5 shows the P-y relationship for a cyclic loaded conductor about a zero and non-zero mean

displacement, a depiction of symmetrically and non-symmetrically applied loads, showing the backbone curve, transient and steady state load cycles.

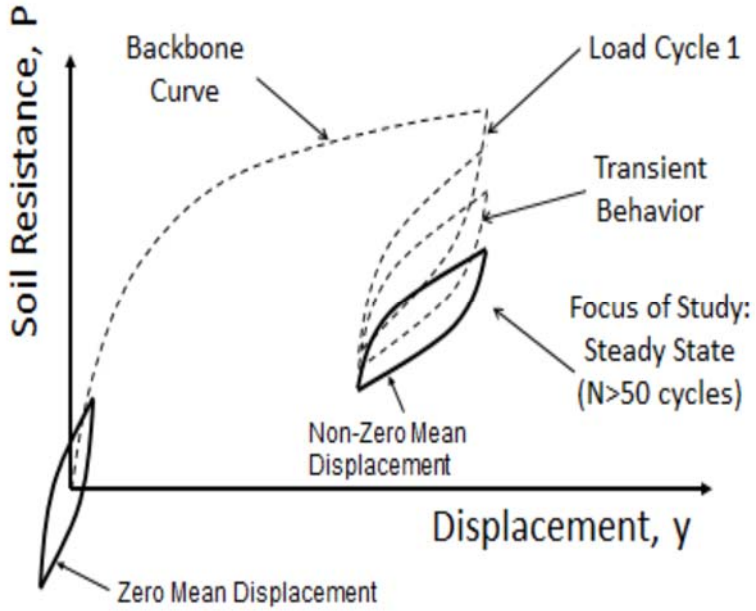

Fig. 1.5: Sketch of the P-Y Relationship for a Cyclic Loaded Conductor About a Zero and Non-Zero Mean Displacement (Reprinted from Aubeny, 2012).

The use of data from the centrifuge is being adopted more because it provides good simulations of field conditions in a controlled environment and the desired parameters can be measured with good accuracy and precision. In the past, designers of dynamically loaded structures only had results of full-scale tests as the principal source of information for modeling the nonlinear behavior of soil surrounding dynamic laterally loaded piles. Much time and capital is required to carry out full-scale tests; the inhomogeneity of in-situ soil strata often makes full scale tests yield data which is site dependent, Prevost et al. (1983). The dynamic response of SSI of a cyclic loaded offshore conductor was carried out with the use of the centrifuge which permitted

similitude effects to be properly accounted. The model Conductor was instrumented with strain gages at varying depths along the conductor, and embedded in clay layer in a centrifuge box. From the experiments, bending moments at discrete strain gage locations were interpreted from strain gage data. Calibrations to the centrifuge experimental data was carried out to obtain model parameters for the power law and the Ramberg-Osgood model relating the soil resistance and deflection. The quality of fit of these models was carefully checked, then back-calculated bending moments were compared to the measured experimental moments.

CHAPTER II

BACKGROUND

2.1 Overview

An appreciable amount of research study has been conducted over the years on obtaining load-deflection relationship for laterally loaded structures in sands, and clays, with the P-y method being the most common approach. A great deal of these research efforts had been concentrated on static analysis, with very few dealing with cyclic loading.

In the course of analyzing and designing laterally loaded piles, different approaches have been adopted for developing P-y curves with a clear distinction made for sand, soft and stiff clays, a brief enumeration of these approaches have been described by Whiteside (1995).

2.2 Soil-Structure Interaction

Soil-structure interaction is usually considered for most dynamic systems in contact with the earth either in seismic regions or offshore environments where cyclic loading is expected. It is the process whereby the response of a structure influences the motion of the soil in its zone of influence, or the motion of the soil influences the motion of the structure it supports.

Most civil engineering structures are in contact with soil, or are supported by structures embedded in the ground; these includes offshore structures in contact with the seabed (catenary riser at touchdown) or below the sea bed (shallow and deep foundations, anchors, suction caissons), foundations of high rise buildings, and foundations for wind

turbines. Soil-structure interaction analysis will be expected to be carried out to understand the behavior of the structure relative to the soil supporting it.

The offshore conductor interacts with the sea bed in the manner described above, as the pile deflects, the soil experiences some deformation which influences its ability to support the conductor as it further deflects. There is always a limiting condition acceptable for the deflection of the wellhead which the conductor supports which makes it really important knowing what resistance from the soil to rely on. A factor that will determine the size of the conductor during design, and for fatigue analysis. If the pile experiences serious deflections cycled in two directions, there is tendency for cracks to set in, within a shorter period compared with one subjected to smaller magnitudes of deflections. This continual back and forth movement of the pipes cannot be avoided for it is of natural consequences but can be minimized with accurate predictions of the behavior of the structural response. Therefore, carrying out soil–structure analysis of the conductor will to help determine the associated deflections and cyclic stresses in the conductor caused by motions associated with the floating vessel, hull and the riser, which will be very useful for fatigue analysis, Jeanjean (2009).

2.3 Literature Review

2.3.1 P-y Curves

According to Matlock (1970), the first significant attempt to deal with the nonlinear behavior of soil resistance to lateral deflection of piles was employed by McClelland and Focht (1958). McClelland and Focht (1958) proposed a linear conversion to produce P-y curves for laterally loaded piles from nonlinear laboratory stress-strain curves, and analysis of field test data. Subsequently, Matlock (1970), proposed P-y curves for both static and cyclic loading on piles, but the P-y curves for the cyclic loading were empirically constructed off the static loading curves with a bit of adjustment made on the representative cyclic P-y curves to fit the experimental data. According to Whiteside

(1995), the P-y curve approach was a method developed to account for nonlinearity and produces results that are far more accurate over a wider range of loads than methods based on linear soil behavior.

Based on the P-y approach, the lateral soil-structure interaction can be modeled using empirically derived nonlinear uncoupled springs (p-y curves), as boundary conditions in structural analysis. P-y curves intended for a more generalized use are usually normalized by dividing the soil pressure by using either the ultimate pressure or shear strength; the deflection by the diameter of the pile. The P-y approach is still the most common approach adopted due to its ease of use, and the short computation time required. The finite element analysis (FEA) is being adopted in some computations also to determine soil response from pile forcing. Templeton (2009) carried out nonlinear 3D FEA to determine the lateral interaction between the well conductors and soil, for site conditions at an actual deep water production system location and centrifuge test; then compared results to the centrifuge test results and the 2000 edition of API RP2A recommendations.

Templeton (2009) showed that the P-y curves as formulated by 2000 edition of API RP2A for pile performance underestimates the stiffness of the soil/conductor interaction. Adopting P-y relations closer to the field conditions will be less conservative and can reduce the overall costs associated with conductor sizes and accumulated fatigue stress predictions.

Several plots of normalized P-y curves obtained from a Finite Element Analysis from Templeton (2009), Matlock, API standard, centrifuge test, and proposed empirical curves were presented by Jeanjean (2009), with good correlation shown amongst all curves except those generated from the API and Matlock, which showed softer response in comparison to the other presented P-y curves. The study concluded that within the margin of load interests, API lateral P-y curves produced conservative results for

structures below the mudline in soft normally-consolidated clays, but underestimates the ultimate unit pressure acting on the conductor and predicts a shorter fatigue life, as shown in Fig. 2.1, since the API static P-y curves are shown to underestimate the soil stiffness for soft clays, interpreted cyclic P-y curves will certainly work the same way, which again indicates the need for further study to improve design recommendations.

The P-y relationship for piles/conductors-soil interaction are usually established from large scale or model tests, or empirically. The piles/conductors are usually instrumented with strain gages at discrete points throughout the length of the pile/conductor. The data collected is then reduce from strain gage readings to curvature / bending moment data at the strain gage locations. A smooth function is usually fit to the discrete bending moment, in order to have a continuous function representing the bending moment profile along the entire length of the pile, which is then further interpreted to derive the pressure and the deflection. Some of these methodologies employed to reduce strain gage data to soil resistances and deflection have been described by Rollins and Gerber (2008) and Yang and Liang (2006).

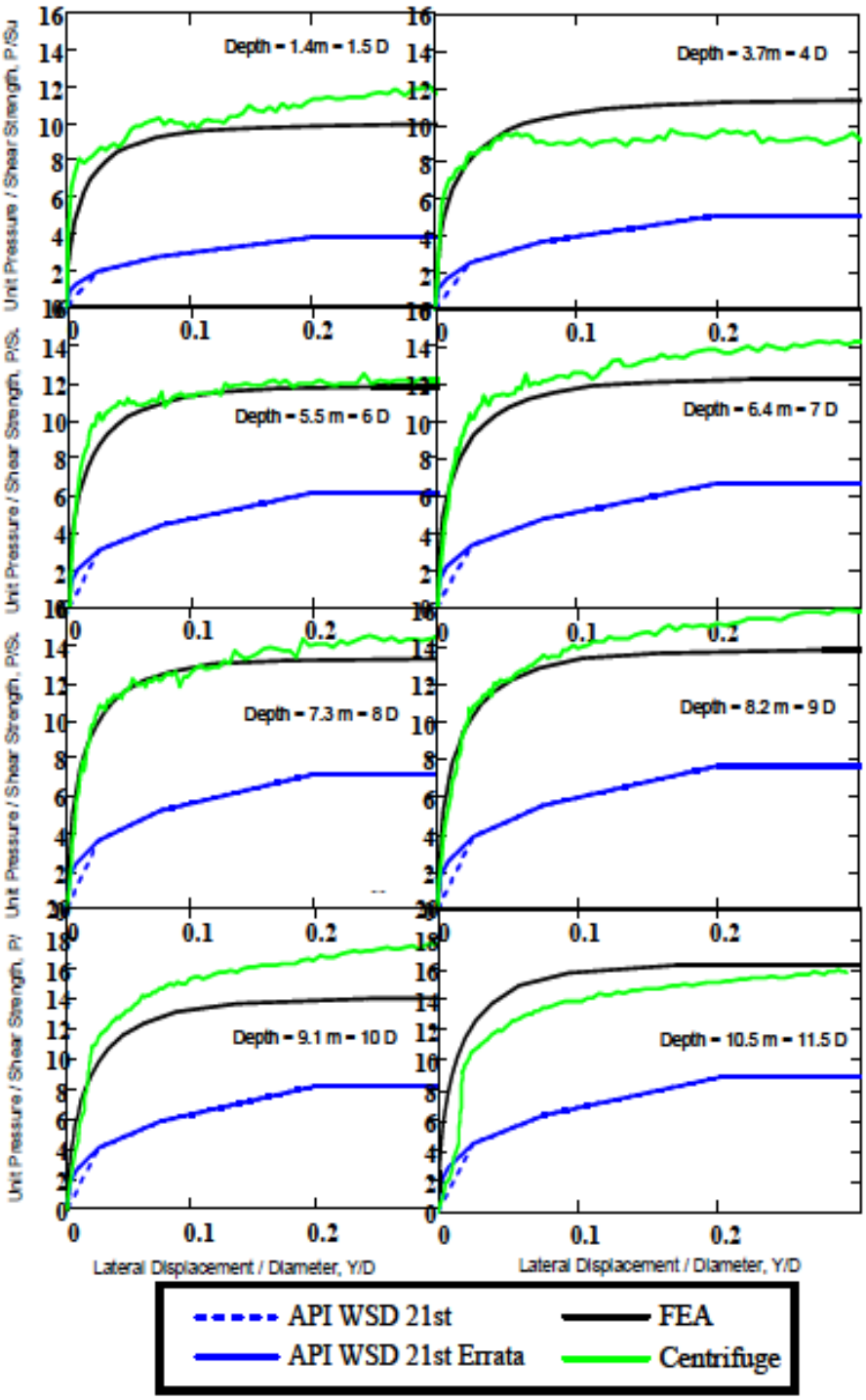

Fig. 2.1: Comparison of Normalized Monotonic P-Y Curve from Centrifuge Test 1 from Jeanjean, 2009, FEA Results from Templeton, 2009, With Those Obtained from API Recommendation (Reprinted from Jeanjean, 2009).

2.4 Ultimate Resistance on a Laterally Loaded Pile

The ultimate unit resistance that can be exerted by soil on a pile is very crucial in the analysis of laterally loaded piles. The ultimate resistance is usually incorporated in the generated normalized P-y curves, and also used to determine the limiting condition of the soil with respect to the conductor. The ultimate lateral resistance can be obtained from experimental measurements (laboratory and field), simplified wedge analysis (incorporating the principles of plasticity to determine lower bound and upper bound values) or by judgment in conjunction with any of the above methods, Murff and Hamilton (1993). The ultimate lateral resistance on laterally loaded pile embedded in clay in an undrained state has been published by Broms (1964), Randolph and Houlsby (1984), and Murff and Hamilton (1993).

Broms (1964) first treated the problem of finding the failure load on a laterally loaded pile, presenting a limit pressure of $9s_u$ for cohesive soil, which was the same value adopted by Matlock (1970); s_u is the undrained shear strength. Randolph and Houlsby (1984), based on classical plasticity theory presented a lower bound and upper bound solution for plastically deforming cohesive material in undrained conditions due to a laterally loaded pile. The final results from the study are presented below and full description of the derivations can be found in the publication.

Lower bound solution: The lower bound solution is obtained by finding a set of stresses that are in equilibrium with applied loads, however do not violate the yield criterion for the material. The Lower bound formulations are shown in Eqns. 1 – 3.

$$\frac{P}{cd} = \pi + 2\Delta + 2\cos\Delta + 4\left[\cos\left(\Delta/2\right) + \sin\left(\Delta/2\right)\right] \quad \text{Eqn.1}$$

where,

$P = final\ failure\ load\ per\ unit\ lenght\ of\ pile$

$c = shear\ strength$

$d = pile\ diameter$

$\Delta = \arcsin\alpha = a/c$

$$For\ \ \Delta = 0,\ \ \frac{P}{cd} = 6 + \pi = 9.14 \qquad (for\ smooth\ pile) \qquad \text{Eqn.2}$$

$$\Delta = \frac{\pi}{2},\ \ \frac{P}{cd} = 4\sqrt{2} + 2\pi = 11.94 \qquad (for\ perfectly\ rough\ pile) \qquad \text{Eqn.3}$$

Upper bound solution: For the upper bound solution, a failure mechanism is assumed, an associated velocity field consistent with kinematic constraints. The collapse load is estimated by equating the rate of energy dissipation within the deforming mass to the workdone by the external load. The upper bound solution is shown in Eqn. 4.

$$\frac{P}{cd} = \pi + 2\Delta + 4\cos\left(\left(\pi/4\right) - \left(\Delta/2\right)\right)\left(\left(\sqrt{2}\right) + \left(\sin\left(\left(\pi/4\right) - \left(\Delta/2\right)\right)\right)\right) \quad \text{Eqn.4}$$

Murff and Hamilton (1993), also presented an approximate empirical upper bound solution for ultimate pressure on a laterally loaded pile, considering pile-soil adhesion at the front of the pile. Based on the solution, the ultimate unit resistance on the pile is given in Eqn. 5; and the non-dimensional lateral bearing factor (N_p) expression in Eqn. 6.

$$Pult = N_p S_u + \gamma' z \quad \text{Eqn. 5}$$

$$N_p = N_1 - N_2\, exp\left(-\frac{\varepsilon z}{D}\right) \quad \text{Eqn. 6}$$

Where,

$$\varepsilon = 0.25 + 0.05\,\lambda \qquad \lambda < 6 \quad \text{Eqn. 7}$$

$$\varepsilon = 0.55 \qquad \lambda \geq 6 \quad \text{Eqn. 8}$$

$$\lambda = \frac{S_{u0}}{S_{u1}\, D} \qquad \text{Eqn. 9}$$

N_1 *is limiting value at depth*; 9.0 *for the smooth pile*

$(N_1 - N_2)$, *is soil surface intercept*; N_2 *is* 7.0 *for the smooth pile*

The value for the intercept $(N_1 - N_2)$ was slightly modified by Jeanjean (2009) where, $N_1 = 12, and\ N_2 = 4$

It is also important to note that the value of N_p at depth has been limited to 12 in order to be consistent with exact Lower and Upper bound plasticity solutions proposed by Randolph and Houlsby (1984). This is the frame work that has been adopted in this thesis even though some measurements indicate apparently higher values. Fig. 2.2 shows plots of Normalized lateral pressure and depth along the pile, showing measurements from centrifuge and numerical simulation being above 12. The reason for measured data exceeding the theoretical upper bound is unclear. Possible reasons can include inaccuracy in soil strength measurements and strain rate effects.

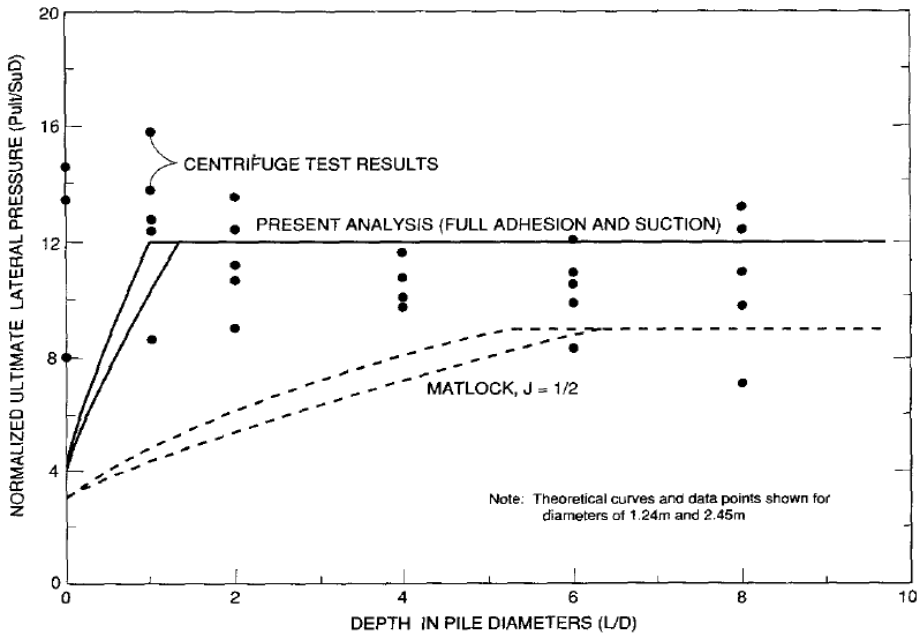

(a) Normalized Lateral Ultimate Pressure Along Pile Depth (Reprinted from Murff and Hamilton (1993))

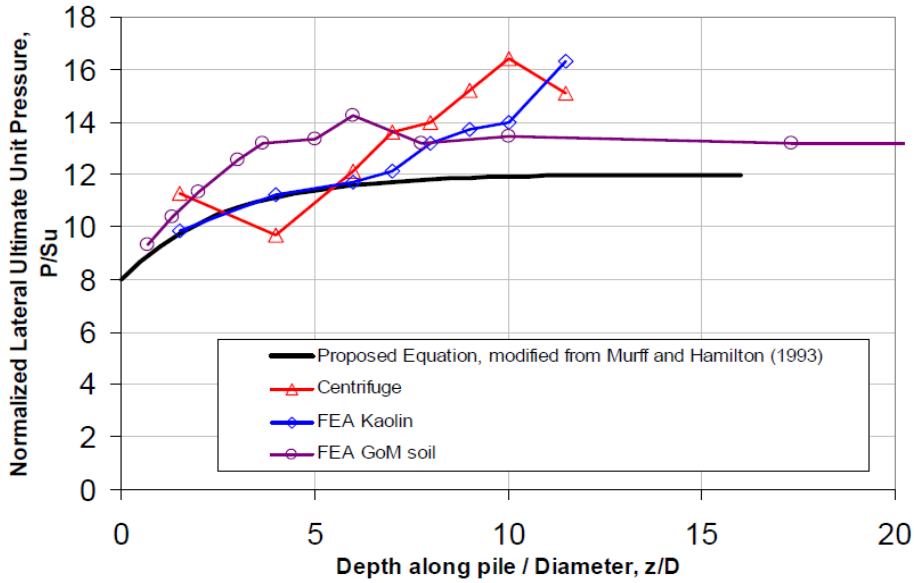

(b) Normalized Lateral Ultimate Unit Pressure from Centrifuge Test 1, FEA Analysis and Modified Murff and Hamilton (1993) Equation (Reprinted from Jeanjean (2009))

Fig. 2.2: Normalized Unit Pressure Suggesting Values of Np Higher Than 12.

CHAPTER III

P-Y CURVE GENERATION PROCEDURE

3.1 Overview

Bending moments were calculated from strain gage measurements along the pile shaft obtained from a centrifuge test on a conductor subjected to cyclic lateral loading. The test was carried out on a small-scale conductor model in soft normally to slightly over-consolidated Alwhite Kaolin clay under displacement control, Jeanjean (2009).

The purpose of this test was to:
Investigate the behavior of well conductors under cyclic loading, locate the position of maximum bending moment in the conductor as it is subjected to cyclic loading, and determine the influence of the considered loading regime on the potential flexural fatigue of the conductor.

The model conductor was instrumented with 13 strain gages to measure the bending perpendicular to the axis of bending. The test was carried out at 48g in a large geotechnical centrifuge with a loading frequency of 1Hz. The pile head rotation, displacement, force were measured as well as strains at the 13 strain gage locations. Bending moments at these 13 locations along the depth of the conductor were computed from the measured strains. The deformed shape of the pile was computed through double integration of the measured curvature ($y'=M/EI$), and invoking the boundary constraints of measured y' and y values at the reference point near the pile head. Similarly, the second derivative of the bending moment produced the soil resistance (P) per unit length acting on the conductor. This data reduction procedure produces the soil resistances (P) and deformation (y) along the pile depth at the locations where the strain gages were installed. Different approaches for reducing the bending moment data into soil

resistances and deflection, exists. The bending moment information is obtained at discrete points along the conductor, however, a continuous profile is required. Some researchers will fit an nth order continuous function of to the entire data points, while others will fit a piecewise nth order function to the data points. Yang and Liang, (2006), considered different methods to fit the discrete bending moment data, and concluded that the piecewise cubic polynomial curve fitting method yielded the least error on predicted deflections. Least square quadratic and cubic polynomial curve fitting methods were considered during the data reduction process, however, better results were obtained with the quadratic polynomial, when predicted pile head loads were compared to the measured values. Therefore, the quadratic polynomial was chosen for the data reduction. The results of Yang and Liang, (2006), ensures more confidence with the use of the piecewise approach as this should be less sensitive to noise and scatter in the data.

3.2 Centrifuge Test Data Set

Test data relevant for the analysis included the pile geometry information, undrained shear strength (s_u), bending moment (M), pile head rotation (y'(0)), and pile head deflection (y(0)). The conductor (model and prototype) geometry and test parameters are shown in Table 1.

Five sets of cyclic tests were carried out on this conductor, each for 1000 cycles, as depicted earlier in Fig. 1.4, which consisted of a mixture symmetric, and asymmetric loading schemes. Fig. 3.1 shows an image of the conductor and the test bed at the end of the cyclic tests, and monotonic push.

Table 1: Conductor (Model and Prototype) Geometry and Test Parameters.

Parameter	Prototype	Model
Scale	1	48
Material	Steel	
Diameter (m)	0.9144	0.01905
Thickness (m)	0.0508	0.00106
SMYS (MPa)	476.9	476.9
Length (m)	22.43	0.421

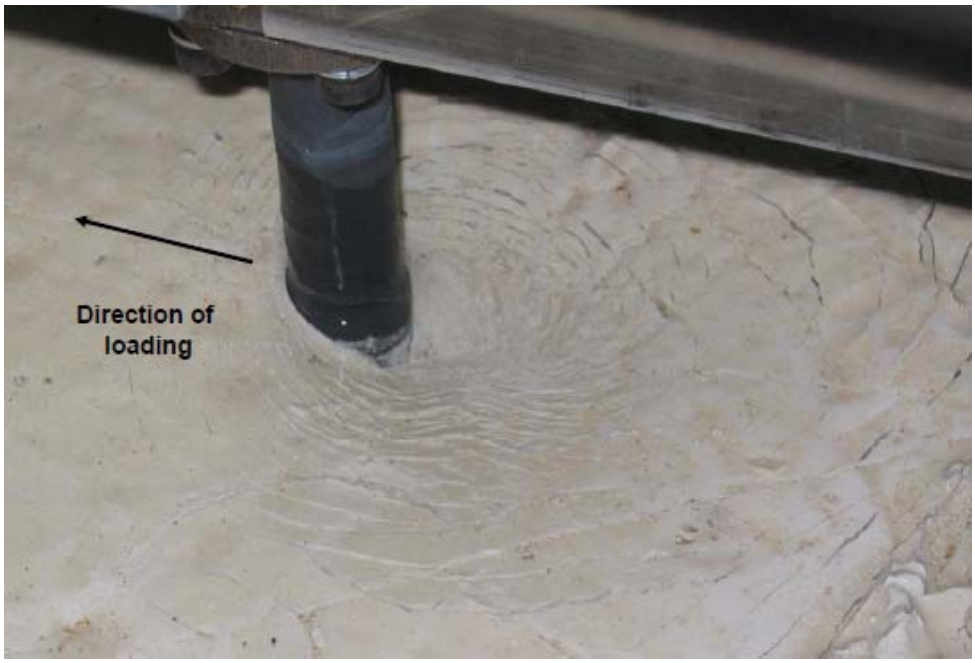

Fig. 3.1: A View of the Conductor and the Test Bed at the End of the Cyclic Test, After a Monotonic Push (Reprinted from Jeanjean (2009)).

3.3 Data Reduction

The bending moment information obtained from the strain gages along the pile were reduced to line load and deflection using basic beam theory from structural analysis. The Winkler beam theory was adopted and springs were fixed along the length of the pile at the locations of the strain gages. A schematic of the beam in undeformed and deformed configuration is shown in Fig. 3.2. A beam subjected to pure bending, within the elastic range has its curvature of the neutral surface as expressed in Eqn. 10. Eqn. 11 – Eqn. 14, show the relationship between the deflection, and moment, shear, line load, and soil resistance respectively.

For the analysis, elevations are referenced to a point z = 3.312m above the mudline, the top of the conductor pipe, which is slightly below the actual point of the load application during the tests. Table 2 lists the sensor locations in terms of three reference points, the base of the loading bracket, the pin connection, and the mudline.

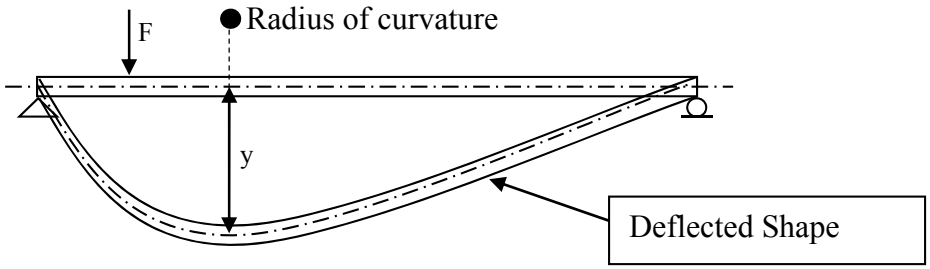

Fig. 3.2: Schematic of a Beam in Undeformed and Deformed Configuration.

Deflection: $\boldsymbol{y}$

Curvature: $\frac{\mathbf{1}}{\boldsymbol{\rho}} = \frac{\boldsymbol{M}}{\boldsymbol{EI}} = \frac{\boldsymbol{d^2y}}{\boldsymbol{dx^2}}$ Eqn. 10

Moment: $\boldsymbol{M} = \boldsymbol{EI}\ \frac{\boldsymbol{d^2y}}{\boldsymbol{dx^2}}$ Eqn. 11

Shear: $\boldsymbol{V} = \frac{\boldsymbol{dM}}{\boldsymbol{dx}} = \boldsymbol{EI}\ \frac{\boldsymbol{d^3y}}{\boldsymbol{dx^3}}$ Eqn. 12

Line Load: $\boldsymbol{w} = \frac{\boldsymbol{dV}}{\boldsymbol{dx}} = \boldsymbol{EI}\ \frac{\boldsymbol{d^4y}}{\boldsymbol{dx^4}}$ Eqn. 13

Soil Resistance: $\boldsymbol{P = K_s y}$ Eqn. 14

Modulus of Elasticity: $\boldsymbol{E}$

Moment of Inertia across the section about its neutral axis: $\boldsymbol{I}$

Secant Modulus: $\boldsymbol{K_s}$

3.3.1 Double Integration

The deflection at each strain gage location was obtained by integrating the curvature (M/EI) twice using the trapezoidal rule. The first integration of the curvature to obtain slope along the pile, with the measured slope at the pile head providing the necessary integration constant. A second integration of the curvature produced the deflected shape of the pile, using the measured deflection at the pile head to obtain the second integration constant.

Table 2. Centrifuge Test Measurements and Locations.

Depth below reference point z_{ref} (m)	Depth below pin connection z_{pin} (m)	Depth below mudline z_{mud} (m)	Measurement
-1.056	0.0	-4.368	Pile head displacement, y
-1.056	0.0	-4.368	Pile head tilt, y’
-1.056	0.0	-4.368	Pile head force
1.685	2.741	-1.627	SG13 Moment
2.601	3.657	-0.711	SG12 Moment
4.886	5.942	1.574	SG11 Moment
7.173	8.229	3.861	SG10 Moment
9.001	10.057	5.689	SG9 Moment
9.916	10.972	6.604	SG8 Moment
10.830	11.886	7.518	SG7 Moment
11.745	12.801	8.433	SG6 Moment
12.659	13.715	9.347	SG5 Moment
14.030	15.086	10.718	SG4 Moment
15.859	16.915	12.547	SG3 Moment
18.145	19.201	14.833	SG2 Moment
20.889	21.945	17.577	SG1 Moment

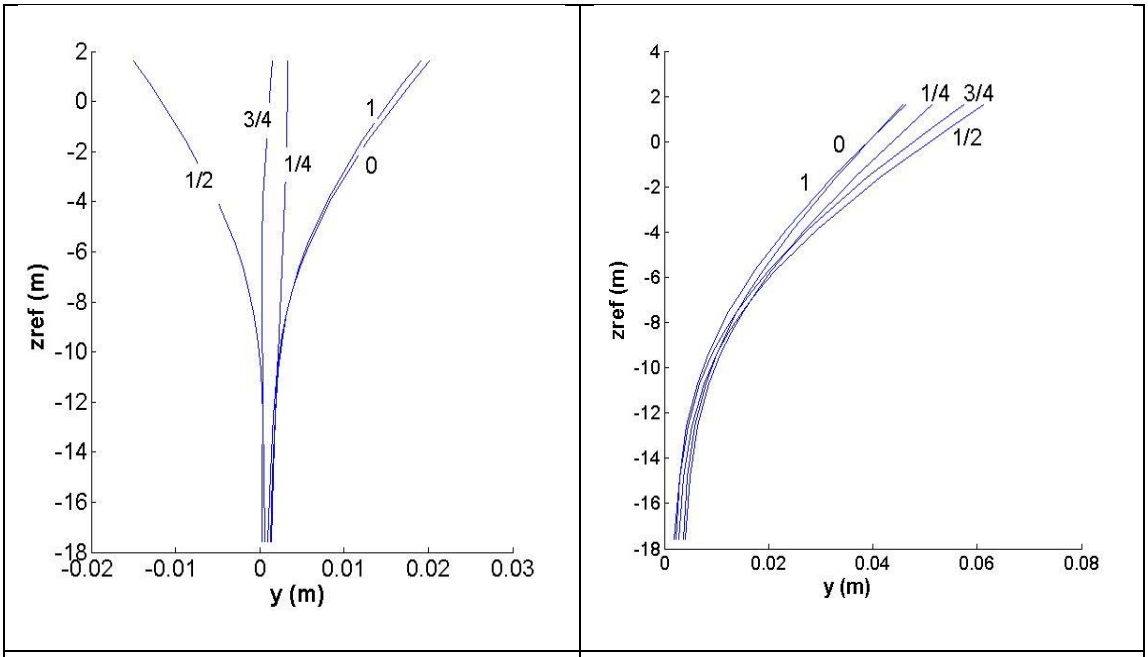

a. Zero Offset | b. 0.05 m Offset

Fig. 3.3: Profiles of Lateral Deflection along Conductor (Reprinted from Aubeny (2012)).

3.3.2 Double Differentiation

The soil resistance was obtained by differentiating the bending moment (M) twice. The second derivatives were computed numerically by locally fitting a least squares second order polynomial through the 5 nearest data points surrounding the point of interest. A least squares fit has the advantage that it tends to be smooth through noise in the data while giving maximum weight to the data in the immediate vicinity of the point of interest. For the extreme two points at the pile head and toe, 2 and 3 data points were considered respectively for the least square fitting exercise. Fig. 3.4 shows a sample moment fit to the bending moment data from the test, and Fig. 3.5 show profiles of soil resistance P at ¼ cycle increments for a load cycle.

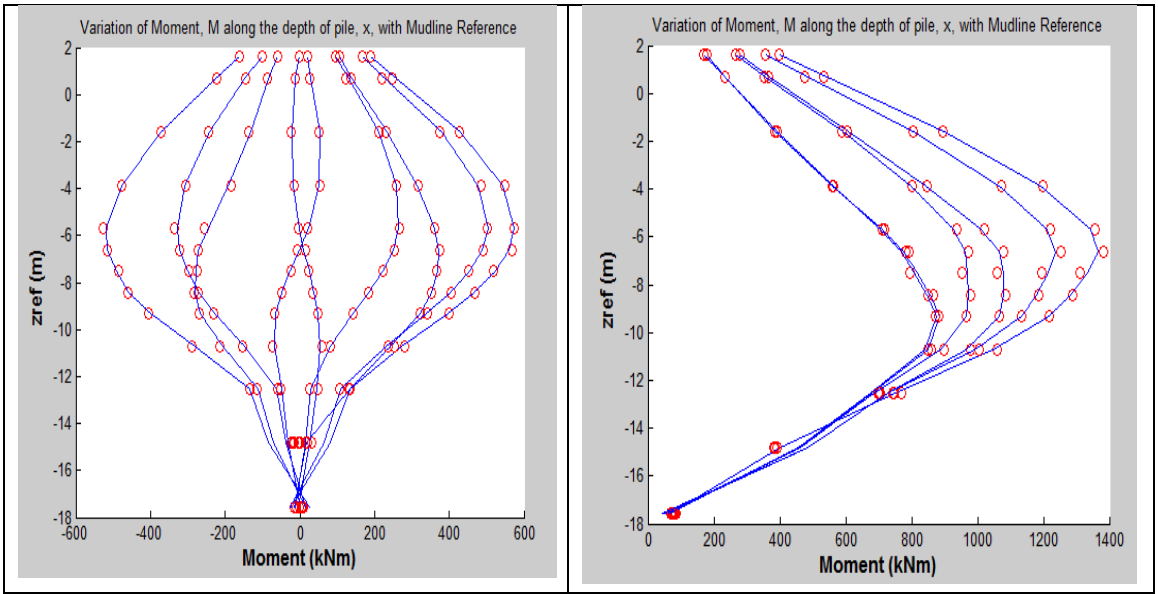

a. Zero Offset | b. 0.05 m Offset

Fig. 3.4: Profiles of Bending Moment along Conductor.

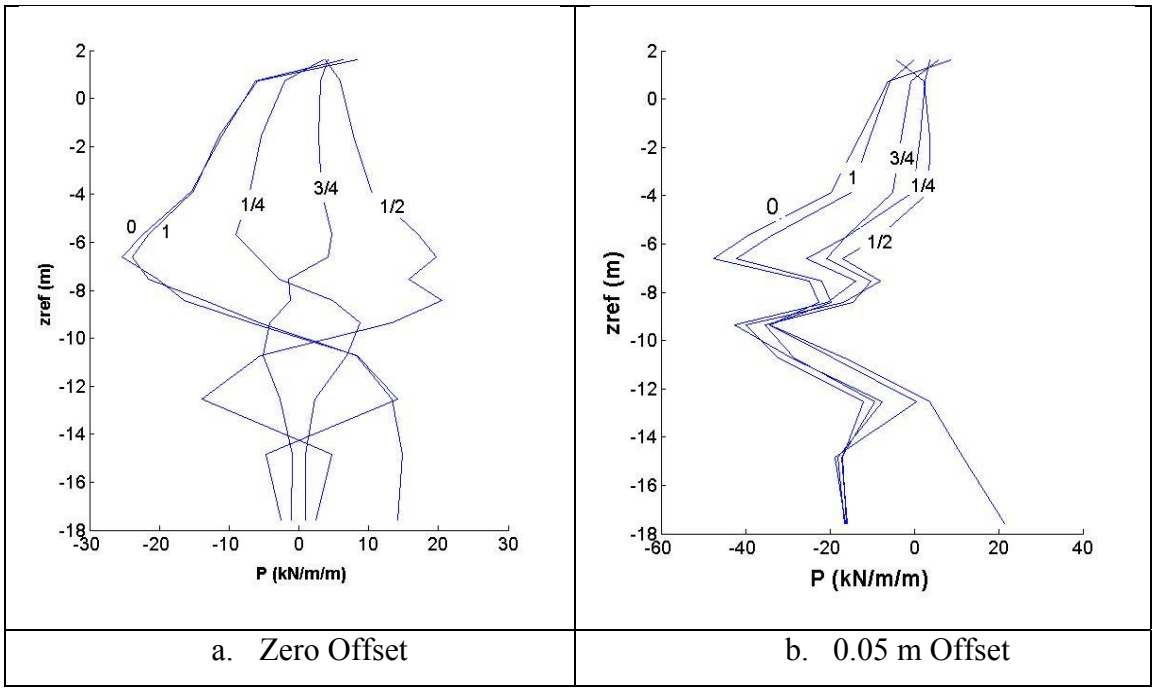

a. Zero Offset | b. 0.05 m Offset

Fig. 3.5: Profiles of Soil Resistance along Conductor (Reprinted from Aubeny (2012)).

Schematics of the steps described above is shown in Fig. 3.6. Detailed steps of the numerical differentiation procedure are contained in Appendix A. At any instant of time, profiles of displacement and soil resistance can be computed using the procedure described above, which has been implemented in a MATLAB program. The inputs of this program are pile head displacement, rotation, and force measurement; the bending moments along the depth of the pile, in prototype scale. Note that the displacement curves, being a product of double integration, are very smooth. By contrast, the soil resistance curves, being a product of numerical double differentiation of relatively widely spaced data are more irregular, but nevertheless suitable for their intended purpose.

For back-calculating soil stiffness, a continuous history of P and y throughout a given load cycle is required. Fig. 3.7 shows a typical result of the data extraction and processing. The blue data points denote unloading from the peak to trough, while the red data points denote reloading from the trough to peak. A finite difference scheme implemented in a MATLAB program was used to back-calculate the moment using the secant stiffness obtained from the Power law and Ramberg-Osgood curve fit parameters.

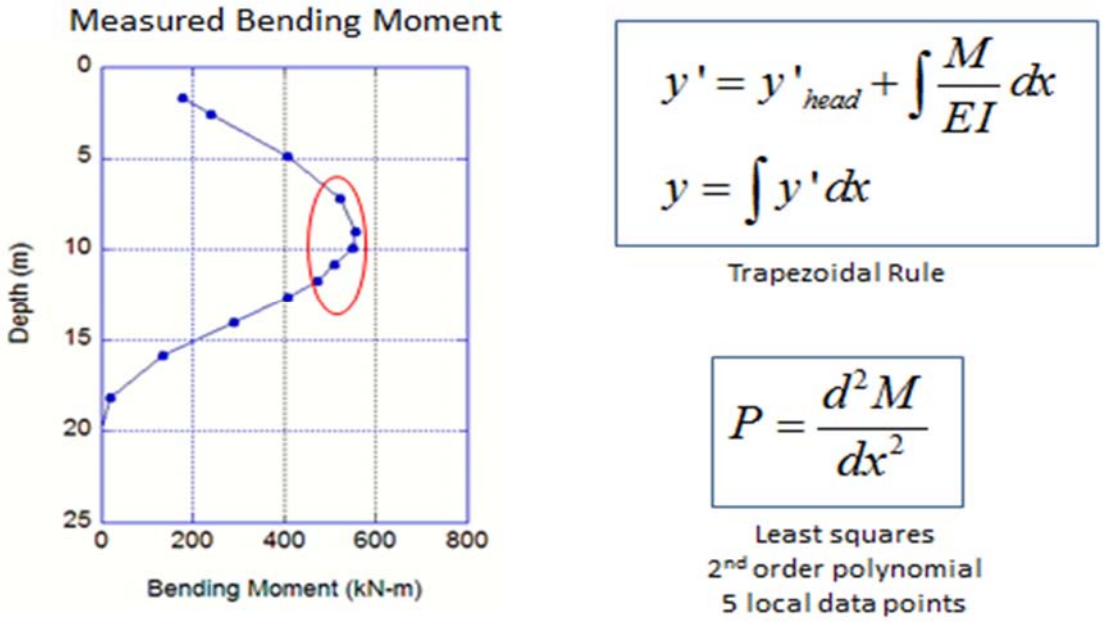

Fig. 3.6: Reduction of Centrifuge Test Data (Bending Moment) to Soil Resistance (P), and Deflection (Y) (Reprinted from Aubeny (2012)).

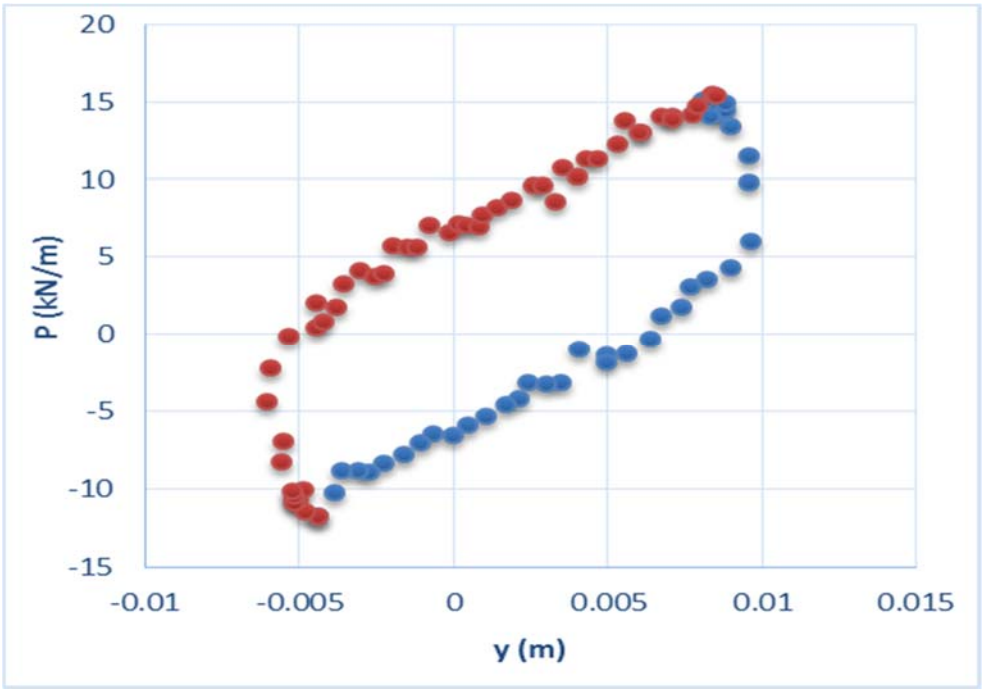

Fig. 3.7: Typical P-Y Loop Obtained from Data Analysis Procedure.

3.3.3 Power Law Model

Initially, a hyperbolic fitting function was applied to the dataset. However, after several trials and comparisons, it was concluded that a power law function provided a better fit.

The power law function employed is of the form expressed below:

$$P = K_0 \left(\frac{y}{D}\right)^n \quad \text{Eqn. 15}$$

where K_0 and n are curve fit parameters, and D is pipe diameter.
As will be shown subsequently, values of K_0 and n were both found to be dependent on depth, z.

In a general nonlinear analysis of laterally loaded piles, the soil resistance as a function of lateral displacement can be input directly into the model in the form of a nonlinear soil resistance function. In the framework of a linear analysis, approximate characterization of nonlinear soil resistance can be modeled using an equivalent secant stiffness and damping. For the power law function, closed form solutions were obtained for the secant stiffness and damping ratio.

$$K_{sec} = \frac{K_0}{D} \left(\frac{y}{D}\right)^{n-1} \quad \text{Eqn. 16}$$

$$\beta = \frac{1}{\pi} \left(\frac{1}{n+1} - \frac{1}{2}\right) \quad \text{Eqn. 17}$$

While the secant stiffness for a power law relationship is a function of displacement magnitude, the damping ratio is solely a function of the exponent n. At large displacement amplitudes, the damping would be expected to increase. Accordingly, Eqn. 17 should be considered valid only for small displacements. Note that when n = 1, the P-y relationship is linear and the damping becomes zero.

Expressing the secant modulus, K_{sec} in Eqn. 16 in normalized form can facilitate generalization of the model test results to other soil profiles. For this purpose, the ultimate soil resistance (P_{ult}) was chosen as the normalization parameter. An attempt was made to evaluate P_{ult} from the bending moment and displacement measurements taken at the final stage of the test when a large lateral displacement was applied to the pile. P_{ult} values were evaluated in exactly the same manner as that described for evaluating P. However, the P_{ult} values derived from this approach were judged to be excessively large. This was attributed to the fact that the monotonic loading to ultimate capacity was not conducted in a soil in pristine state; i.e., a number of episodes of cyclic loading and consolidation occurred prior to the monotonic loading.

To provide an alternative estimate of P_{ult}, consistent with published values, the modified Murff-Hamilton equation for the bearing factor (N_p) by Jeanjean (2009) was used in conjunction with the undrained soil strength profile. In the upper reach of the soil profile relevant to the zone in which the data interpretation was focused, the undrained soil strength profile over depth z (in meters) was taken as:

$$s_u = 2.4\ kPa + (0.555\ kPa/m)\ z \qquad \text{Eqn. 18}$$

3.3.4 Ramberg-Osgood Model

The Ramberg-Osgood model has been successfully applied in characterizing stress-strain relationship for cyclic loads in metals, Skelton et al. (1997); also employed in characterizing the stress-strain behavior of cyclically loaded soil by its backbone curve. The Ramberg-Osgood equation shown below in Eqn. 19, as presented by Idriss et al. (1976) is used to represent the actual soil backbone curve.

$$\gamma = \gamma_y \left[\frac{\tau}{G_{max}\,\gamma_y} + \alpha \left(\frac{\tau}{G_{max}\,\gamma_y} \right)^R \right] \quad \text{Eqn. 19}$$

where,

τ = shear stress

γ = shear strain

G_{max} = shear modulus at very small strains

γ_y, α, R = soil parameters

The expression was modified to have it in a relevant form to fit the problem being solved; relating soil resistance to pile deflection. The modified expression is shown in Eqn. 20 and Eqn. 21. The secant stiffness and damping ratio are shown in Eqns. 22 and 23 respectively, all modifications from Idriss et al. (1976).

$$y = y_{ref} \left[\frac{P}{K_{max}\,y_{ref}} + \alpha \left(\frac{P}{K_{max}\,y_{ref}} \right)^R \right] \quad \text{Eqn. 20}$$

$$\frac{y}{y_{ref}} = \text{a P} + \alpha\,(a\,P)^R \quad \text{Eqn. 21}$$

where,

y = deflection

P = soil resistance

y_{ref},a,α, c, R = soil parameters (constants)

$$K_{max} = \frac{1}{a\,y_{ref}}$$

$$\frac{K_{sec}}{K_{max}} = \frac{1}{1+\alpha\left(\frac{P}{K_{max}\,y_{ref}} \right)^{R-1}} \quad \text{Eqn. 22}$$

$$\beta\ (\%) = \frac{100\,\alpha \left(\frac{P}{K_{max}\,y_{ref}} \right)^R}{\left(\frac{y}{y_{ref}} \right)} \quad \text{Eqn. 23}$$

3.4 Inverse Process for Bending Moment

The springs defined by the curve fit parameters that will be presented in Chapter 4 can be applied to the analysis of a laterally loaded conductor pipe subjected to arbitrarily imposed pile head loads or displacements. This analysis can be achieved through well-established finite difference techniques. Specific details of the procedure used in this investigation are described in Appendix B. The back analysis was carried out using displacement control at the pile head, since the centrifuge tests were carried out with a displacement control criteria. This is a verification process to see how the predicted bending moment profile compares with the measured bending moment profile from the centrifuge test. The results of the comparison will be presented in the next Chapter.

CHAPTER IV

RESULTS

4.1 P-y Curves

The centrifuge test as described earlier and depicted in Fig. 1.4, consists of 3 symmetric cyclic tests with zero offset (M1: 0.02D±0.005, M3: 0.02D±0.005, and M5: 0.02D±0.005), 2 symmetric cyclic tests with applied offset about 0.050m (M2: 0.01D±0.005 and M4: 0.01D±0.005). The data reduction process was carried out for the various tests listed above, with focus on the steady state. The steady state condition was considered from the 100th to the last cycle, in incremental steps of 100 cycles. The normalized P-y curves at steady state at the specified step size were grouped together for the various motions. The power law relationship in Eqn. 15, and Ramberg-Osgood relationship in Eqn. 21, were fit to the P-y data to obtain the best line fit.

Fig. 4.1 (a) – (e), shows the normalized pressure and deflection plots for steady state at the various strain gage locations along the pile.

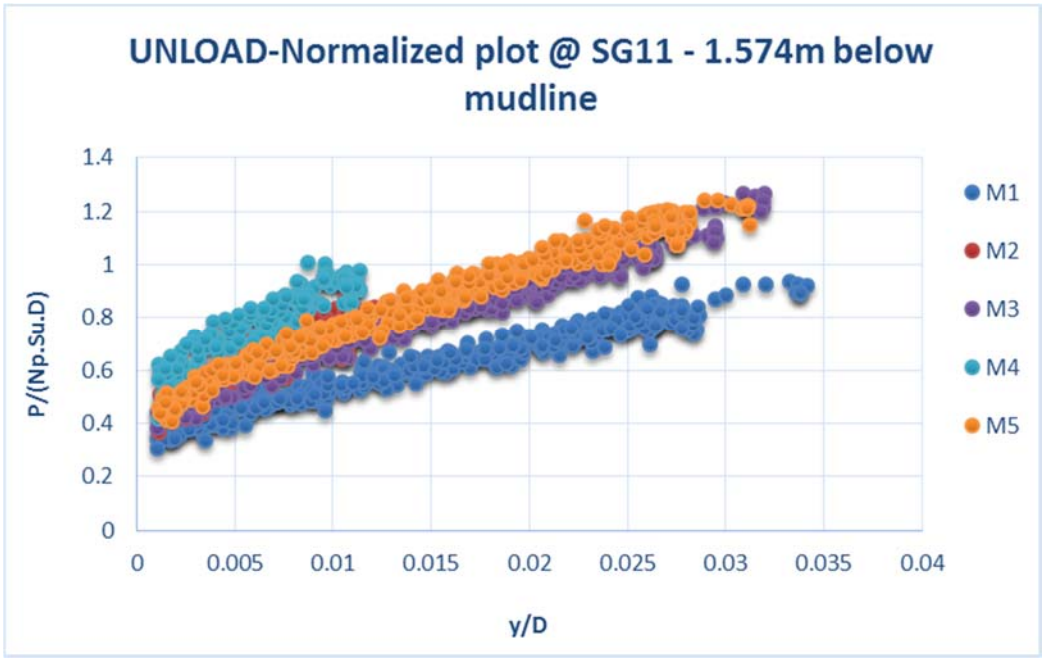

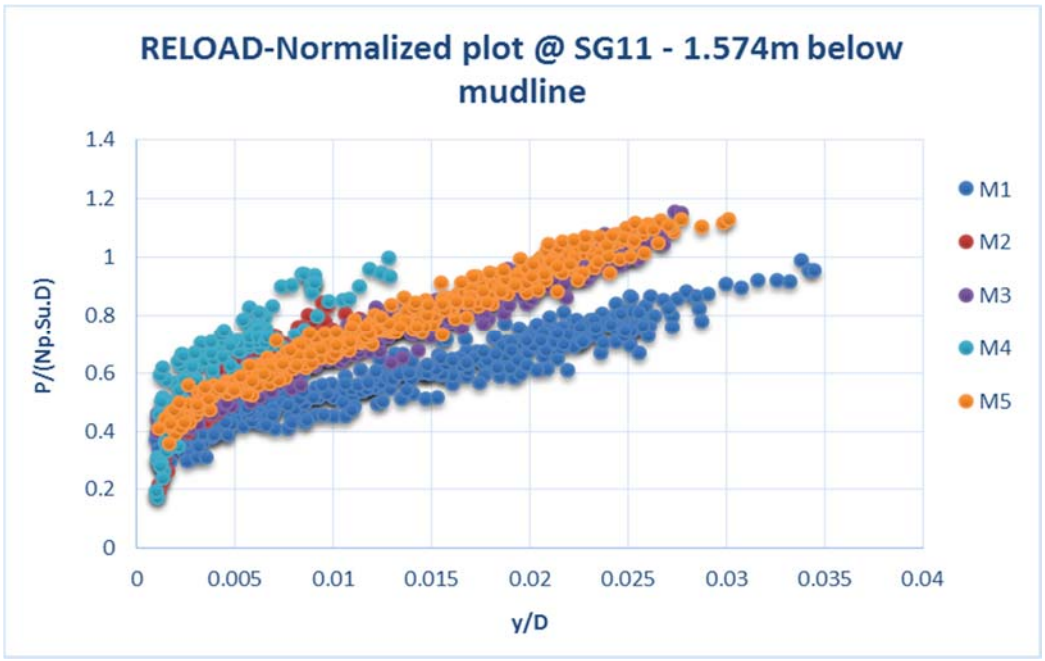

(a) Normalized Soil Resistance and Deflection Relationship at SG11, for Motions M1, M2, M3, M4, and M5

Fig. 4.1: Normalized Soil Resistance and Deflection Plots from Analyzed Data, Test 4.

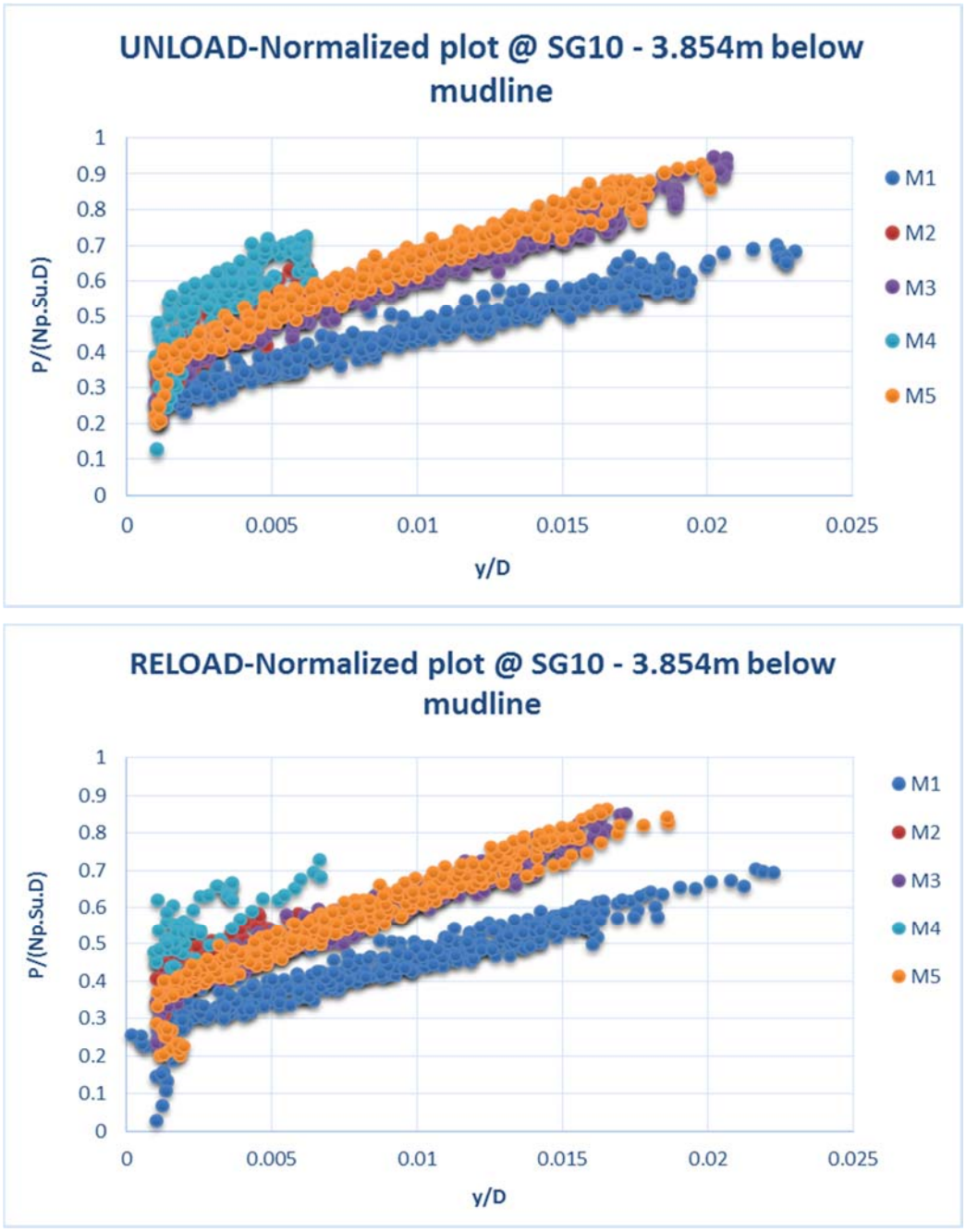

(b) Normalized Soil Resistance and Deflection Relationship at SG 10, for Motions M1, M2, M3, M4, and M5

Fig. 4.1: Continued.

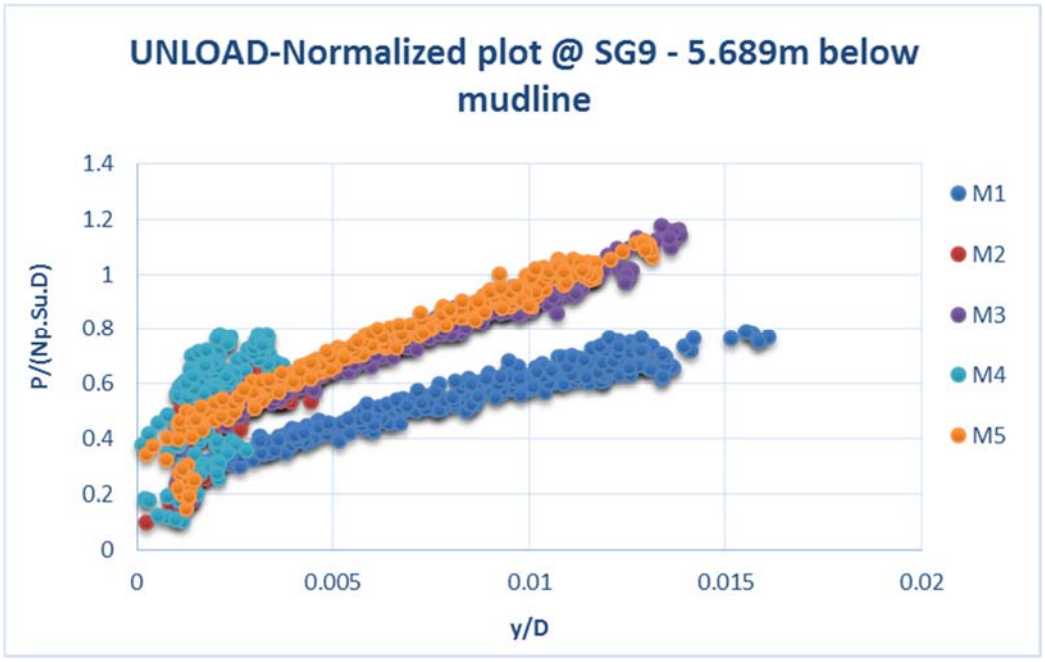

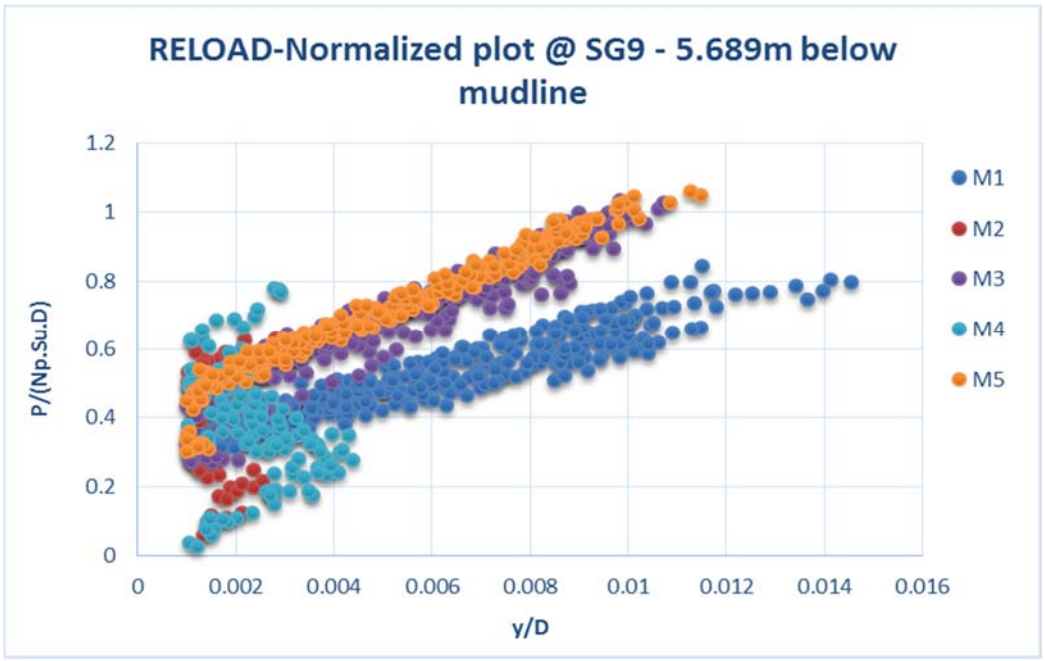

(c) Normalized Soil Resistance and Deflection Relationship at SG 9, for Motions M1, M2, M3, M4, and M5

Fig. 4.1: Continued.

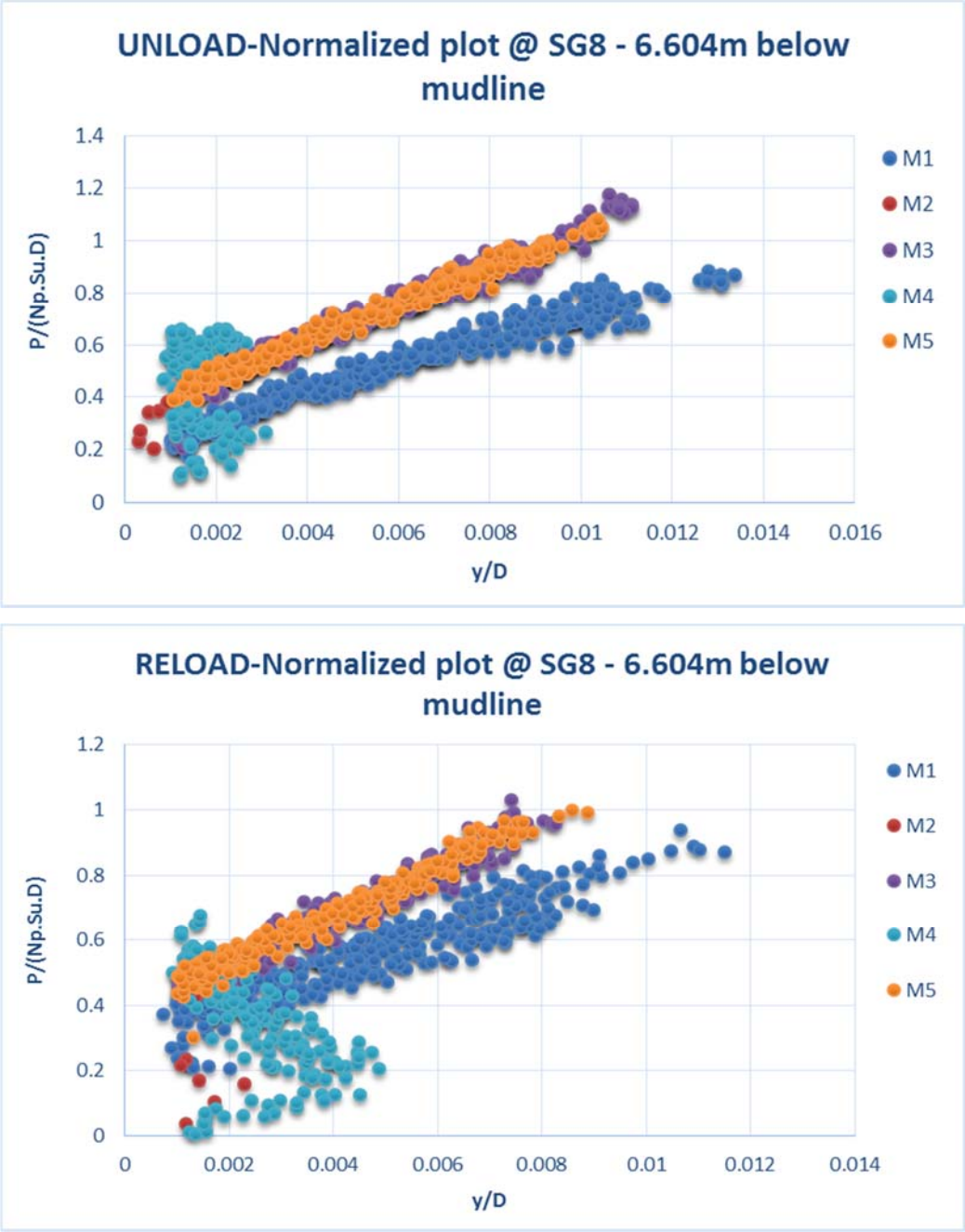

(d) Normalized Soil Resistance and Deflection Relationship at SG 8, for Motions M1, M2, M3, M4, and M5

Fig. 4.1: Continued.

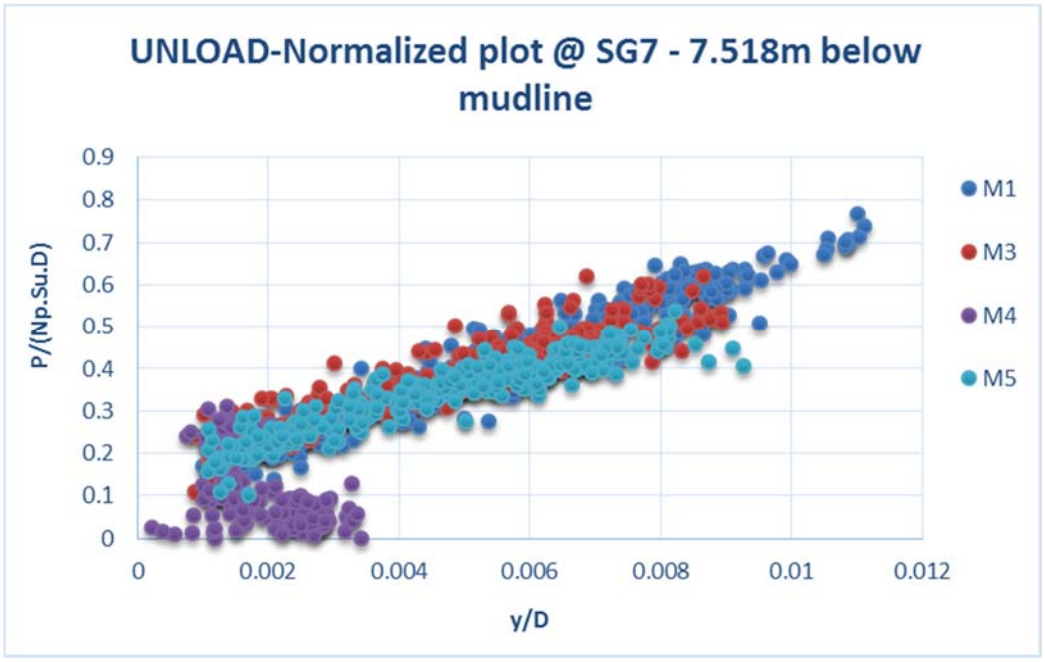

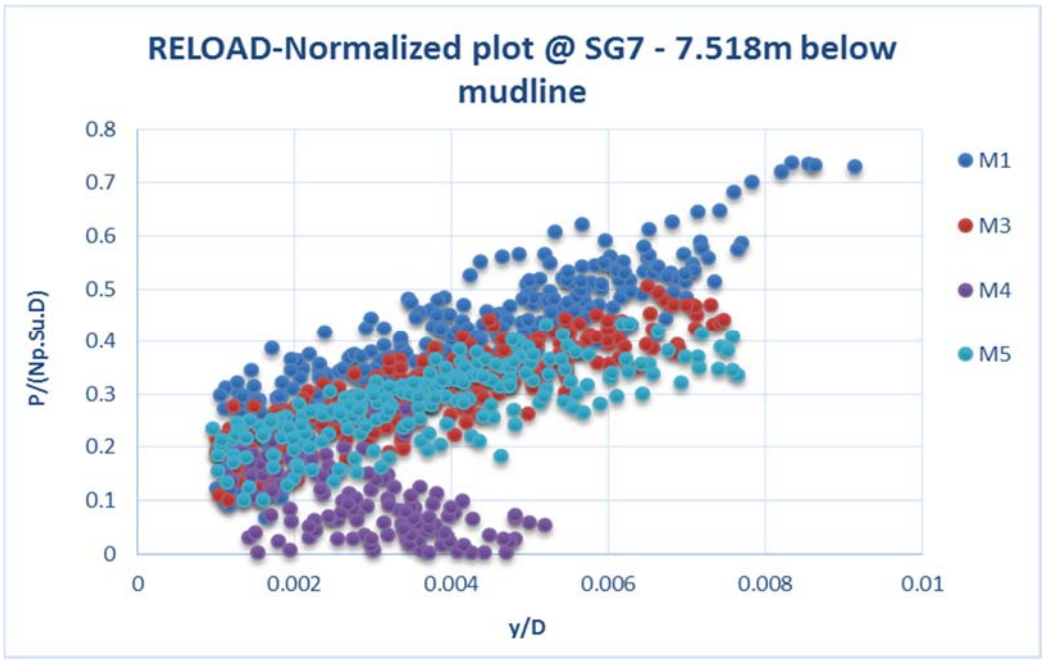

(e) Normalized Soil Resistance and Deflection Relationship at SG 7, for Motions M1, M2, M3, M4, and M5

Fig. 4.1: Continued.

4.1.1 Power Law Model

In applying the Power law model to the test data, curve fits to individual cycles (unload and reload loop) were initially carried out for motions M1 and M2; an example is shown in Fig. 4.2 and 4.3. Instead of having several parameters unique to each individual cycle, a preferable approach was considered where the interpreted P-y data from the steady state region were grouped together to obtain a best power law fit through the entire dataset from which the power law parameters (K_0 and n) were obtained for the various motions (M1 to M5) and strain gage locations along the depth of the pile. The normalized power law intercept, K_0 and exponent, n, as interpreted from the steady state cycles, and the damping ratio is presented in Table 3. The values presented in red in Table 3 indicate a poor fit to the data points. The detailed curve fits to the data from which the K_0 and n values were obtained are all shown in Appendix C, Figs. C-1 – C-24. The interpreted secant stiffness relationship based on the centrifuge test data, is presented in Fig. 4.4. A power law function was fit to the data points as the best fit curve. Upper and lower bounds were established by enveloping the data set with curves having the same n value (the straight-line slope on a log-log plot) with upper and lower bound K_0 values (the straight-line intercept on a log-log plot) bracketing the dataset. The interpreted equivalent damping ratio from the closed form solution presented in Eqn. 17, is shown in Fig. 4.5. The damping ratio is plot against the maximum displacement along the depth of the conductor, which is not dependent on the displacement level with values less than 0.12. The equivalent damping ratio trend obtained from motions M2 and M4 (symmetric motions with offsets), showed a distinct trend different from M1 – M5 (symmetric motions with zero offset).

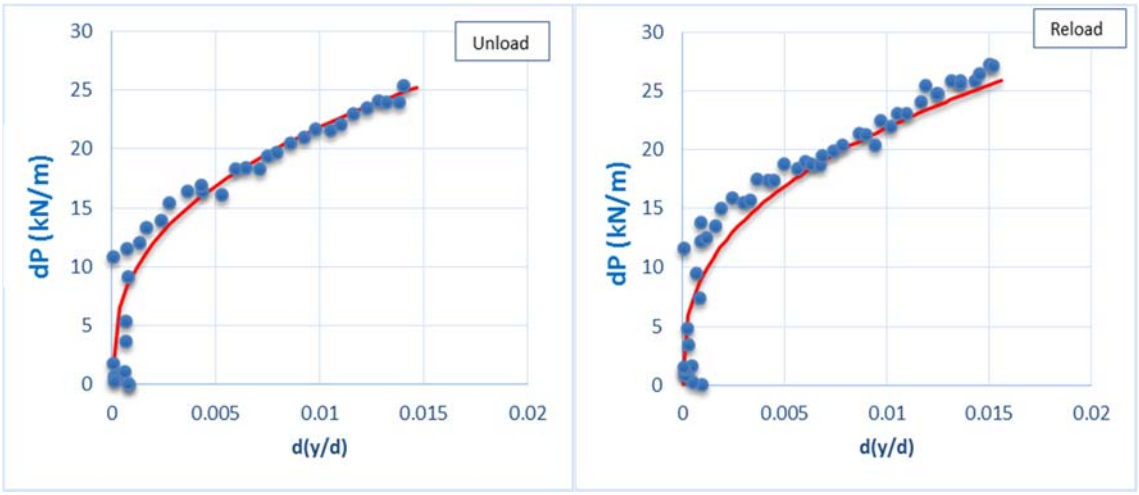

Fig. 4.2: The Power Law Fit to Unload and Reload Portion of Cycle 100, Motion M1.

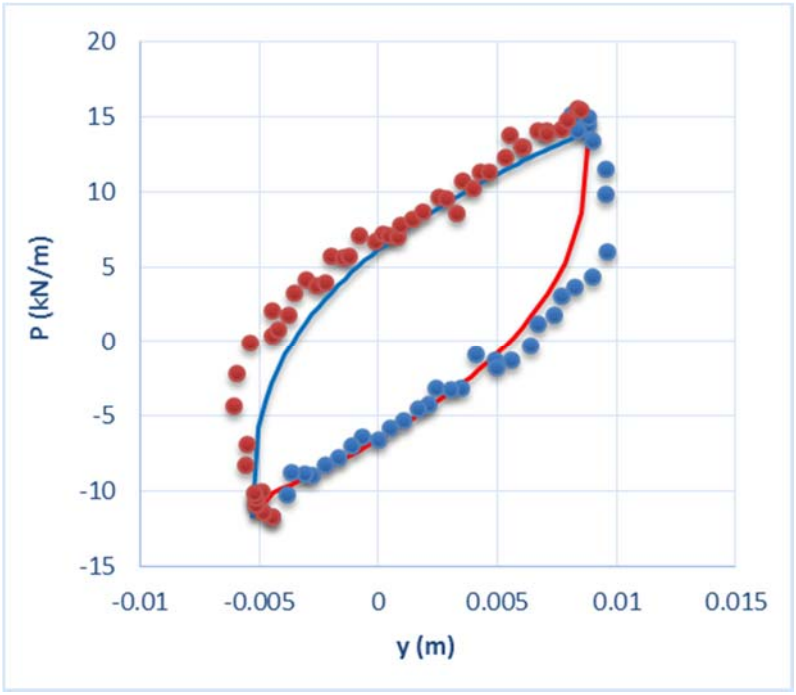

Fig. 4.3: The Power Law Fit to Motion M1, Cycle 100 P-Y Data.

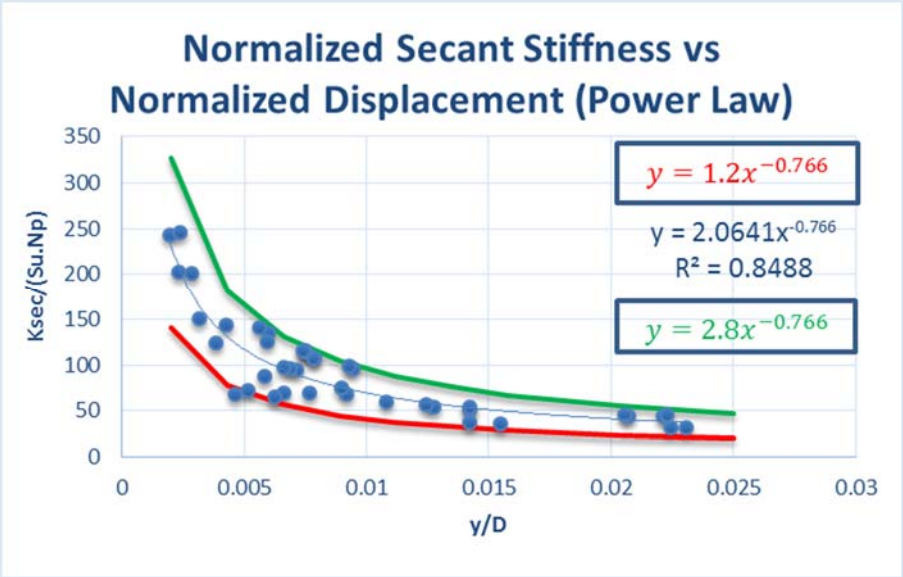

Fig. 4.4: Normalized Fits for Obtaining the Secant Stiffness Based on the Power Law Parameters, Showing the Lower Bound (in Red), Best Line Fit (in Blue), and the Upper Bound (in Green) for the Obtained Data Points.

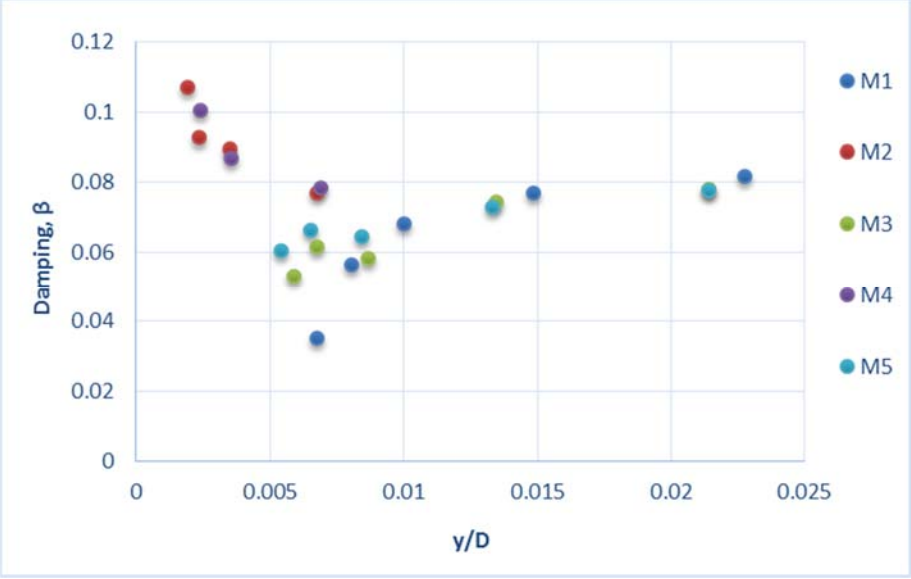

Fig. 4.5: The Equivalent Damping Ratio Variation Along the Conductor Depth, Interpreted from the Power Law Exponent for the Different Motions M1 – M5.

4.1.2 Ramberg-Osgood Model

The P-y curve fit parameters (y_{ref}, K_{max}, α and R) obtained from the Ramberg-Osgood fit to the centrifuge data are shown in Table 4. The values presented in red in Table 4 provided no fit to the data considered, and the damping ratios presented are at the maximum displacement level. The curve fits to the data from which the fit parameters were obtained from, are all shown in Appendix D, Figs. D-1 – D-24. From the normalized Ramberg-Osgood parameters, the interpreted secant stiffness relationship based on the centrifuge test data, is presented in Fig. 4.6. A power law function was fit to the data points as the best line curve, and in order to have a range of bounded values, the same lower and upper bound as with the power law model was used and provides reasonable bound to the data points. The closed form solution for damping presented in Eqn. 22 is dependent on the displacement level, so for all motions (M1 – M5), both low and high displacement levels are needed to be considered. Fig. 4.7 shows the variation of the damping ratio with varied displacement levels along the depth of the conductor.

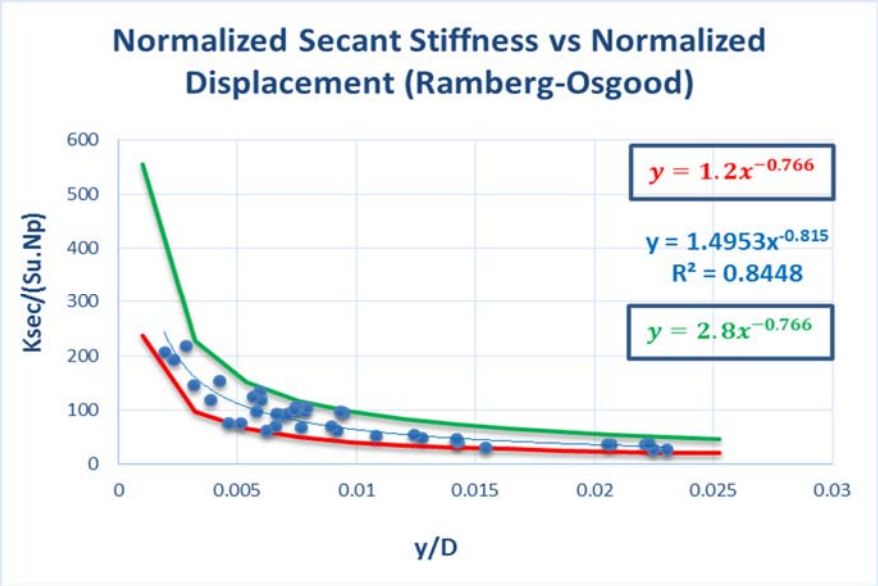

Fig. 4.6: Normalized Fits for Obtaining the Secant Stiffness Based on the Ramberg-Osgood Parameters, Showing the Lower Bound (in Red), Best Line Fit (in Blue), and the Upper Bound (in Green) for the Obtained Data Points.

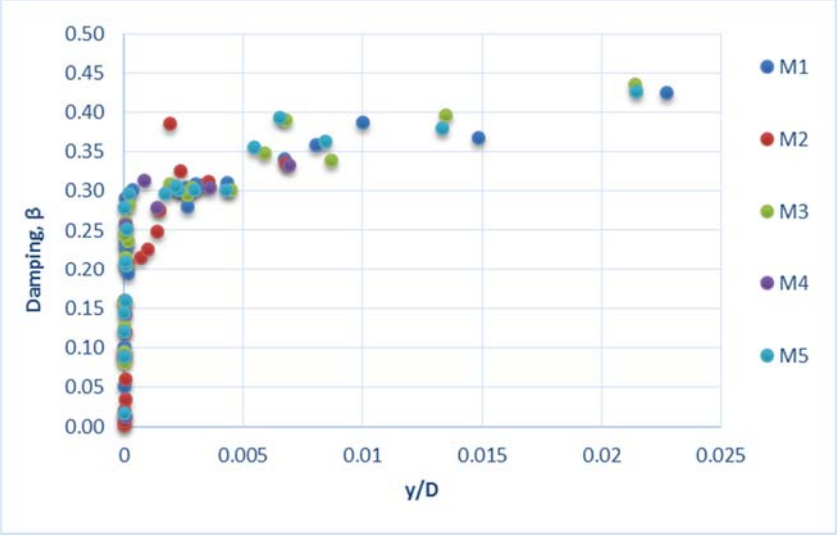

Fig. 4.7: The Equivalent Damping Ratio Variation Along the Conductor Depth, Interpreted from the Ramberg-Osgood Parameters, Dependent on the Deflection Level for Motions M1 – M5.

Table 3. Interpreted Power Law Parameters (Normalized K_0 and n) and Equivalent Damping Ratio.

Strain gage	Depth (m)		M1 K0/(Np.Su.D)	n	Damping (β)	M2 K0/(Np.Su.D)	n	Damping (β)	M3 K0/(Np.Su.D)	n	Damping (β)
SG 11	1.5744	UNLOAD	2.4646	0.3207		2.6751	0.2822		3.6503	0.3502	
		RELOAD	2.4196	0.3203	0.0819	5.1262	0.4139	0.0770	3.3212	0.3342	0.0780
SG 10	3.8544	UNLOAD	2.3879	0.3517		2.7072	0.3114		3.4991	0.3700	
		RELOAD	2.3058	0.3441	0.0770	1.9981	0.2492	0.0895	3.2711	0.3556	0.0744
SG 9	5.6880	UNLOAD	4.6834	0.4398		11.518	0.5264		9.2192	0.498	
		RELOAD	3.3663	0.3596	0.0683	0.4352	0.0411	0.0928	6.8566	0.4326	0.0581
SG 8	6.6048	UNLOAD	8.6195	0.5395		5.3804	0.3897		9.5505	0.4904	
		RELOAD	5.1636	0.4124	0.0565	4.8762	0.44	0.1072	6.041	0.3925	0.0617
SG 7	7.5168	UNLOAD	14.234	0.6763					5.7094	0.5029	
		RELOAD	11.035	0.5988	0.0352				5.1012	0.4991	0.0529

Strain gage	Depth (m)		M4 K0/(Np.Su.D)	n	Damping (β)	M5 K0/(Np.Su.D)	n	Damping (β)
SG 11	1.5744	UNLOAD	2.8123	0.2501		3.7619	0.3413	
		RELOAD	6.6949	0.4287	0.0785	3.5891	0.3467	0.0777
SG 10	3.8544	UNLOAD	5.5203	0.4034		3.6204	0.3661	
		RELOAD	1.7052	0.1851	0.0868	3.7029	0.3781	0.0728
SG 9	5.6880	UNLOAD	9.0888	0.4533		7.6218	0.4519	
		RELOAD	0.2012	-0.083	0.1003	5.9995	0.3972	0.0643
SG 8	6.6048	UNLOAD	0.1595	-0.146		7.6293	0.4469	
		RELOAD	0.0276	-0.386		5.6265	0.378	0.0662
SG 7	7.5168	UNLOAD	0.0033	-0.492		5.0299	0.4959	
		RELOAD	1.00E-04	-1.11		2.7565	0.4037	0.0604

Table 4. Interpreted Ramberg-Osgood Parameters (Normalized K_0 and n), and Equivalent Damping Corresponding to Maximum Displacement.

Strain gage		M1			M2			M3		
		Unload	Reload	Damping (β)	Unload	Reload	Damping (β)	Unload	Reload	Damping (β)
	a	0.2690	0.9990	0.4262	0.3070	0.9950	0.3368	0.8770	0.1530	0.4353
SG 11	yref	0.0003	0.0005		0.0008	0.0010		0.0010	0.0001	
	Kmax	14869.8885	2176.0891		4071.6612	1005.0251		1175.5163	46685.3408	
	α	9733.6193	113.5218		900.5317	14.3913		34.4330	32529.3313	
	R	2.9017	2.8053		2.9406	2.1376		2.8237	2.7597	
	a	0.6060	0.8350	0.3687	0.9680	0.9730	0.3127	0.6620	0.1670	0.3967
SG 10	yref	0.0008	0.0003		0.0009	0.0009		0.0010	0.0003	
	Kmax	2088.8165	4606.1723		1135.2284	1141.9436		1541.4021	23030.8614	
	α	366.7028	258.8899		28.7374	28.9252		94.8541	13409.4934	
	R	2.7165	2.1602		2.6959	3.0442		2.6487	2.6234	
	a	0.7630	0.8140	0.3873	0.9850	0.9870	0.2684	0.9580	0.8540	0.3387
SG 9	yref	0.0003	0.0005		0.0009	0.0004		0.0005	0.0004	
	Kmax	5242.4640	2670.6548		1080.0302	2814.3645		1933.0395	3345.6005	
	α	197.7925	94.0188		5.8103	3.9303		20.0613	38.8310	
	R	2.1713	2.4378		1.3915	-0.0576		1.8227	2.0290	
	a	0.8630	0.9400	0.3582	0.6330	0.3690	0.3003	0.3620	0.2440	0.3903
SG 8	yref	0.0007	0.0010		0.0010	0.0004		0.0002	0.0006	
	Kmax	1632.0402	1085.5406		1612.0192	7324.3976		17265.1934	6610.2591	
	α	31.7386	15.5226		32.2709	4.1346		427.7384	448.6995	
	R	1.8391	2.1091		2.4786	0.0320		1.9328	2.4013	
	a	0.6770	0.0100	0.3409				0.3410	0.8810	0.3481
SG 7	yref	0.0010	0.0000					0.0008	0.0009	
	Kmax	1507.2499	10000000.0000					3858.6202	1207.5253	
	α	29.8476	329879.0217					170.9922	23.1348	
	R	1.3833	1.2248					1.6550	1.4484	

Table 4. Continued.

Strain gage		M4			M5		
		Unload	Reload	Damping (β)	Unload	Reload	Damping (β)
	a	0.7890	0.9810	0.3331	0.4740	0.8920	0.4272
SG 11	yref	0.0005	0.0003		0.0006	0.0006	
	Kmax	2347.0873	3640.6000		3575.7706	1900.1292	
	α	52.8267	31.7108		277.8302	55.3549	
	R	3.3833	1.7841		2.8298	2.8301	
	a	0.02300	0.89200	0.3044	0.7240	0.4970	0.3865
SG 10	yref	0.00004	0.00004		0.0009	0.0002	
	Kmax	1086956.52174	28026.90583		1485.1779	10589.8549	
	α	100886.69448	433.94664		70.7760	696.1554	
	R	1.63186	2.88842		2.6967	2.3350	
	a	0.9120	0.3970	0.2320	0.5730	0.0780	0.3630
SG 9	yref	0.0004	0.0002		0.0009	0.0004	
	Kmax	2963.4898	13257.3247		1939.1119	33738.1916	
	α	6.7507	10.4526		33.1194	10065.6012	
	R	0.6580	-0.0468		2.0222	2.3237	
	a	0.3940	0.6470	0.1860	0.3130	0.7940	0.3940
SG 8	yref	0.0009	0.0008		0.0001	0.0005	
	Kmax	2729.1087	2060.7934		24576.0629	2737.9257	
	α	1.1678	2.1763		992.0503	36.2423	
	R	-0.1518	-0.1659		2.1746	2.5501	
	a	0.9640	0.8900	0.2073	0.1790	0.8390	0.3562
SG 7	yref	0.0001	0.0004		0.0004	0.0009	
	Kmax	17289.0733	2881.0141		14701.5584	1385.9246	
	α	23.7643	4.3060		1438.0487	25.7682	
	R	-0.0747	-0.1619		1.7288	1.3483	

4.2 Bending Moment Profile

The secant stiffness obtained from the Power law and Ramberg-Osgood parameters, was input into a finite difference MATLAB program, and used to compute the peak to peak bending moment profile for the conductor due to maximum peak to peak cyclic pile head displacement. During this exercise, it was observed that reducing the exponent made the computed moment profile closer to the measured profile at depth, and the intercept slightly controlled the magnitude of maximum bending moment. A modification to the upper bound was considered, and employed in the back analysis were the approximate intercept of 2.9, and slope of 0.667. Fig. 4.8 shows the modified curve of the upper bound falling within the lower and upper bound curves.

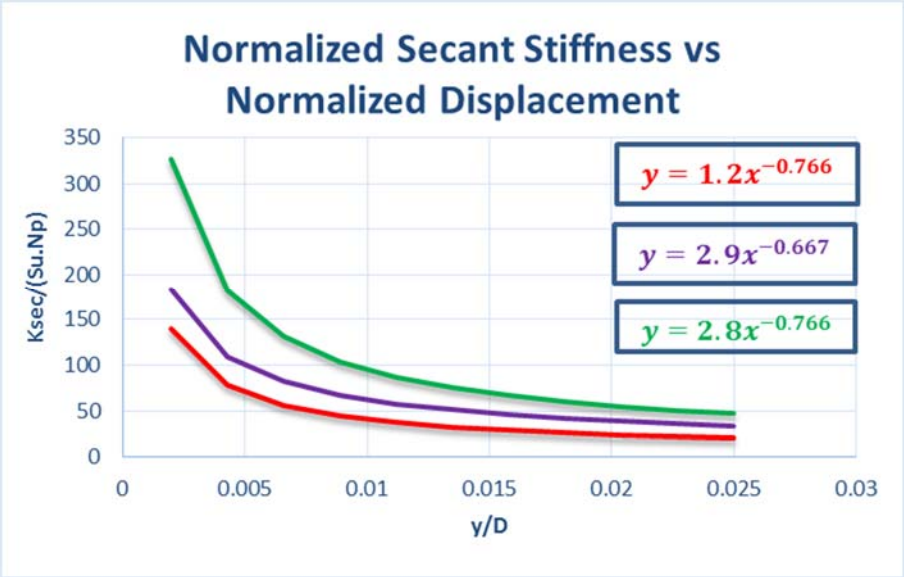

Fig. 4.8: Normalized Fits for Obtaining the Secant Stiffness Based on the Lower Bound (in Red), Modified Upper Bound Slope (in Purple), and the Upper Bound (in Green) for the Obtained Data Points.

The equation presented by Matlock (1970) for soft clay (Eqn. 24), can be simplified in a form comparable to the power law equation and further simplified to obtain an expression for the secant stiffness as presented in Eqn. 25.

$$P = 0.5 \left(\frac{y}{y_{50}}\right)^{1/3} Pult \qquad \text{Eqn. 24}$$

Noting that y_{50} = 2.5 ε_{50}D, where ε_{50} is strain level at 50% of the failure stress.

$$K_{sec} = 0.5 \left(\frac{1}{y_{50}}\right)^{1/3} y^{-\left(\frac{2}{3}\right)} Pult \qquad \text{Eqn. 25}$$

Strain levels at 50% of the failure stress are typically taken as ε_{50} = 0.02, 0.01, and 0.005 for soft, medium, and stiff clays, respectively.

The interesting observation is that the Matlock formulations for secant stiffness in Eqn. 25, after substituting the value for y_{50} for soft clay and medium clay, the intercept is approximately 1.398, and 1.762 respectively; slope 0.667. This is the same slope used in the modified upper bound equation but with the Matlock values having a lesser intercept.

Figs. 4.9 – 4.13 shows the comparison between the measured bending moment profile, and the computed bending moment profile along the conductor for the soil, conductor, and loading conditions imposed during the centrifuge test, M1 – M5 respectively for cycle N=100. The bending moment profiles for motions M1 – M5, for cycles 200, 300, 400, and 500, are shown in Figs. E.1 – E.19 in Appendix E.

The comparisons show reasonable agreement between calculated and measured maximum bending moments. In addition, the overall shape of the computed bending moment profile from the Power law and Ramberg-Osgood model agrees with the measured bending moment.

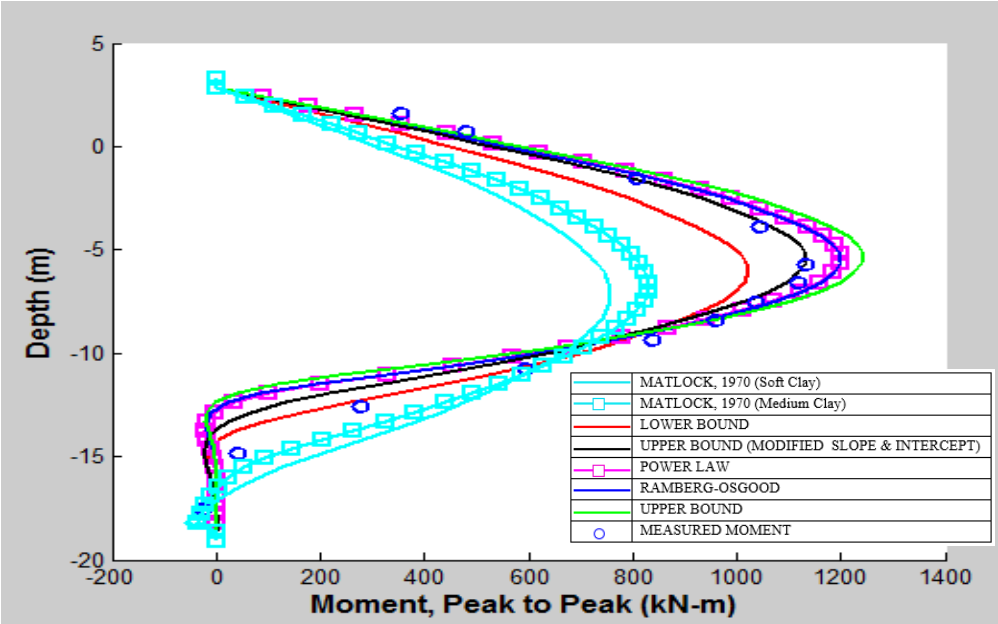

Fig. 4.9: Calculated Versus Measured Bending Moment Profiles from Centrifuge Test 4, M1 Load - Cycle 100 with Zero Offset.

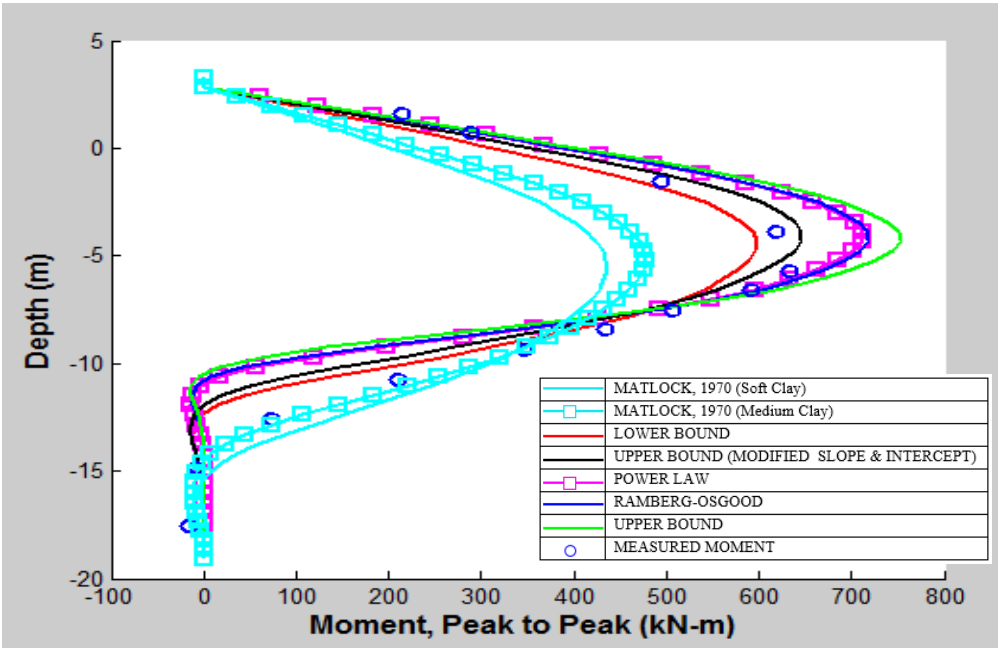

Fig. 4.10: Calculated Versus Measured Bending Moment Profiles from Centrifuge Test 4, M2 Load - Cycle 100 with 0.05 Offset.

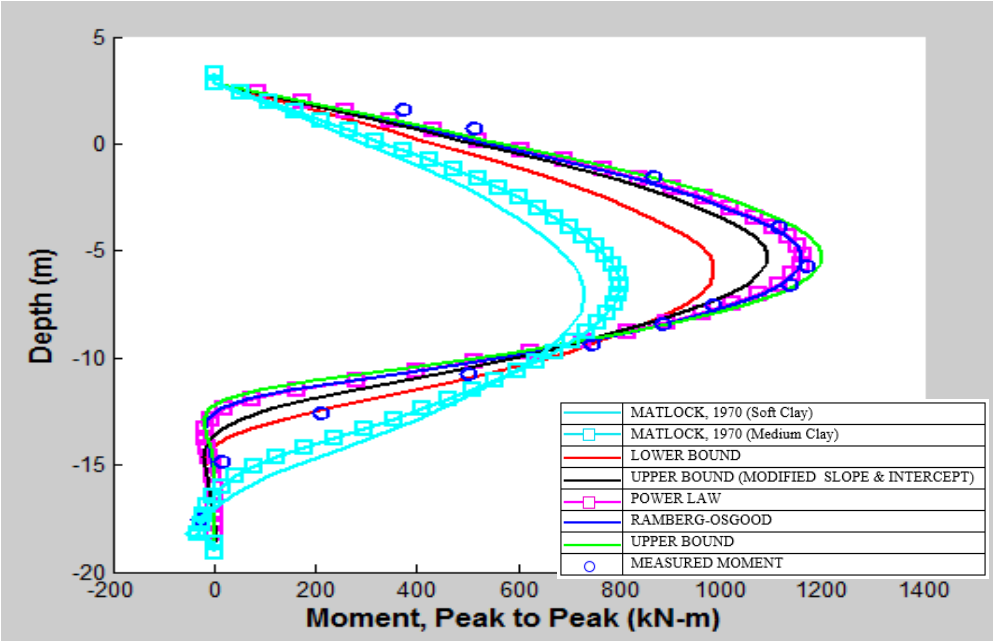

Fig. 4.11: Calculated Versus Measured Bending Moment Profiles from Centrifuge Test 4, M3 Load - Cycle 100 with Zero Offset.

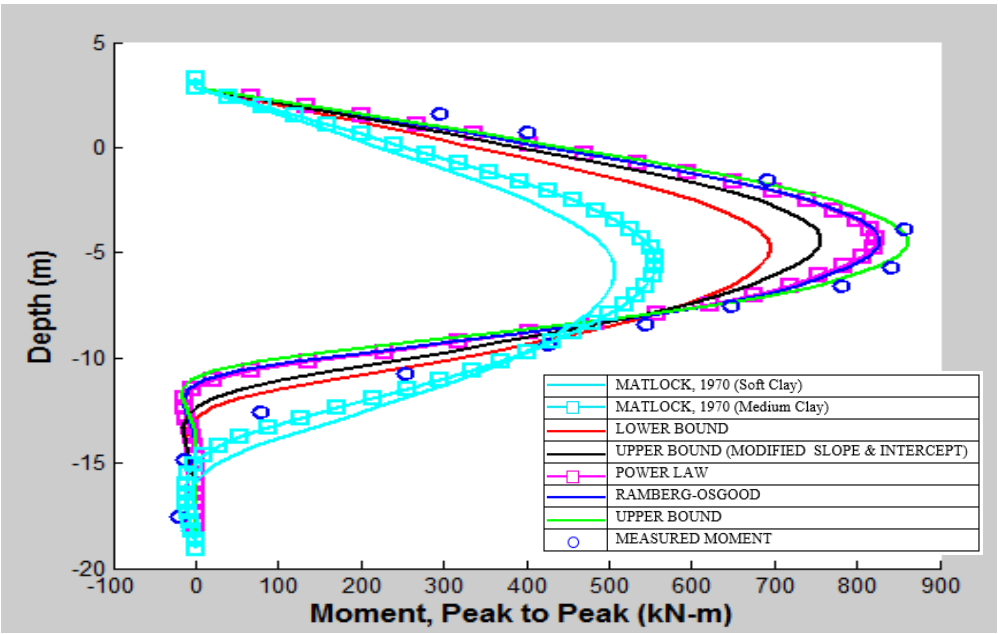

Fig. 4.12: Calculated Versus Measured Bending Moment Profiles from Centrifuge Test 4, M4 Load - Cycle 100 with 0.05 Offset.

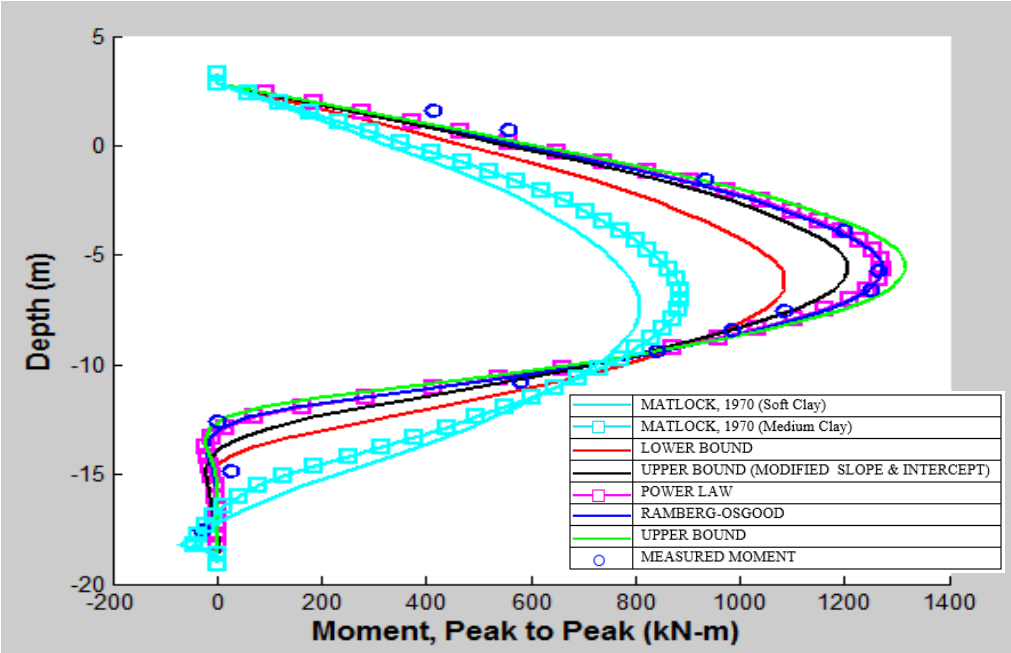

Fig. 4.13: Calculated Versus Measured Bending Moment Profiles from Centrifuge Test 4, M5 Load - Cycle 100 with Zero Offset.

4.3 Result Interpretation

4.3.1 M1 Motion

The moment profiles from the M1 motion applied at the conductor head, suggest that the moment profile from Matlock (1970) recommendation has the softest springs when compared to the measured moment from the centrifuge test. The maximum moment compared to the measured varied within -30% to -35%. That for the power law and Ramberg-Osgood varied within 4% and 10%, the modified upper bound was within ±1% and ±2%. The bounding limits (lower and upper) were within ±8% to ±12%.

4.3.2 M2 Motion

The moment profiles from the M2 motion applied at the conductor head, suggest that the moment profile from Matlock (1970) recommendation has the softest springs when compared to the measured moment from the centrifuge test. The maximum moment compared to the measured varied within -24% to -42%. That for the power law and Ramberg-Osgood was within 2% to 20%, the modified upper bound was within ±3% to ±10%. The bounding limits (lower and upper) were within ±8% to ±12%.

4.3.3 M3 Motion

The moment profiles from the M3 motion applied at the conductor head, suggest that the moment profile from Matlock (1970) recommendation has the softest springs when compared to the measured moment from the centrifuge test. The maximum moment compared to the measured varied within -35% to -42%. That for the power law and Ramberg-Osgood was within -2% to -6%, the modified upper bound was within -3% to -15%. The bounding limits (lower and upper) were within ±1% to ±20%.

4.3.4 M4 Motion

The moment profiles from the M4 motion applied at the conductor head, suggest that the moment profile from Matlock (1970) recommendation has the softest springs when compared to the measured moment from the centrifuge test. The maximum moment compared to the measured was within -40% to -45%. That for the power law and Ramberg-Osgood was within -3% to -10%, the modified upper bound was within -12% to -16%. The bounding limits (lower and upper) were within -1% to -24%.

4.3.5 M5 Motion

The moment profiles from the M5 motion applied at the conductor head, suggest that the moment profile from Matlock (1970) recommendation has the softest springs when compared to the measured moment from the centrifuge test. The maximum moment compared to the measured was within -45% to -47%. That for the power law and Ramberg-Osgood was within -4% and -10%, the modified upper bound was within -10% to -13%. The bounding limits (lower and upper) were within -1% to -27%.

CHAPTER V

SUMMARY AND CONCLUSIONS

5.1 Summary

A less complicated and less time consuming way of modelling soil-structure interaction problems concerning conductors is achieved by assuming that non-linear soil springs are attached to the conductors (Equivalent spring approach). In addition to the soil springs, dashpots could also be attached to the conductors when inertial effects need to be considered. To obtain the stiffness of the soils springs and the damping coefficient for the dashpot, P-y relations are usually used. In this study, the soil resistances have been obtained by carrying out double differentiation of the bending moment data, and the deflection by double integration of the conductor curvature (M/EI). To get the required parameters needed for modelling, the P-y data were fit to two models (Power law and Ramberg-Osgood). The results of the fits were best for the zero offset motion, the non-zero offset motions fits were not good all the time. This suggests that deeper understanding of the non-zero offset motions is needed. Analytical expressions for the secant stiffness and the equivalent damping ratio were derived for both models, from which secant stiffness and damping ratios were computed. The secant stiffness was used in back-calculating the moments, using displacement boundary condition. The obtained results showed some consistent trends, however, a few departures from the observed trend occurred; reasons for the departure is not clear at the moment.

5.1.1 Power Law

The power law model was fit to the P-y data using the data reduction process described in section 4.1 to obtain the power law parameters K_0 and n. For the purpose of comparison, the Matlock equation relating the soil resistance and deflection was reduced

to a form similar to the equations used in this study. The derived secant stiffnesses were input into a finite difference MATLAB program to back-calculate bending moment profiles. The computed bending moments were then compared to the measured bending moment. Generally, the obtained results suggests that the Matlock's equation underestimated the maximum bending moment, while the power law equations derived from the centrifuge tests calculated maximum bending moments that were much closer to the measured values. The equivalent damping ratio obtained were not displacement level dependent and were less than 0.12.

5.1.2 Ramberg-Osgood

The Ramberg-Osgood model was also fit to the P-y data to obtain the desired fit parameters, as described in section 4.1. The data reduction process revealed that the curve fits were not sensitive to the values of y_{ref} and K_{max} individually; i.e., multiple combinations of y_{ref} and K_{max} produced similar quality curve fits. The secant stiffness obtained from the Ramberg-Osgood equation was also input into the finite difference MATLAB program to back-calculate the bending moment. The results obtained were very similar to that of the Power law model. The equivalent damping ratio obtained were displacement level dependent and shown mostly higher values than that obtained from the power law.

The lower and upper bound equation of the secant stiffness were presented to provide a bound to the measured data, because the equation could take any intercept and slope different from that obtained from the power law and Ramberg-Osgood and still give a meaningful result. The modified upper bound equation lay between the lower and upper limits and was able to match better the maximum bending moment as well as the entire moment profile. This equation had approximately the same slope as that using the Matlock's equation but a higher intercept, and from the presented results was a better match to the measured moment profile.

The significance of the departure of the centrifuge test data from the Matlock equations should not be overstated. The Matlock equations were designed for monotonic loading and were not necessarily intended for the small displacement loading of interest in the current study.

5.2 Conclusions

The conclusions from this study include the following:

1. For the relatively small pile head displacements under consideration in this study, about 0.01 to 0.02 pile diameters - reasonable P-y curves could be extracted from the bending moment measurements down to a depth of about 6-8 diameters below the mudline. Below this depth, the overall displacement levels were too small to produce reliable interpretations.
2. Under uniform cyclic displacement loading at the pile head, a steady state condition develops after about 50 load cycles; data analysis was carried out at 100 load cycles and above, to ensure that only the steady state was considered.
3. The unload and reload segment of the P-y loops under cyclic loading has been be characterized in terms of:

   A Power law relationship (Eqn. 15); results shown in Appendix C, Figs. C-1 – C-24, which illustrates the general quality of the curve fits. The power law relationship involves two parameters: a coefficient K_0 controlling soil stiffness and an exponent n controlling the degree of nonlinearity.

   A Ramberg-Osgood relationship (Eqn. 20); results shown in Appendix D, Figs. D-1 – D-24, which illustrates the general quality of the curve fits. The Ramberg-Osgood relationship involves four parameters: y_{ref}, K_{max}, α, and R.
4. To facilitate extrapolating the results of centrifuge test programs such as this to other soil and site conditions, the coefficient K_0 has be normalized by P_{ult}, the

ultimate line load per unit depth acting on the pile. In this investigation P_{ult} was computed by multiplying the soil undrained shear strength s_u by the dimensionless bearing factor Np proposed by Jeanjean, (2009).

5. The secant stiffness obtained from the Power law and the Ramberg-Osgood were bounded by the same limits, even though they had different intercepts and slopes, they presented similar results when used to back calculate the bending moment. However, the information retrieved for the damping were very different, the reason for this is not known, but it would be conservative to use the small damping ratios, since the displacements considered were small the absorbed energy is also expected to be small. Using less damping will actually be more conservative, than using a higher value than what can be relied upon.

5.3 Recommendations for Future Research

Recommendations for future study include the following:

1. Include larger cyclic displacement magnitudes at the pile head to: (1) permit better quality P-y measurements at depths beyond 5 diameters, and (2) verify the validity of the relationships and parameters derived from this study for greater displacement magnitudes.
2. Perform at least one monotonic load to failure in pristine soil to provide an unambiguous measure of P_{ult}, which is important for developing reliable normalized model parameters.
3. Perform numerical studies to establish the validity and limitations of the simplified P-y secant stiffness approach considered in this study. The equivalent linear model developed in this study can be readily modified to accommodate a true nonlinear analysis, where the actual P-y path can be tracked.
4. Perform supplemental single-element laboratory test-bed soils, such as cyclic direct simple shear tests. Such tests can be useful in interpreting softening phenomena in the centrifuge tests and can provide a useful guide in extrapolating

the centrifuge test results to other soils having different strength, shear modulus, and sensitivity characteristics.

5. Further study is required to gain better understanding of the non-zero offset motions, also needed is understanding fully how series of past cyclic motions affect present cyclic motions.

REFERENCES

Aubeny, C. P., "Development of Soil-Spring Model for Conductor Fatigue Evaluation", unpublished manuscript, Texas A&M University, December, 2012.

API Recommended Practice 2A- WSD, "Recommended Practice for Planning, Designing and Constructing Fixed Offshore Platforms – Working Stresses Design," Reaffirmed October, 2010.

Broms, B. B. "Lateral Resistance of Piles in Cohesive Soils," Journal of the Soil Mechanics and Foundations Division, ASCE, Vol. 90, No. SM2, Proceeding Paper 3825, 1964: pp. 27-63.

Idriss, I. M., Dobry, R.,Doyle E.H., and Singh, R. D. "Behavior of Soft Clays Under Earthquake." In Offshore Technology Conference, Houston, Texas, 1976: OTC-2671-MS.

Hamilton, J, M. and Murff, J. D. "Ultimate Lateral Capacity of Piles in Clay." In Offshore Technology Conference. Houston, Texas, 1995.

Jeanjean, Philippe. "Re-Assessment of P-Y Curves for Soft Clays from Centrifuge Testing and Finite Element Modeling." In Offshore Technology Conference. Houston, Texas, 2009.

Matlock, Hudson. "Correlation for Design of Laterally Loaded Piles in Soft Clay." In Offshore Technology Conference. Houston, Texas, 1970.

McClelland, Bramlette and John A. Focht, Jr. "Soil Modulus of Laterally Loaded Piles," Transactions, ASCE, Vol. 123, New York, 1958: pp. 1049-1063.

Murff, J., and J. Hamilton. “P-Ultimate for Undrained Analysis of Laterally Loaded Piles.” Journal of Geotechnical Engineering 119, No. 1, 1993: 91-107.

Pilisi, Nicolas, and David Bradley Lewis. “Hydrodynamic Loads, Soil and Structure Interaction in Conductor Design for Offshore Platforms and Jack-up Rigs.” In IADC/SPE Drilling Conference and Exhibition. San Diego, California, USA: IADC/SPE Drilling Conference and Exhibition, 2012.

Prevost, Jean H., and Robert H. Scanlan. “Dynamic Soil-Structure Interaction: Centrifugal Modeling.” International Journal of Soil Dynamics and Earthquake Engineering, Vol. 2, No. 4, 1983: 212-21.

Randolph, M. J., Houlsby, G. T. “Limiting Pressure on a Circular Pile Loaded Laterally in Cohesive Soil” Geotechnique Vol.34, No. 4, Dec 1984, P613–623.

Reese, L.C., Cox, W.R. and Koop, F.D. “Field Testing and Analysis of Laterally Loaded Piles in Stiff Clay”. Seventh Annual Offshore Technology Conference, Dallas, Texas, 1975: 671-690.

Rollins, Kyle M., and Travis M. Gerber. “Cyclic P-Y Curves for a Pile in Cohesive Soil.” In Geotechnical Earthquake Engineering and Soil Dynamics IV, 2008: 1-10.

Skelton, R. P., Maier, H.J., Christ, H. J. “The Bauschinger effect, Masing model and the Ramberg-Osgood relation for cyclic deformation in metals.” In Materials Science and Engineering A238, 1997: 377-390.

Steve Everley, “60 Percent of Statistics are Made Up”. Retrieved from http://energyindepth.org/national/60-percent-of-statistics-are-made-up/, February, 2013.

Stevens, J. B., and Audibert, J.M.E. “Re-Examination of P-Y Curve Formulations.” In Offshore Technology Conference. Houston, Texas, 1979.

Templeton, John S. “Finite Element Analysis of Conductor/Seafloor Interaction.” In Offshore Technology Conference. Houston, Texas, 2009.

The Encyclopedia of Earth, “A Brief History of Offshore Oil Drilling”. Retrieved from http://www.eoearth.org/article/A_Brief_History_of_Offshore_Oil_Drilling?topic=64403 , February, 2013.

Ting, J. “Full-Scale Cyclic Dynamic Lateral Pile Responses.” Journal of Geotechnical Engineering, Vol.13, No. 1, 1987: 30-45.

Whiteside, W. D. III. “The behavior of laterally loaded single pile: A survey of current methodology.” M.S. thesis, University of California, Berkeley California, 1995.

Yang, Ke and Liang, Robert. “Methods for Deriving P-y Curves from Instrumented Lateral Load Tests” Geotechnical Testing Journal, Vol. 30, No. 1, 2006.

APPENDIX A

Numerical Differentiation of Strain Gage Curvature Measurements

The procedure locally fits a second order polynomial about any point of interest. The polynomial has the form:

$$M = c_1 z^2 + c_2 z + c_3 \qquad \text{(Eqn. A.1)}$$

where M = bending moment in pile

z = depth

c_i = polynomial curve fit coefficients

The polynomial curve fit coefficients c_i can be formed into a matrix C:

$$C = \begin{bmatrix} c_1 \\ c_2 \\ c_3 \end{bmatrix} \qquad \text{(Eqn. A.2)}$$

The basic steps in finding c_i are as follows:

a. Select 5 data points surrounding the point of interest.

b. Construct an array *Z* comprising the polynomial terms of depth z_i of the strain gages.

$$Z = \begin{bmatrix} z_1^2 & z_1 & 1 \\ z_2^2 & z_2 & 1 \\ z_3^2 & z_3 & 1 \\ z_4^2 & z_4 & 1 \\ z_5^2 & z_5 & 1 \end{bmatrix} \qquad \text{(Eqn. A.3)}$$

c. Construct an array *M* containing the measured bending moments M

$$M = \begin{bmatrix} m_1 \\ m_2 \\ m_3 \\ m_4 \\ m_5 \end{bmatrix}$$ (Eqn. A.4)

d. Construct the 3-by-3 matrix equation below:

$Z^T M = Z^T Z C$ (Eqn. A.5)

e. Solve Eqn. A.5 for unknown C

f. The local polynomial curve fit for moment is now defined by Eqn. A.1.

g. The line load Q (soil resisting force per unit depth) acting on the pile is the second derivative of bending moment, or the first derivative of the shear force:

$Q = 2 c_1 = dV/dx$ (Eqn. A.6)

h. The average pressure P acting on the pile is obtained by dividing the line load Q by pile diameter D:

$P = Q / D$ (Eqn. A.7)

APPENDIX B

Analysis of Laterally Loaded Pile

The analysis solves the fourth order differential equation:

$$EI\frac{d^4y}{dz^4}+k_{sec}y=0 \qquad \text{(Eqn. B.1)}$$

where E = elastic modulus of pile

I = moment of inertia of pile

y = lateral displacement of pile

z = depth

k_{sec} = secant stiffness of soil spring

This equation is subject to the following boundary constraints for a pile of length L:

Imposed displacement δ at pile head: $y(0) = \delta$ (Eqn. B.2)

Zero moment at pile head: $y''(0)=0$ (Eqn. B.3)

Zero moment at pile tip: $y''(L)=0$ (Eqn. B.4)

Zero displacement at pile tip: $y(L) = 0$ (Eqn. B.5)

Eqn. B.1 is solved with finite difference methods by discretizing the pile into n segments of length $\Delta z = L/n$, which will generate n+1 equations. Equations 3 through n-2 have the form:

Equation i: $y_{i-2} - 4\, y_{i-1} + (6 + k_{sec}\, \Delta z^4/ EI)\, y_i - 4\, y_{i+1} + y_{i+2} = 0$ (Eqn. B.6)

The four boundary constraints are provided through the following additional equations:

$y_1 = \delta$ (Eqn. B.7)

$y_1 - 2y_2 + y_3 = 0$ (Eqn. B.8)

$y_{n-2} - 2y_{n-1} + y_n = 0$ (Eqn. B.9)

$y_n = 0$ (Eqn. B.10)

If one chooses to impose a force F rather than displacement a displacement at the pile head, Eqn. B.7 may be replaced with the following 3rd order finite difference equation:

$-y_1 + 3y_2 - 3y_3 + y_4 = F\, \Delta z^3/ EI$ (Eqn. B.11)

Eqns. B.6 through B.10 (or B.8 through B.11) comprise a non-singular matrix equation that can be solved directly through Gauss elimination.

Finally, bending moments at any location along the pile can be computed from:

$$M_i = EI\,(y_{i-1} - 2y_i + y_{i+1}) \qquad \text{(Eqn. B.12)}$$

Eqn. B.6 is nonlinear due to the dependence of the secant stiffness k_{sec} on displacement. The solution algorithm proceeds iteratively according to the following sequence:

1. Estimate a displacement distribution for iteration j, $y_j(z)$. For the first estimate, assume displacement varies linearly from $y = \delta$ at the pile head to $y=0$ at the tip.
2. Compute secant stiffness along the depth of the pile using Eqn. 2.
3. Construct the system of equations defined by Eqns. B.7 - B.10.
4. Solve for displacement for iteration j+1, $y_{j+1}(z)$.
5. Compute the maximum difference between bending moments in iterations j and j+1. If the difference is within tolerance, the solution has converged. If not, repeat Steps 1-5 with the updated displacement distribution $y_{j+1}(z)$. A tolerance of 0.1% was used in this study.

It is noted that the pile head displacements (or forces) used in the back analysis are not absolute displacements, rather, they are the amplitude of the cyclic component of loading. In the analysis of a given load cycle from the centrifuge tests, the cyclic component of displacement at the pile head was taken as:

$$\delta = (y_{max} - y_{min}) \qquad \text{(Eqn. B.13)}$$

Where, y_{max} and y_{min} are the maximum and minimum measured displacements at the pile head. Similarly, the moments in Eqn. B.12 denote the cyclic component of moments occurring in the pile. The computed cyclic moments should be compared to measured cyclic moments, which were computed from measured moments as follows:

$$M_{cyc} = (M_{max} - M_{min}) \qquad \text{(Eqn. B.14)}$$

APPENDIX C

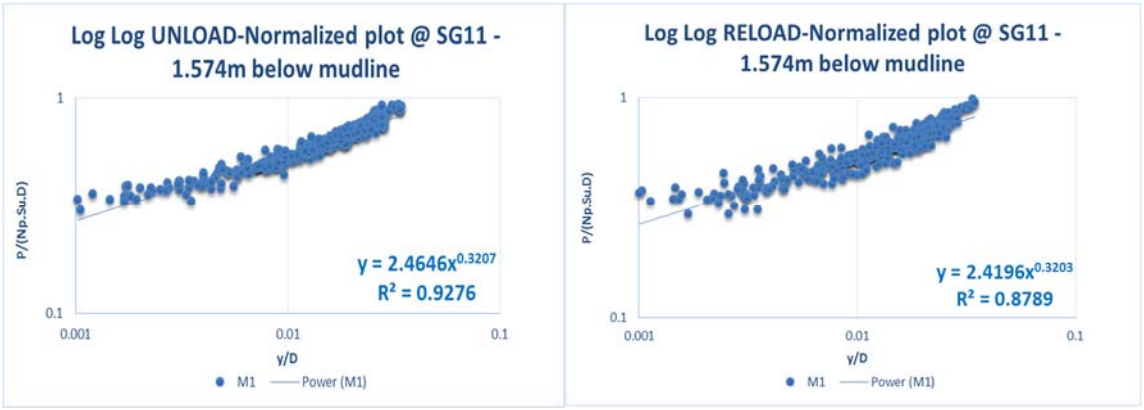

Fig. C-1: Power Law Fit To the Steady State Region of the Unload and Reload Loop of SG 11, for Motion M1

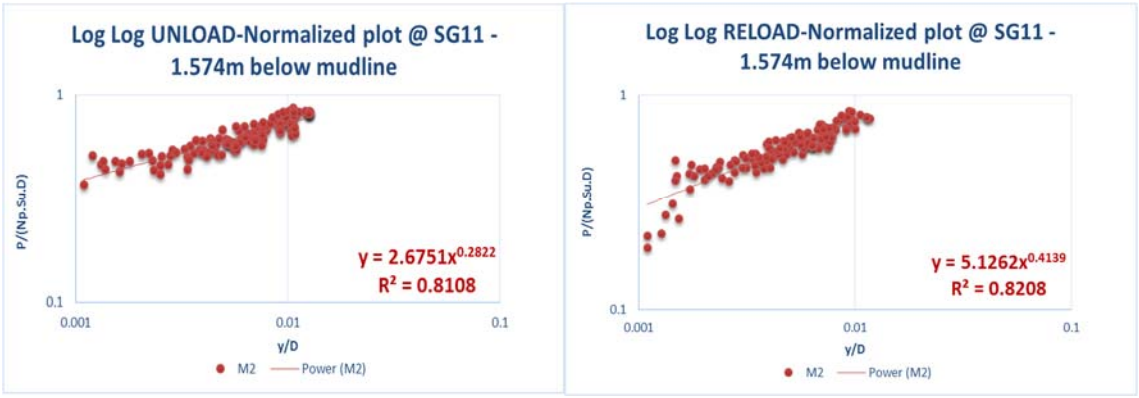

Fig. C-2: Power Law Fit To the Steady State Region of the Unload and Reload Loop of SG 11, for Motion M2

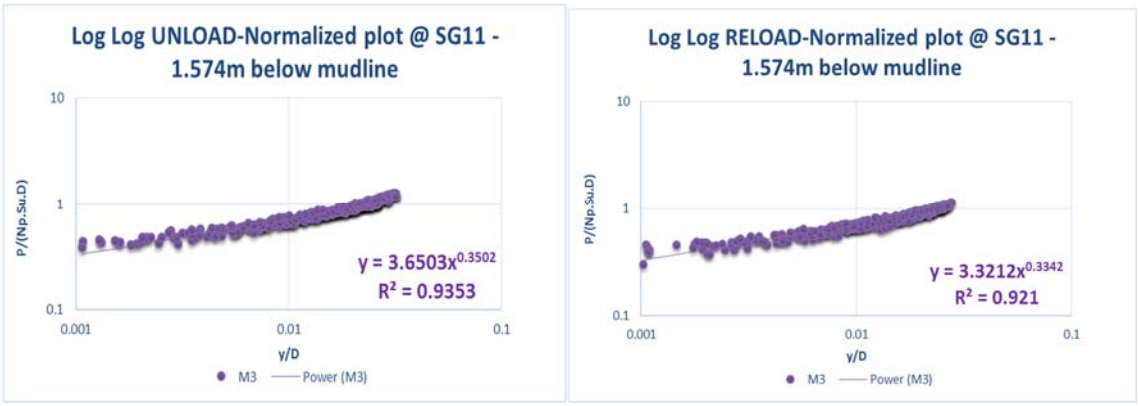

Fig. C-3: Power Law Fit To the Steady State Region of the Unload and Reload Loop of SG 11, for Motion M3

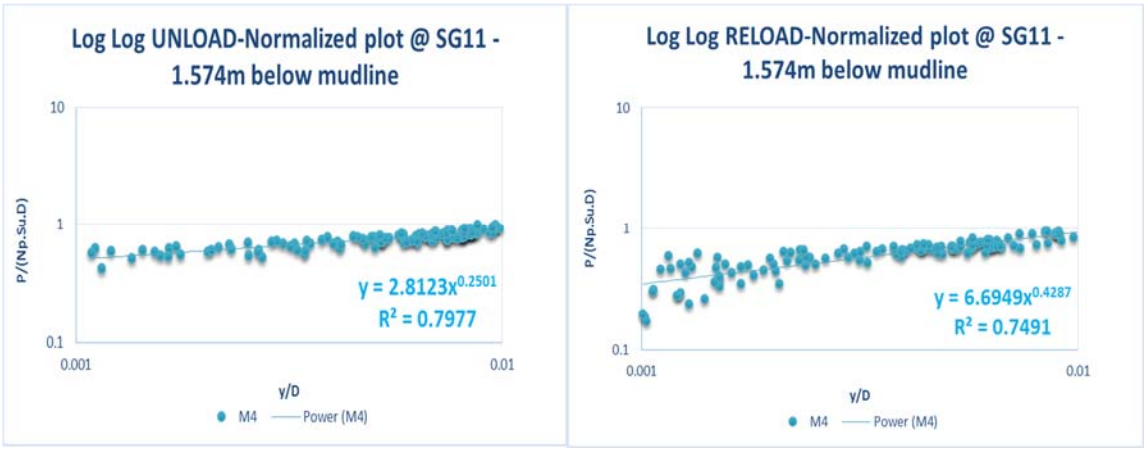

Fig. C-4: Power Law Fit To the Steady State Region of the Unload and Reload Loop of SG 11, for Motion M4

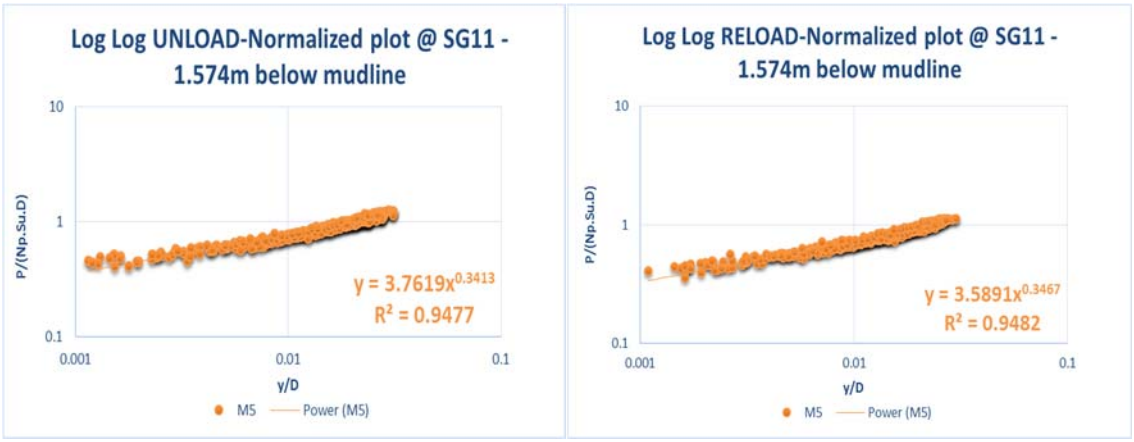

Fig. C-5: Power Law Fit To the Steady State Region of the Unload and Reload Loop of SG 11, for Motion M5

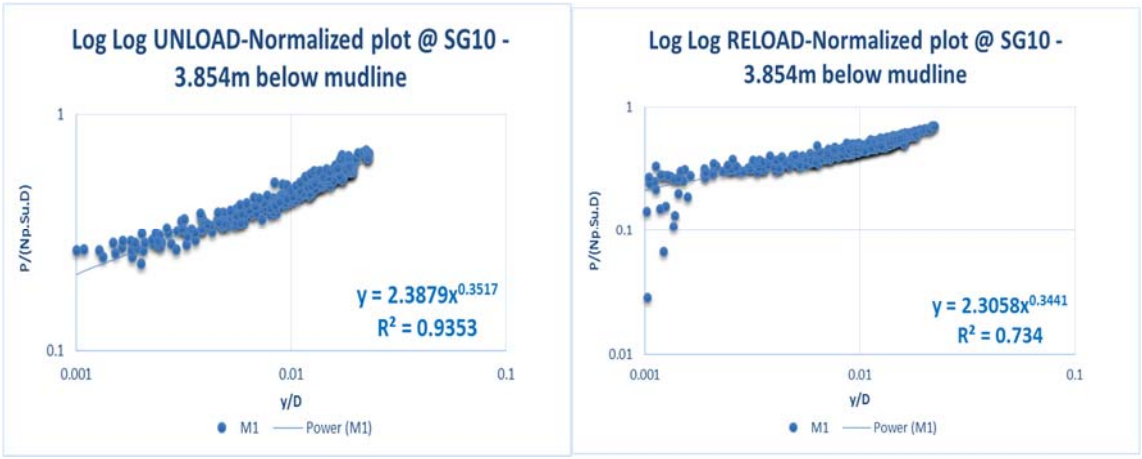

Fig. C-6: Power Law Fit To the Steady State Region of the Unload and Reload Loop of SG 10, for Motion M1

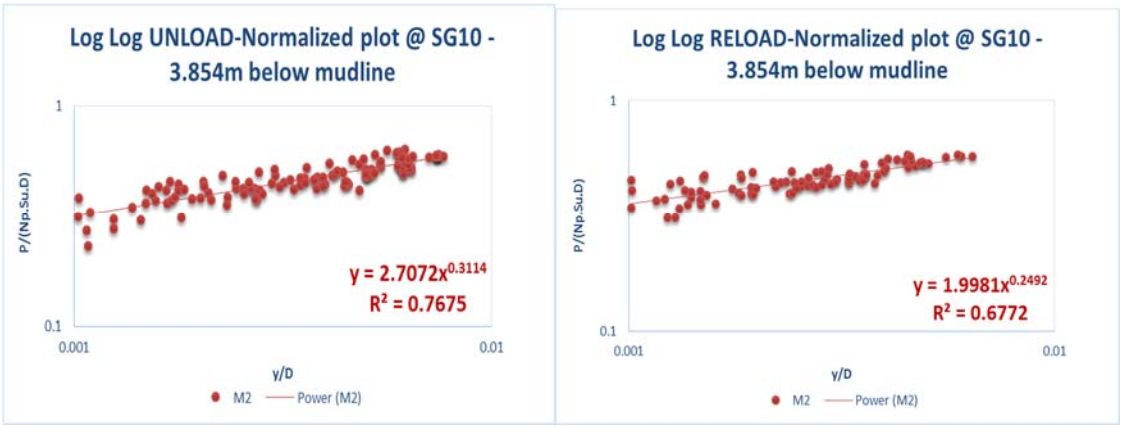

Fig. C-7: Power Law Fit To the Steady State Region of the Unload and Reload Loop of SG 10, for Motion M2

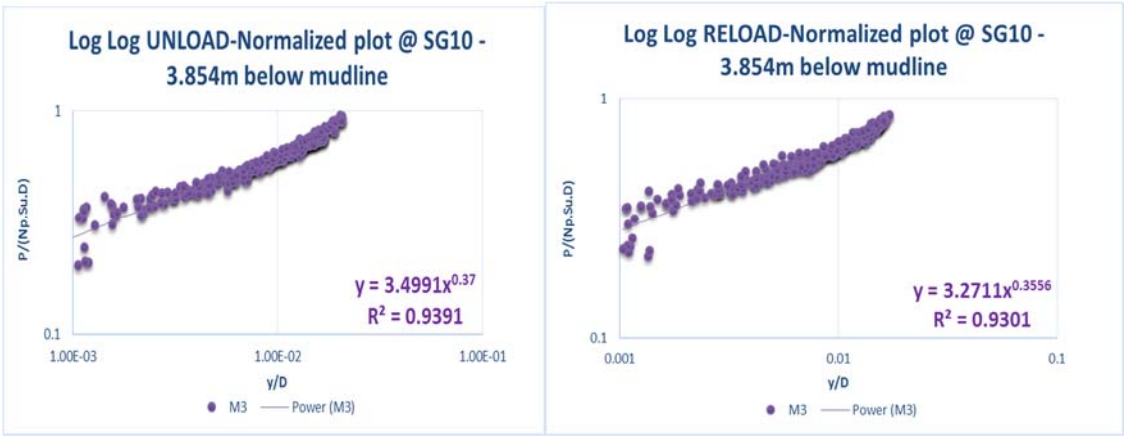

Fig. C-8: Power Law Fit To the Steady State Region of the Unload and Reload Loop of SG 10, for Motion M3

Fig. C-9: Power Law Fit To the Steady State Region of the Unload and Reload Loop of SG 10, for Motion M4

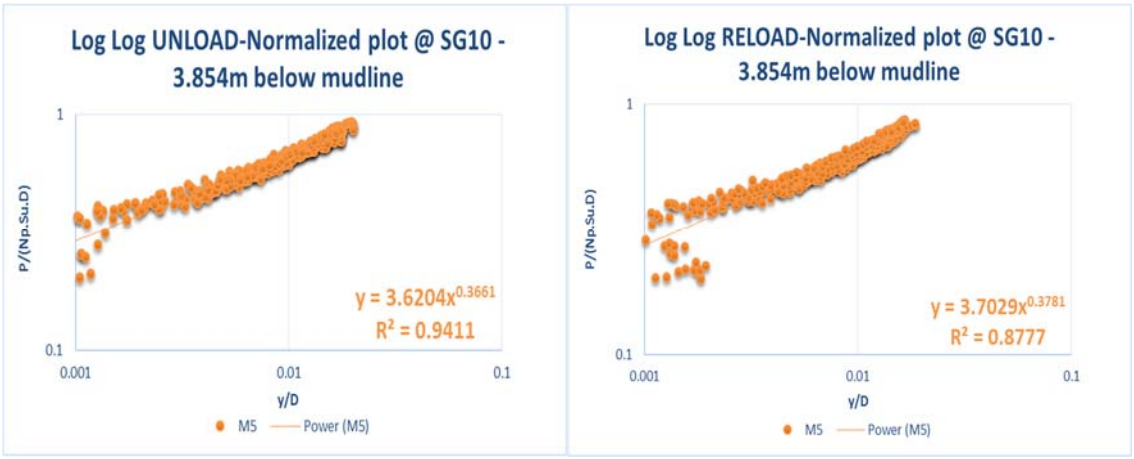

Fig. C-10: Power Law Fit To the Steady State Region of the Unload and Reload Loop of SG 10, for Motion M5

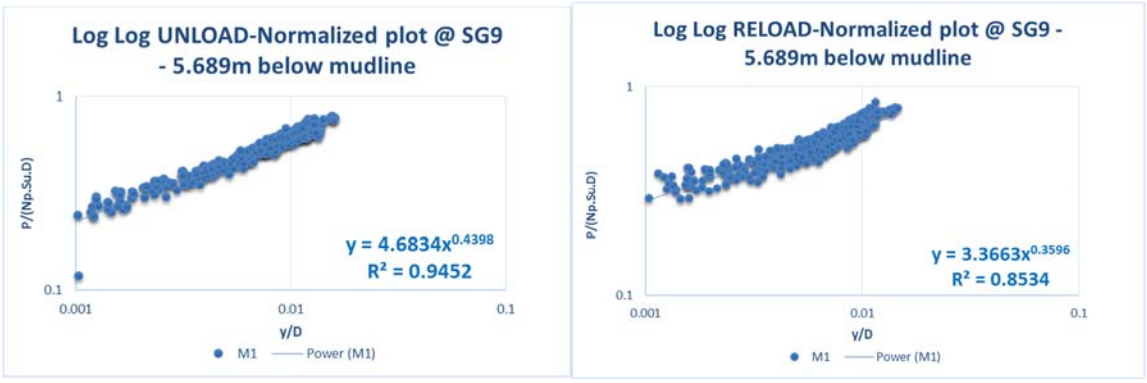

Fig. C-11: Power Law Fit To the Steady State Region of the Unload and Reload Loop of SG 9, for Motion M1

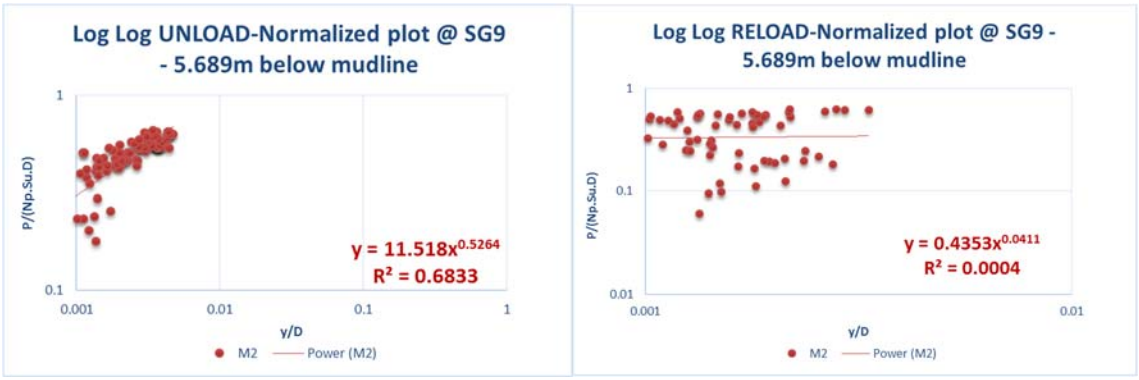

Fig. C-12: Power Law Fit To the Steady State Region of the Unload and Reload Loop of SG 9, for Motion M2

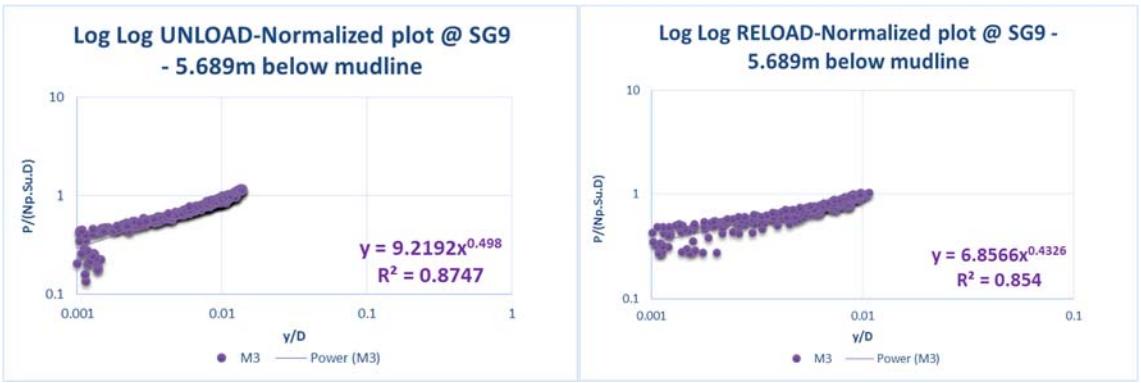

Fig. C-13: Power Law Fit To the Steady State Region of the Unload and Reload Loop of SG 9, for Motion M3

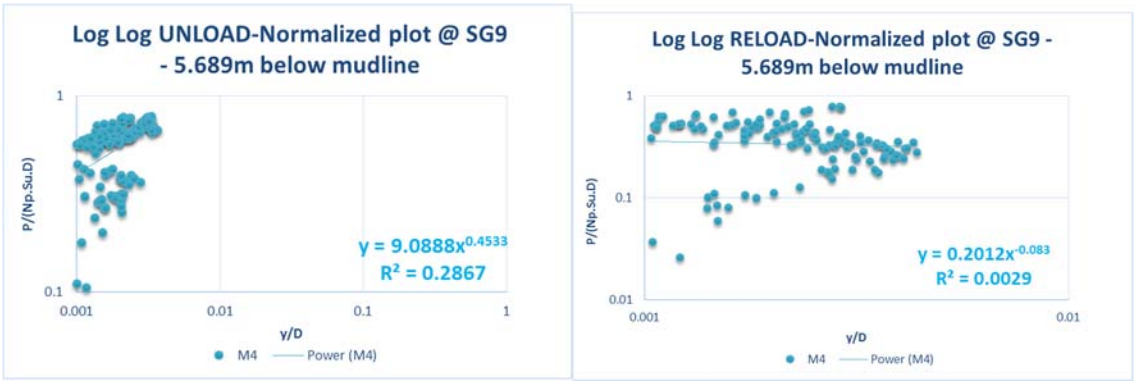

Fig. C-14: Power Law Fit To the Steady State Region of the Unload and Reload Loop of SG 9, for Motion M4

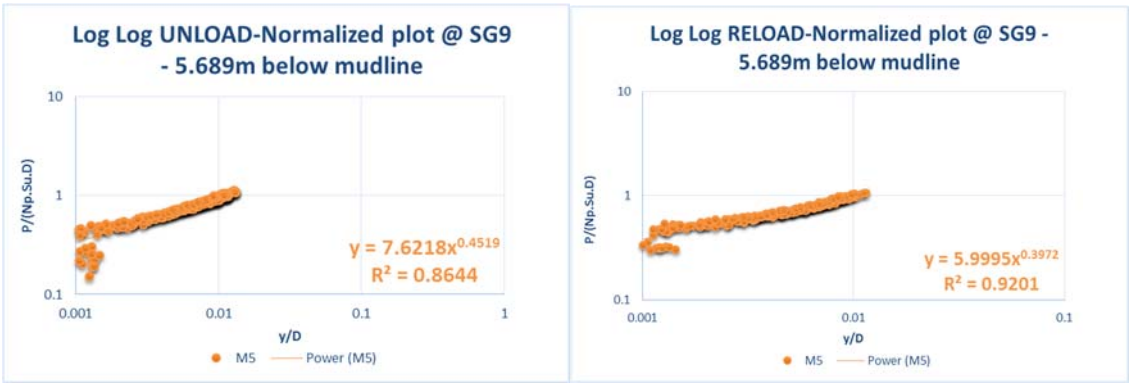

Fig. C-15: Power Law Fit To the Steady State Region of the Unload and Reload Loop of SG 9, for Motion M5

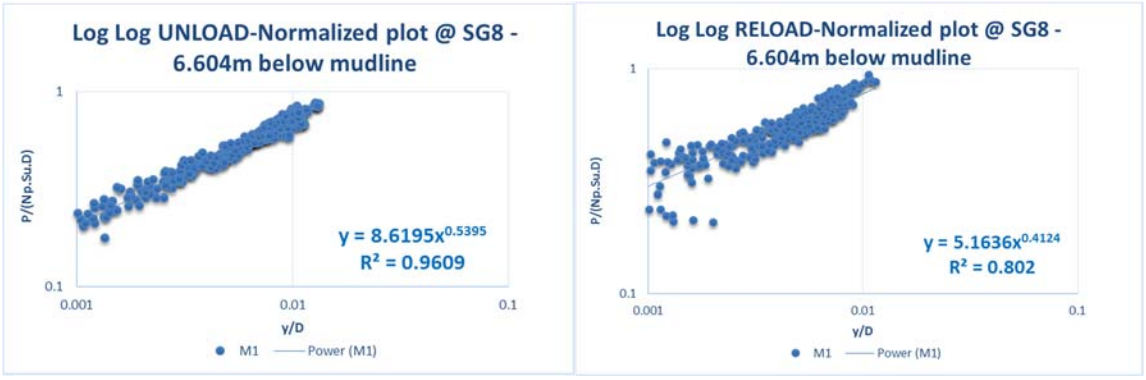

Fig. C-16: Power Law Fit To the Steady State Region of the Unload and Reload Loop of SG 8, for Motion M1

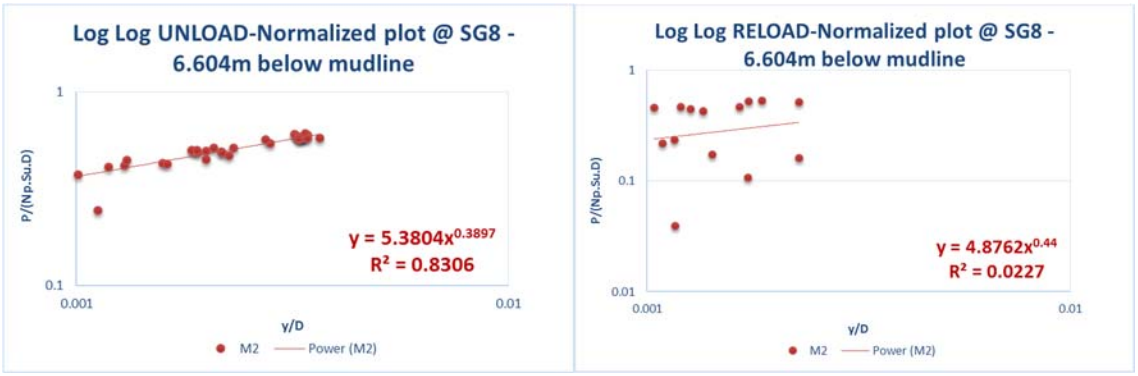

Fig. C-17: Power Law Fit To the Steady State Region of the Unload and Reload Loop of SG 8, for Motion M2

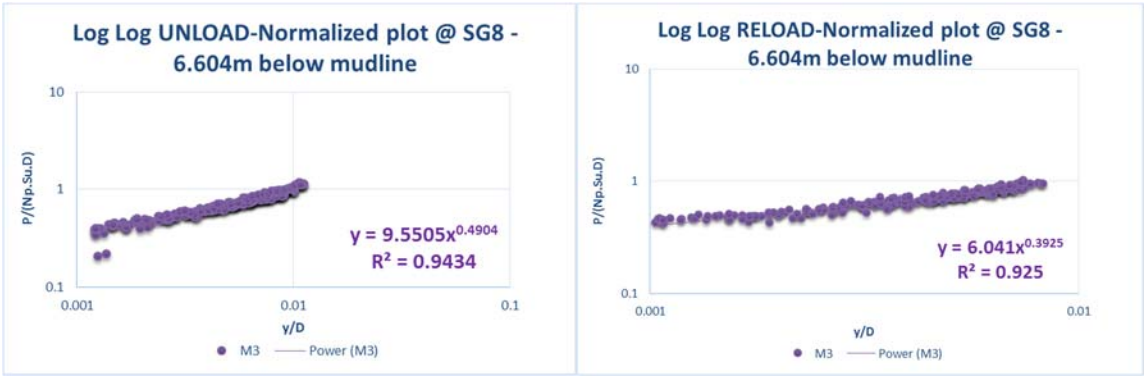

Fig. C-18: Power Law Fit To the Steady State Region of the Unload and Reload Loop of SG 8, for Motion M3

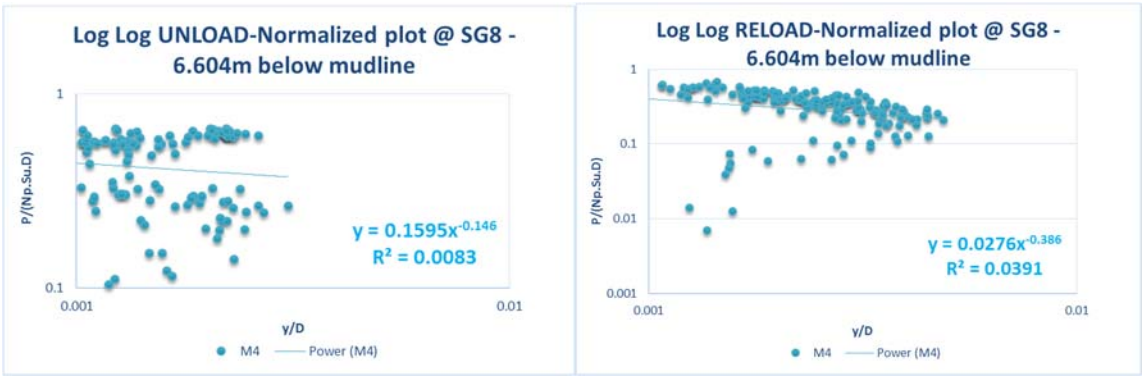

Fig. C-19: Power Law Fit To the Steady State Region of the Unload and Reload Loop of SG 8, for Motion M4

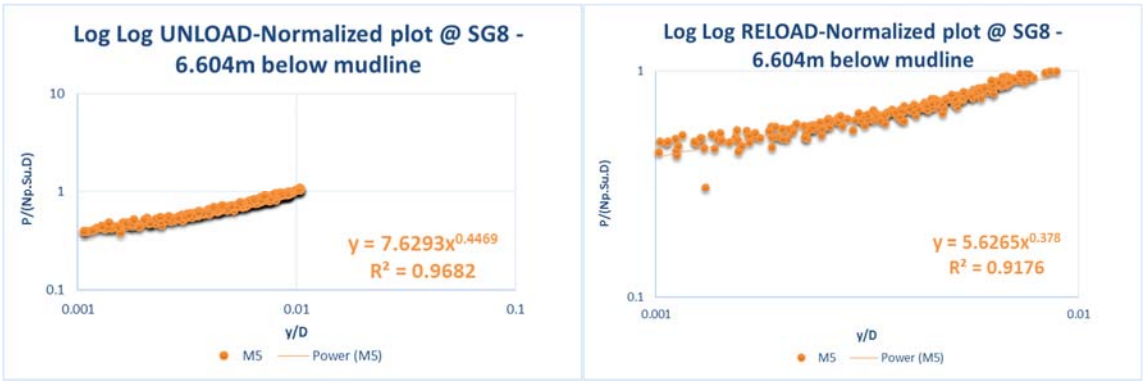

Fig. C-20: Power Law Fit To the Steady State Region of the Unload and Reload Loop of SG 8, for Motion M5

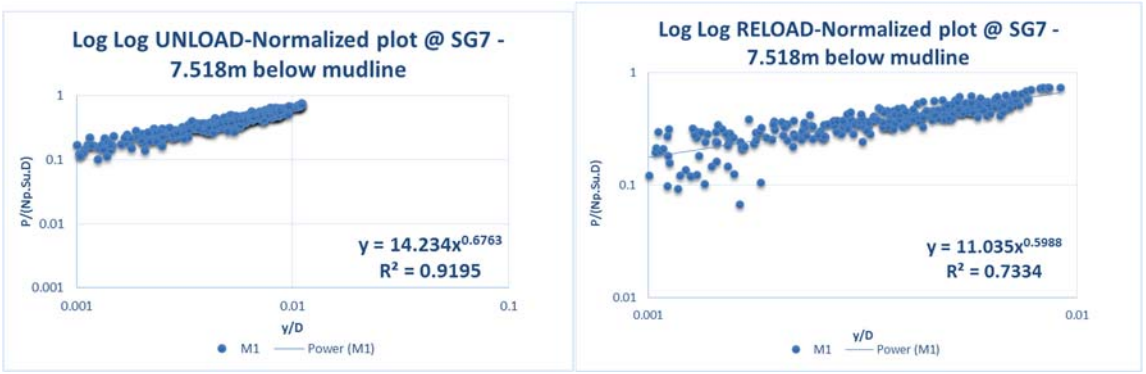

Fig. C-21: Power Law Fit To the Steady State Region of the Unload and Reload Loop of SG 7, for Motion M1

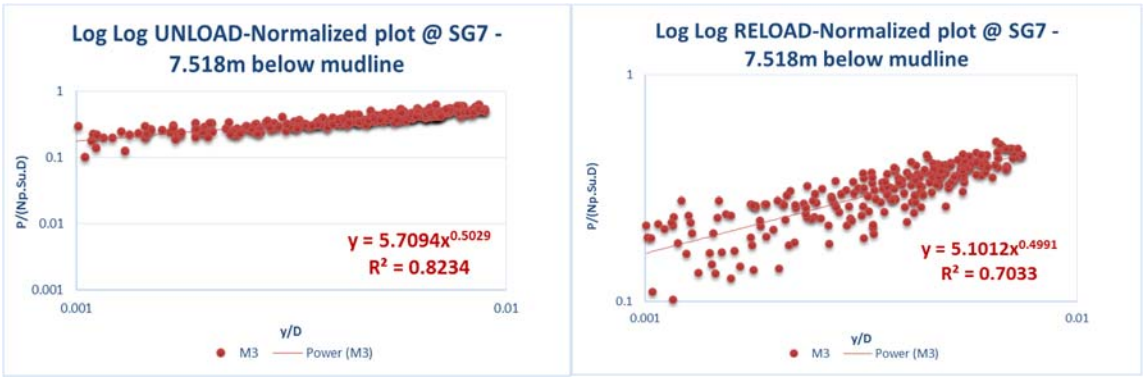

Fig. C-22: Power Law Fit To the Steady State Region of the Unload and Reload Loop of SG 7, for Motion M3

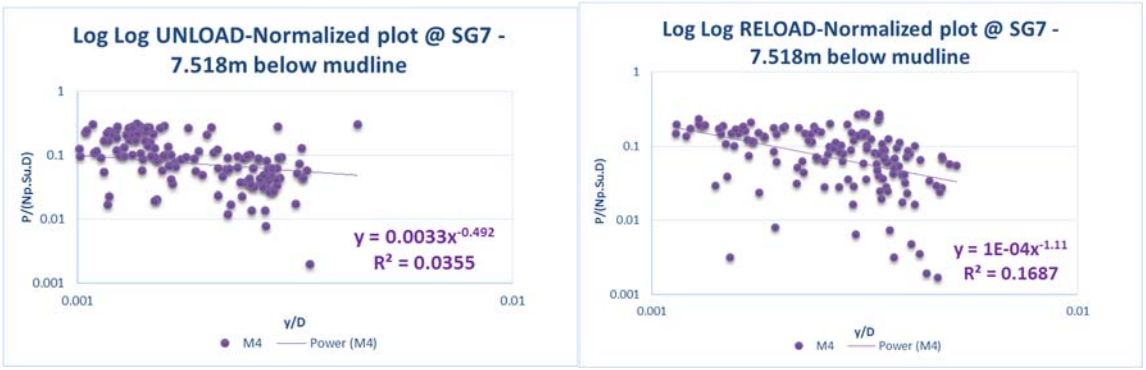

Fig. C-23: Power Law Fit To the Steady State Region of the Unload and Reload Loop of SG 7, for Motion M4

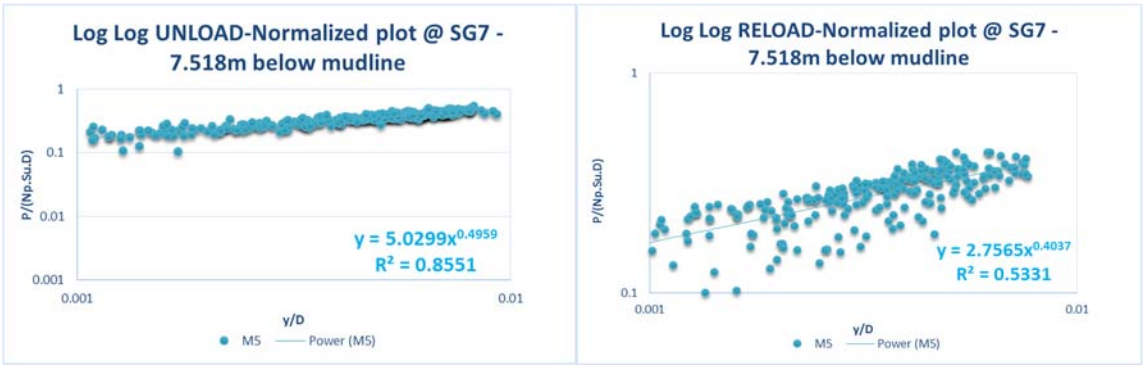

Fig. C-24: Power Law Fit To the Steady State Region of the Unload and Reload Loop of SG 7, for Motion M5

APPENDIX D

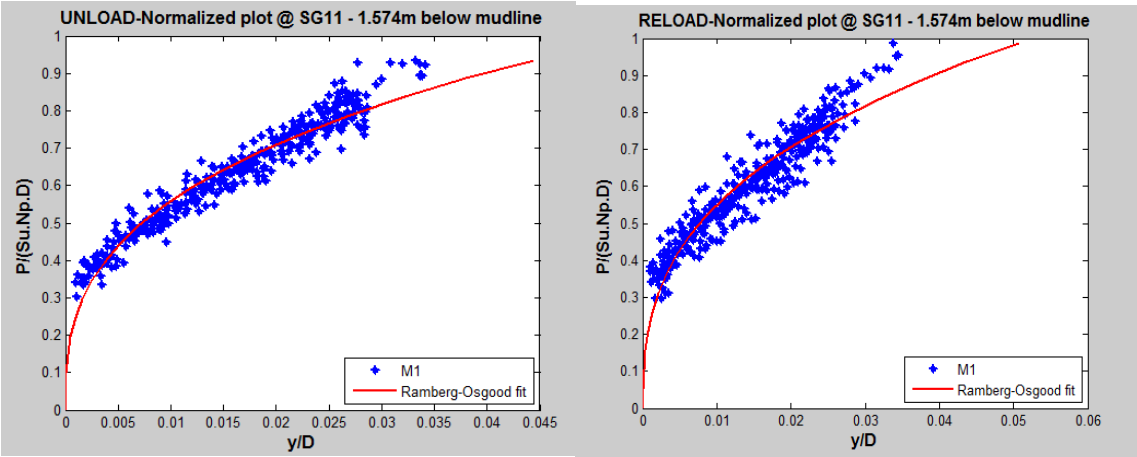

Fig. D-1: Ramberg-Osgood Fit to the Steady State Region of the Unload and Reload Loop of SG 11, for Motion M1

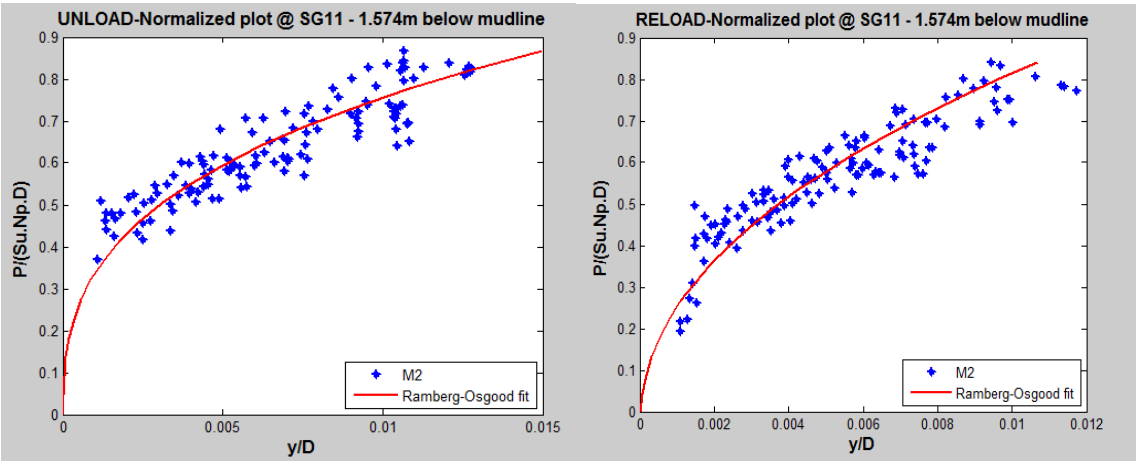

Fig. D-2: Ramberg-Osgood Fit to the Steady State Region of the Unload and Reload Loop of SG 11, for Motion M2

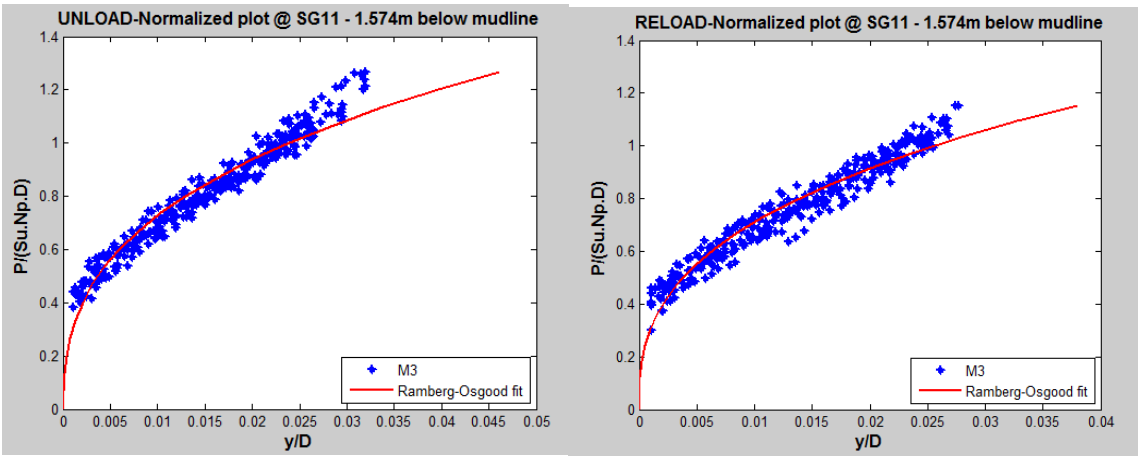

Fig. D-3: Ramberg-Osgood Fit to the Steady State Region of the Unload and Reload Loop of SG 11, for Motion M3

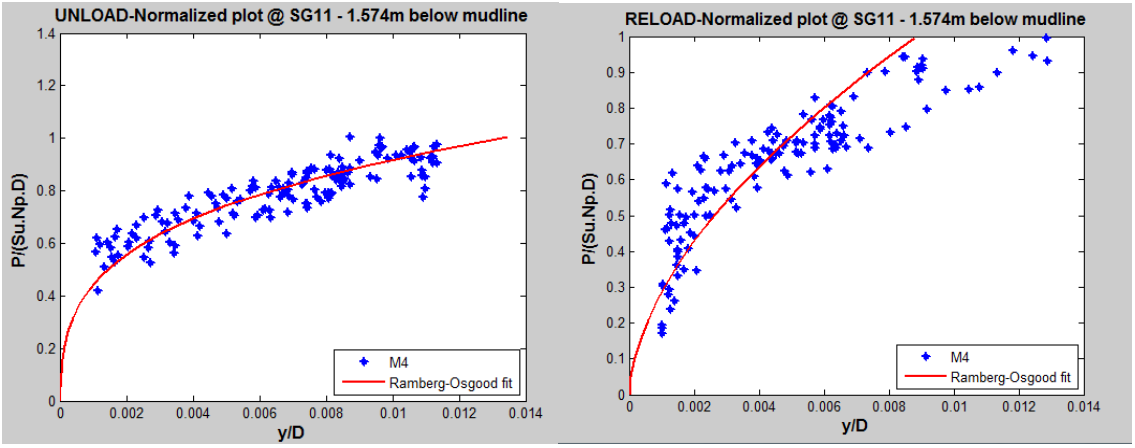

Fig. D-4: Ramberg-Osgood Fit to the Steady State Region of the Unload and Reload Loop of SG 11, for Motion M4

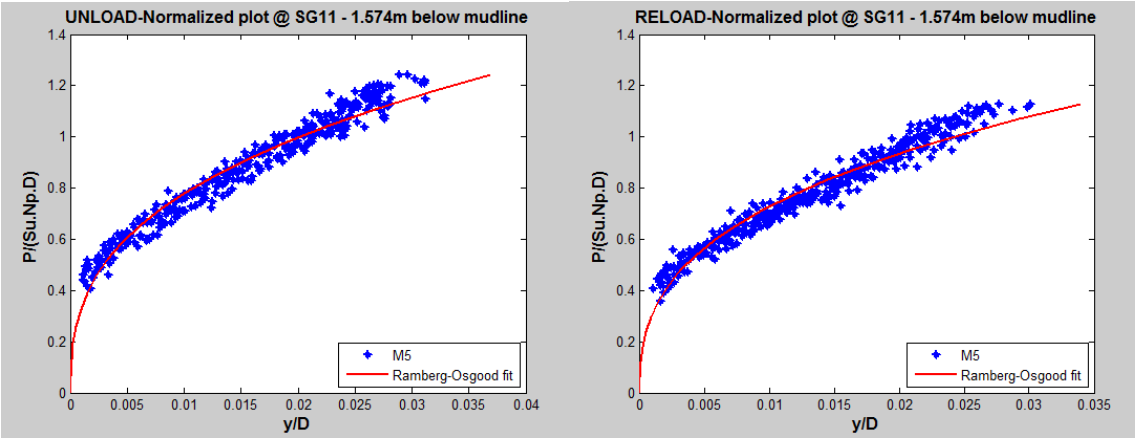

Fig. D-5: Ramberg-Osgood Fit to the Steady State Region of the Unload and Reload Loop of SG 11, for Motion M5

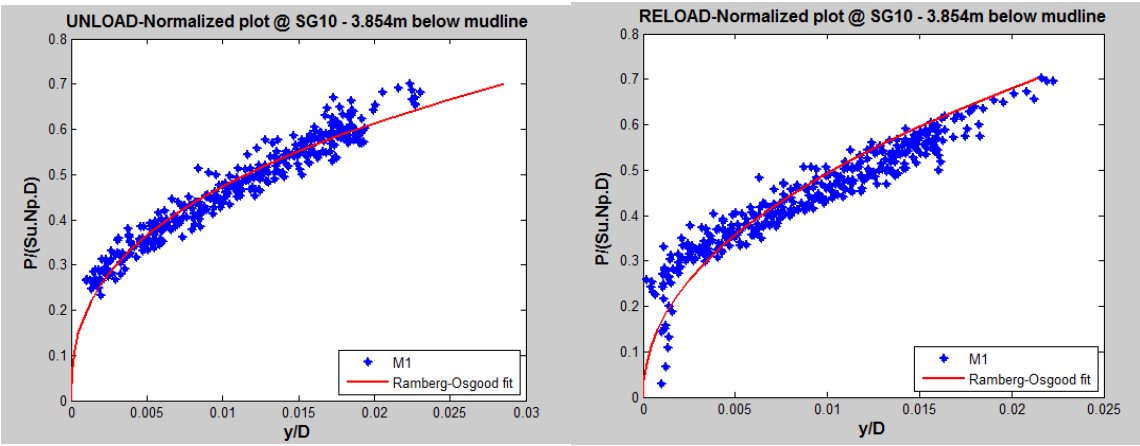

Fig. D-6: Ramberg-Osgood Fit to the Steady State Region of the Unload and Reload Loop of SG 10, for Motion M1

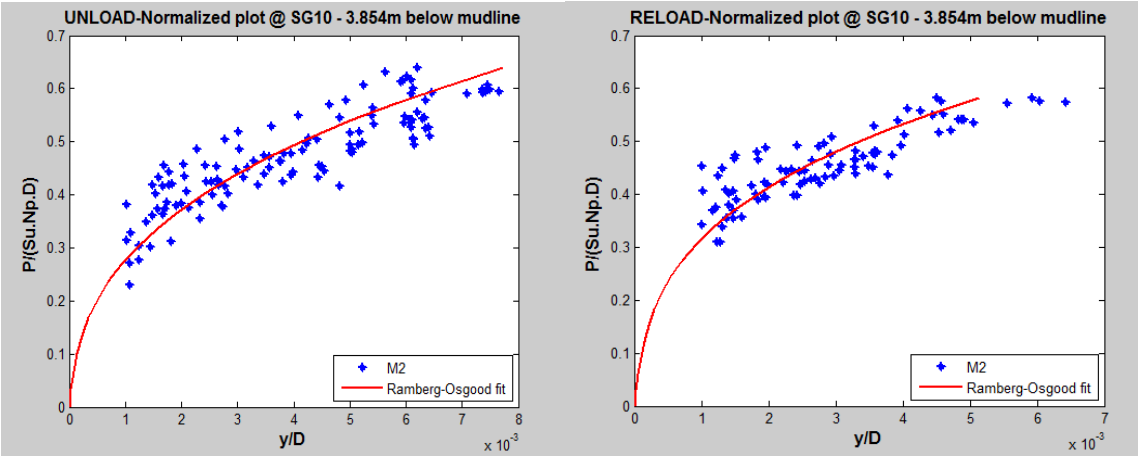

Fig. D-7: Ramberg-Osgood Fit to the Steady State Region of the Unload and Reload Loop of SG 10, for Motion M2

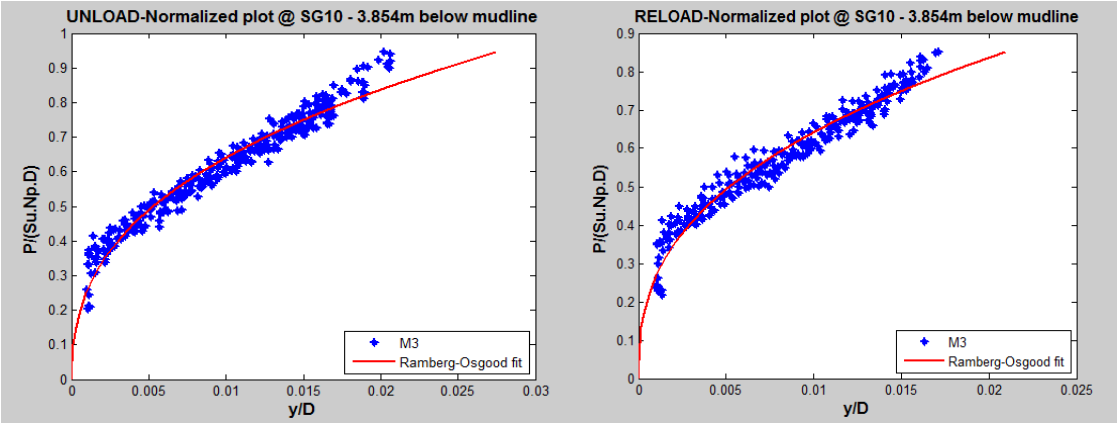

Fig. D-8: Ramberg-Osgood Fit to the Steady State Region of the Unload and Reload Loop of SG 10, for Motion M3

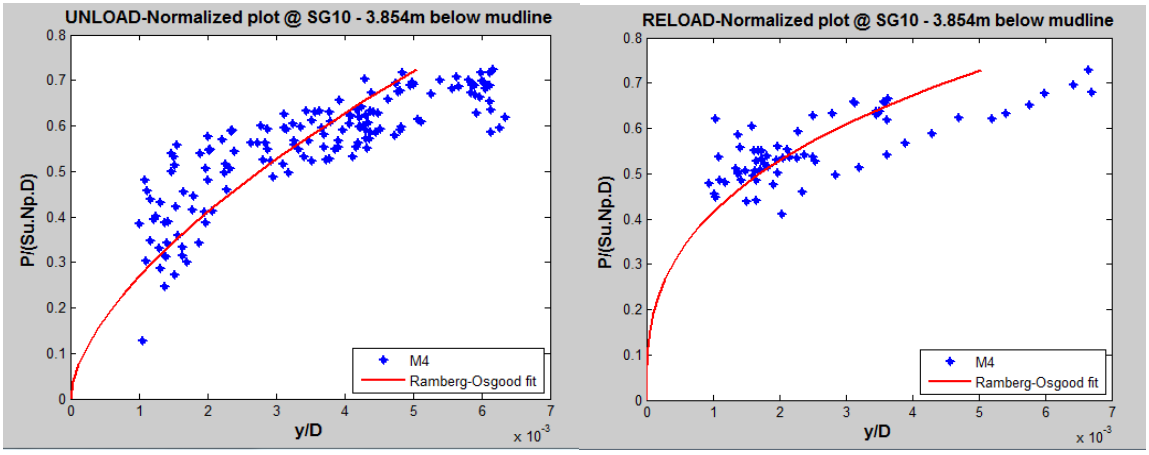

Fig. D-9: Ramberg-Osgood Fit to the Steady State Region of the Unload and Reload Loop of SG 10, for Motion M4

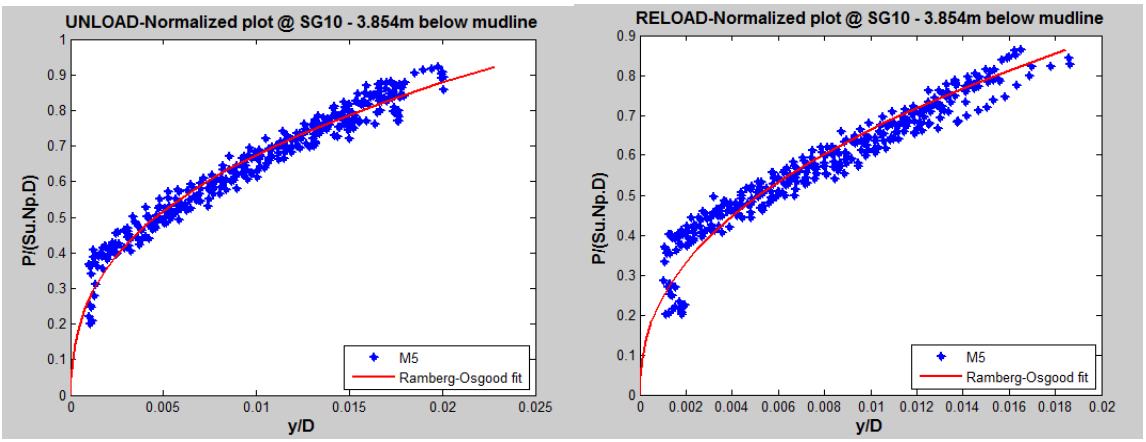

Fig. D-10: Ramberg-Osgood Fit to the Steady State Region of the Unload and Reload Loop of SG 10, for Motion M5

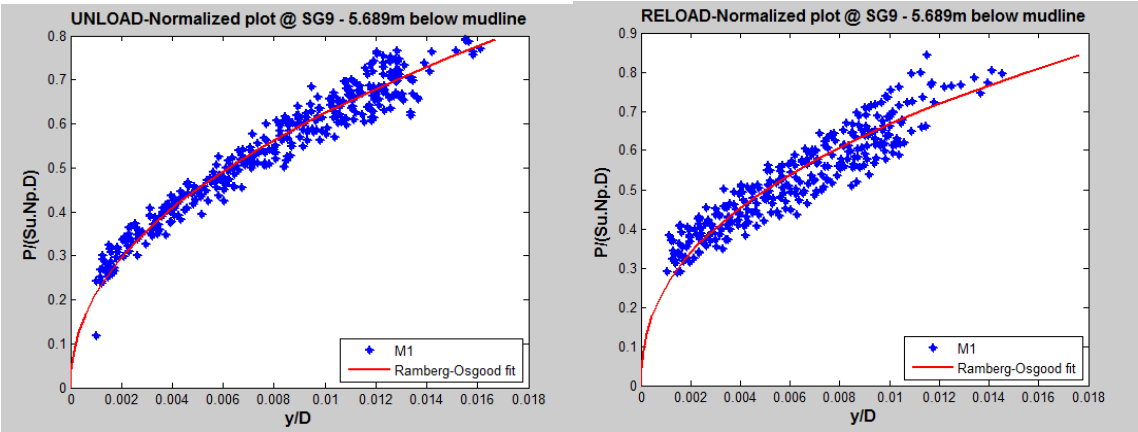

Fig. D-11: Ramberg-Osgood Fit to the Steady State Region of the Unload and Reload Loop of SG 9, for Motion M1

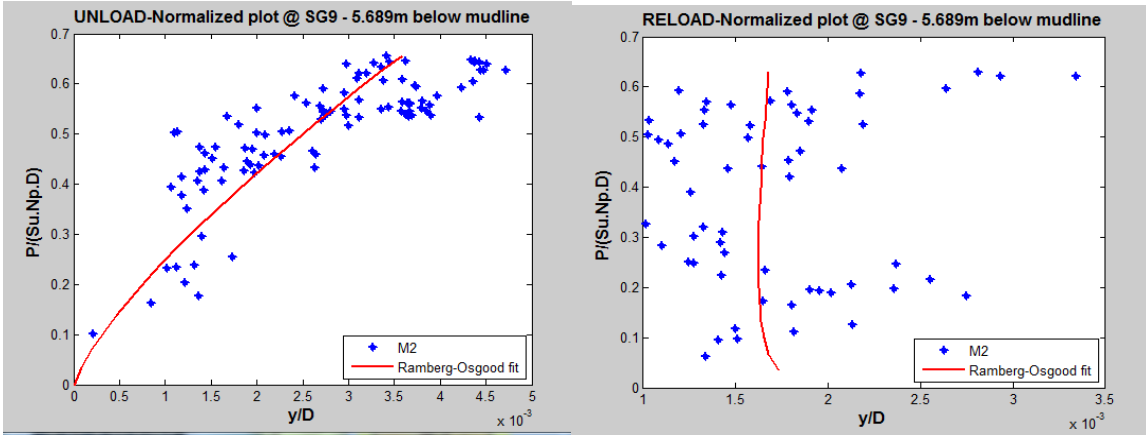

Fig. D-12: Ramberg-Osgood Fit to the Steady State Region of the Unload and Reload Loop of SG 9, for Motion M2, due to scatter of the data points

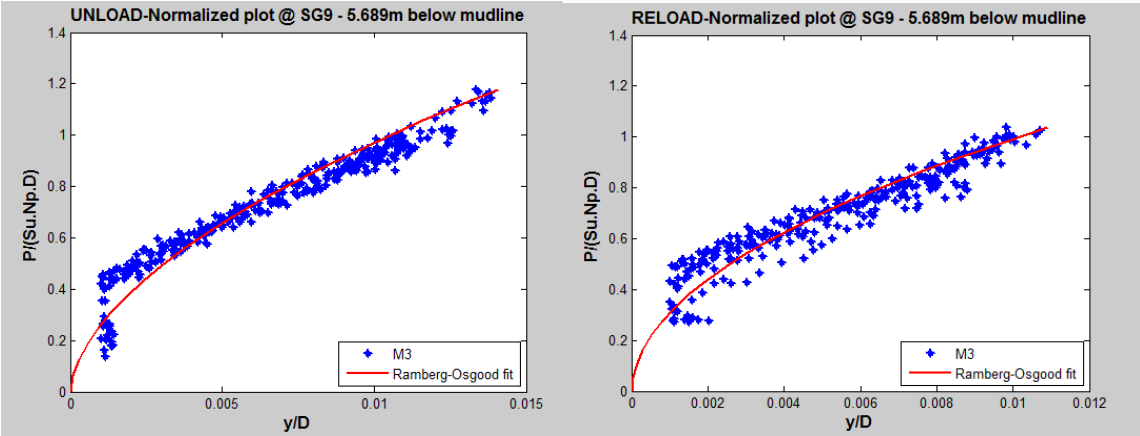

Fig. D-13: Ramberg-Osgood Fit to the Steady State Region of the Unload and Reload Loop of SG 9, for Motion M3

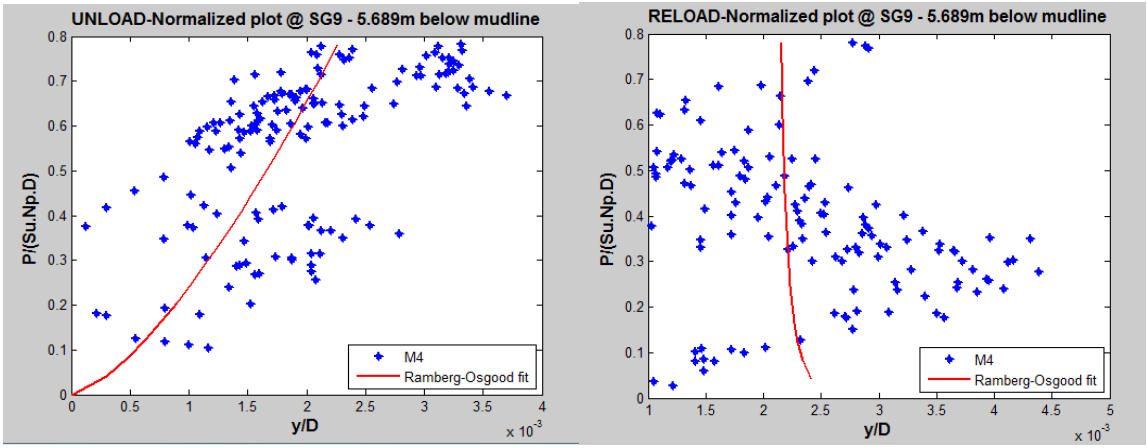

Fig. D-14: Ramberg-Osgood Fit to the Steady State Region of the Unload and Reload Loop of SG 9, for Motion M4, due to scatter of the data points

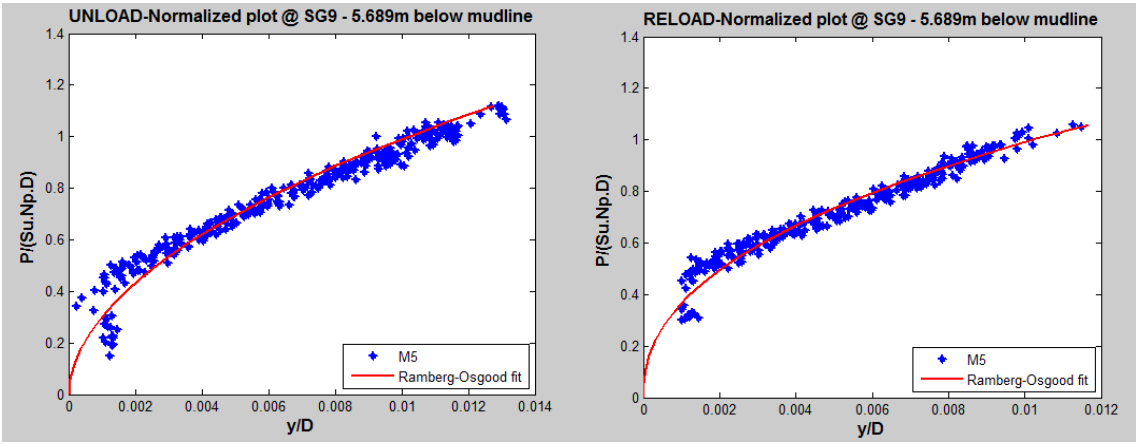

Fig. D-15: Ramberg-Osgood Fit to the Steady State Region of the Unload and Reload Loop of SG 9, for Motion M5

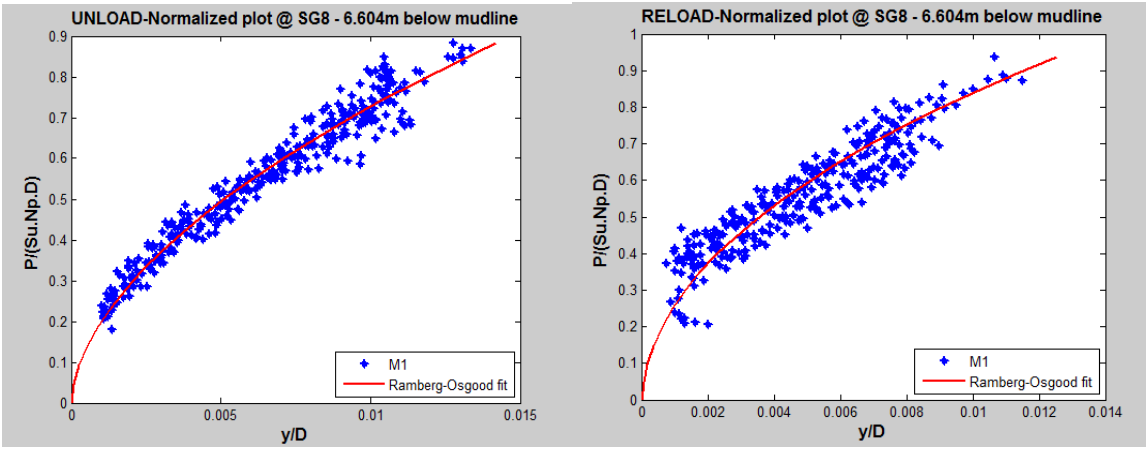

Fig. D-16: Ramberg-Osgood Fit to the Steady State Region of the Unload and Reload Loop of SG 8, for Motion M1

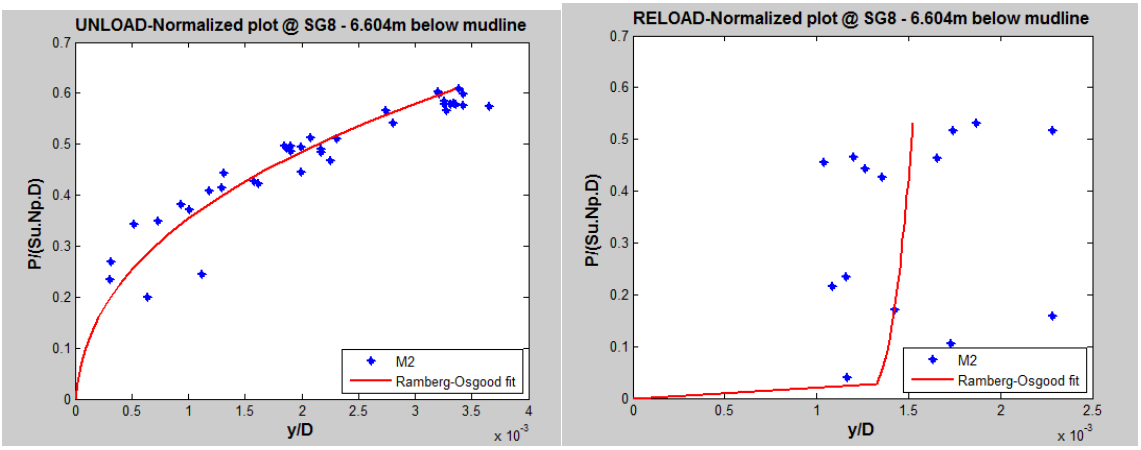

Fig. D-17: Ramberg-Osgood Fit to the Steady State Region of the Unload and Reload Loop of SG 8, for Motion M2

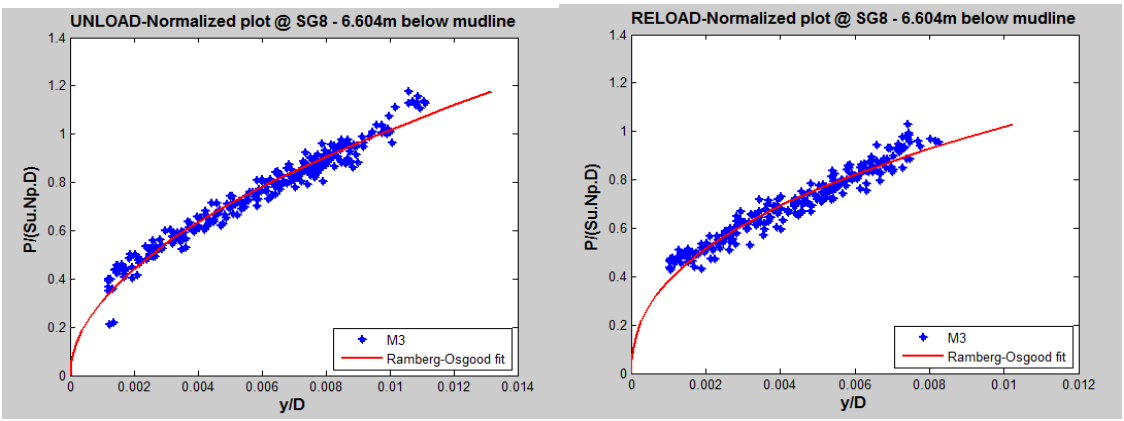

Fig. D-18: Ramberg-Osgood Fit to the Steady State Region of the Unload and Reload Loop of SG 8, for Motion M3

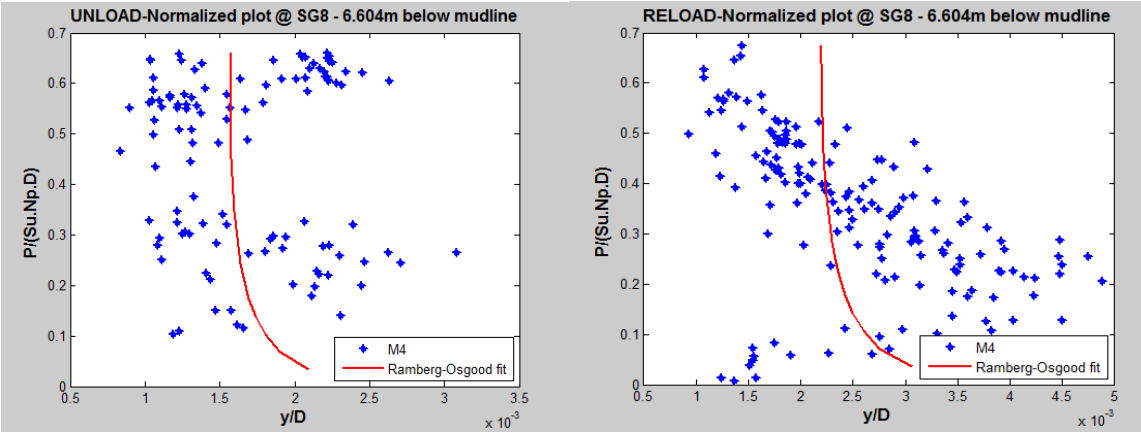

Fig. D-19: Ramberg-Osgood Fit to the Steady State Region of the Unload and Reload Loop of SG 8, for Motion M4, due to scatter of the data points

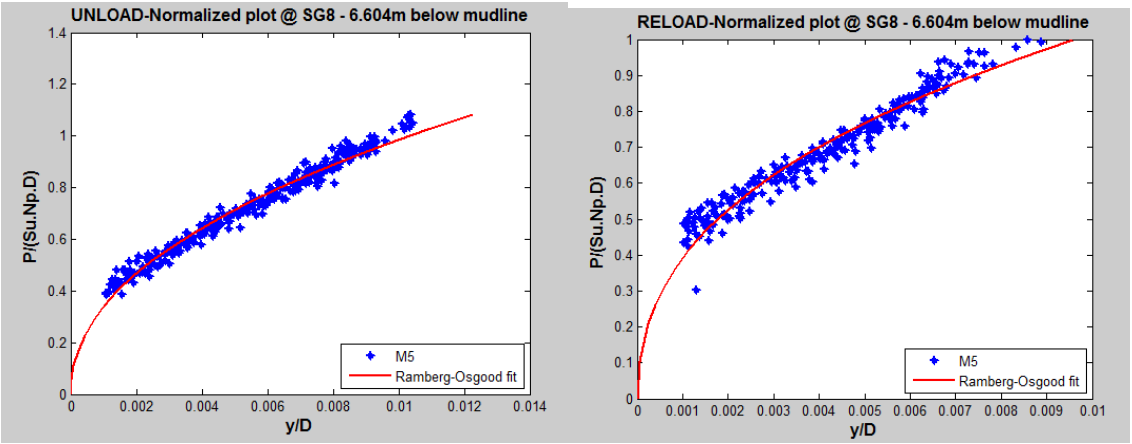

Fig. D-20: Ramberg-Osgood Fit to the Steady State Region of the Unload and Reload Loop of SG 8, for Motion M5

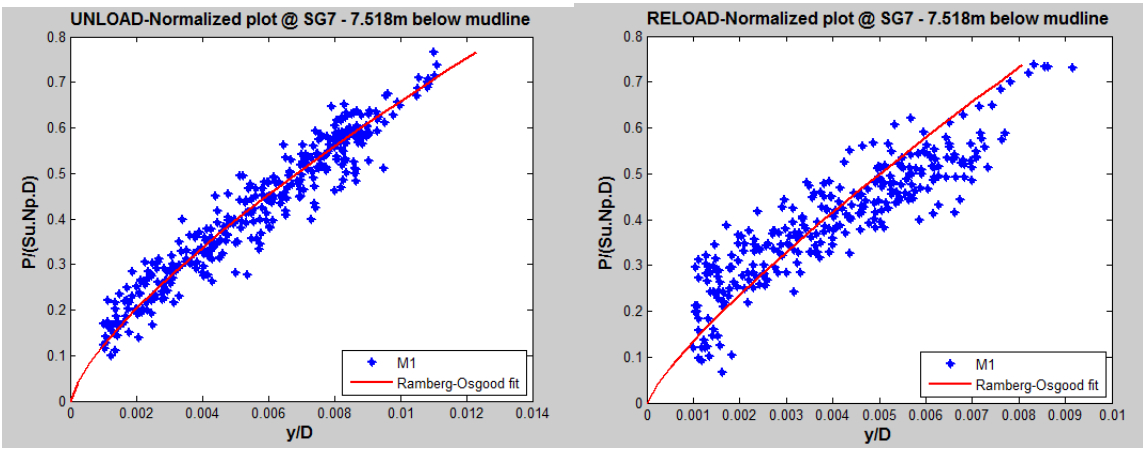

Fig. D-21: Ramberg-Osgood Fit to the Steady State Region of the Unload and Reload Loop of SG 7, for Motion M1

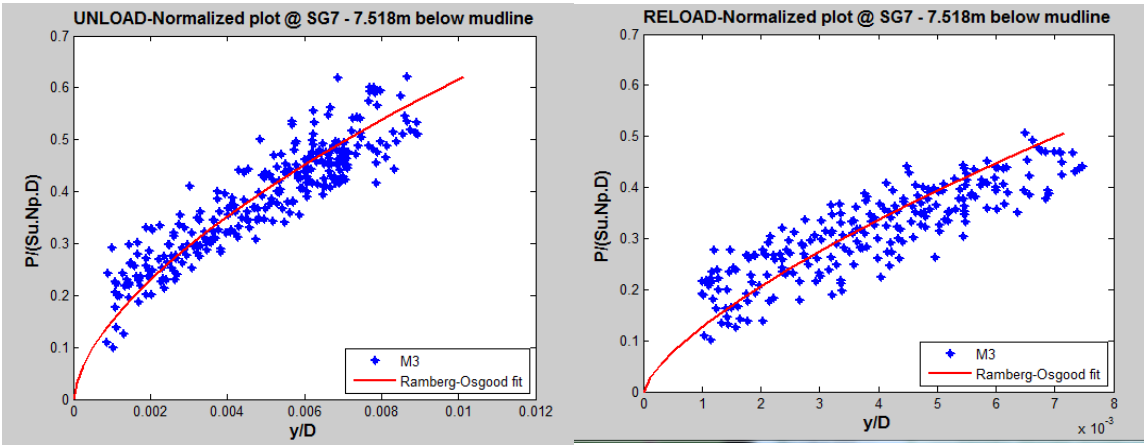

Fig. D-22: Ramberg-Osgood Fit to the Steady State Region of the Unload and Reload Loop of SG 7, for Motion M3

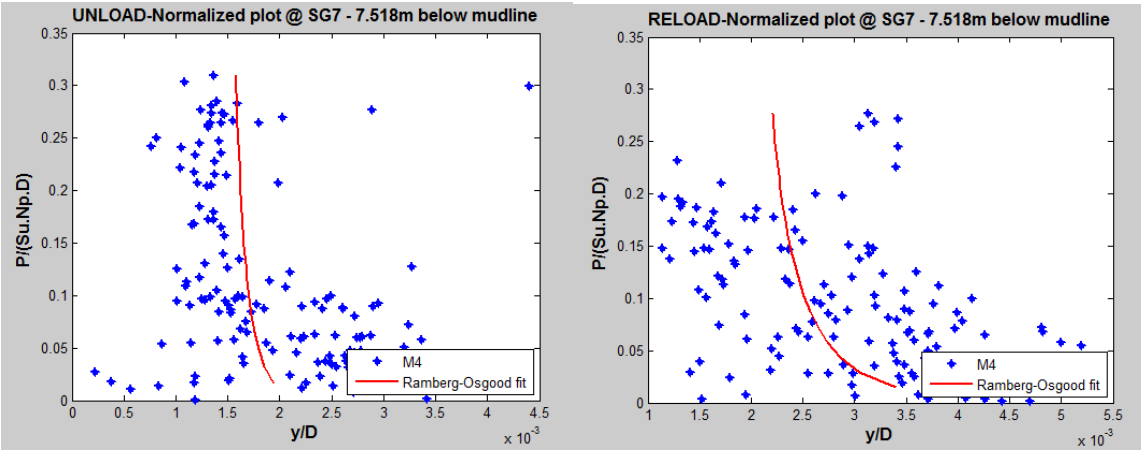

Fig. D-23: Ramberg-Osgood Fit to the Steady State Region of the Unload and Reload Loop of SG 7, for Motion M4, due to scatter of the data points

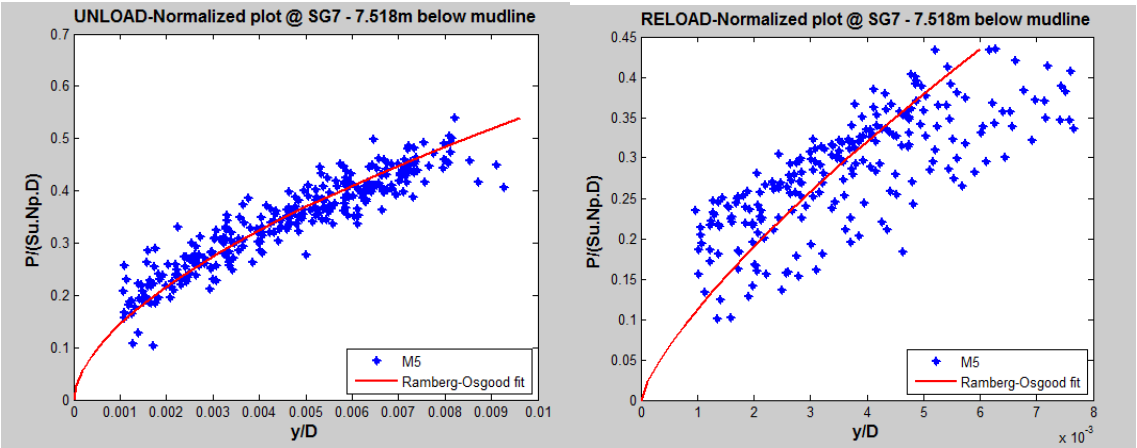

Fig. D-24: Ramberg-Osgood Fit to the Steady State Region of the Unload and Reload Loop of SG 7, for Motion M5

APPENDIX E

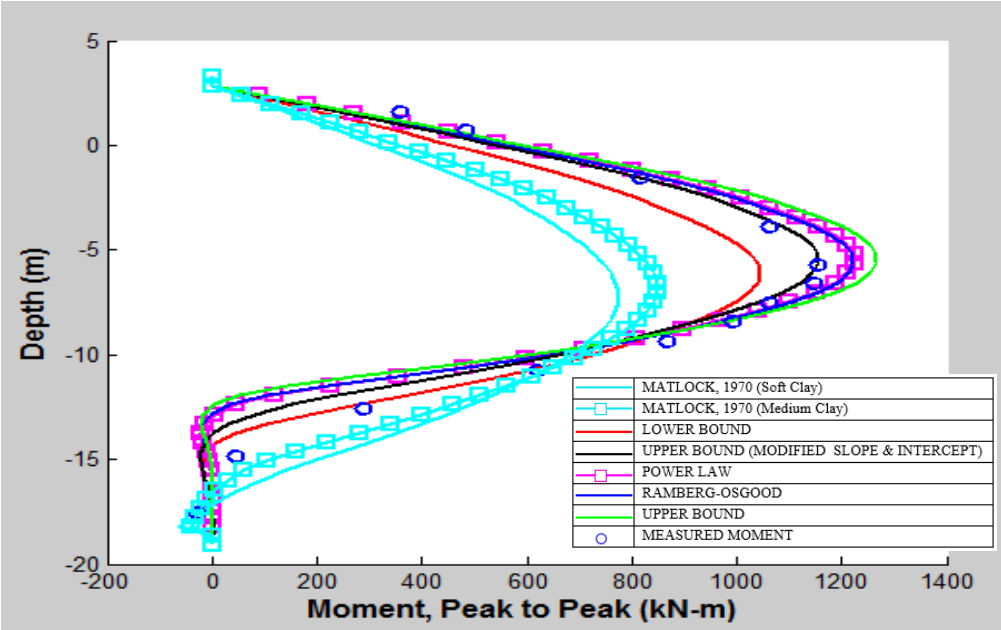

Figure E-1: Calculated Versus Measured Bending Moment Profiles from Centrifuge Test 4, M1 Load - Cycle 200 With Zero Offset.

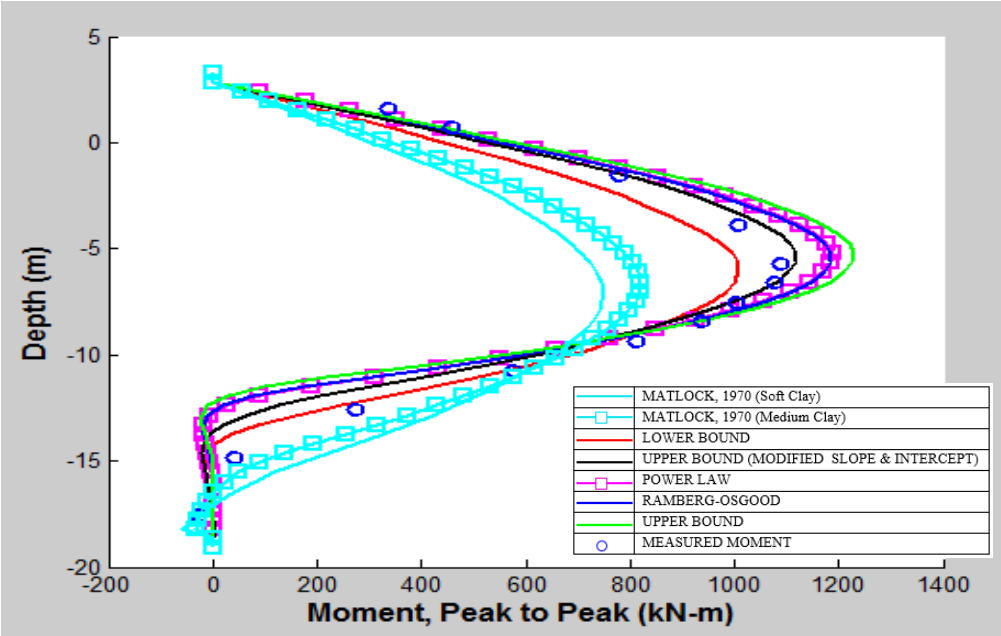

Figure E-2: Calculated Versus Measured Bending Moment Profiles from Centrifuge Test 4, M1 Load - Cycle 300 With Zero Offset.

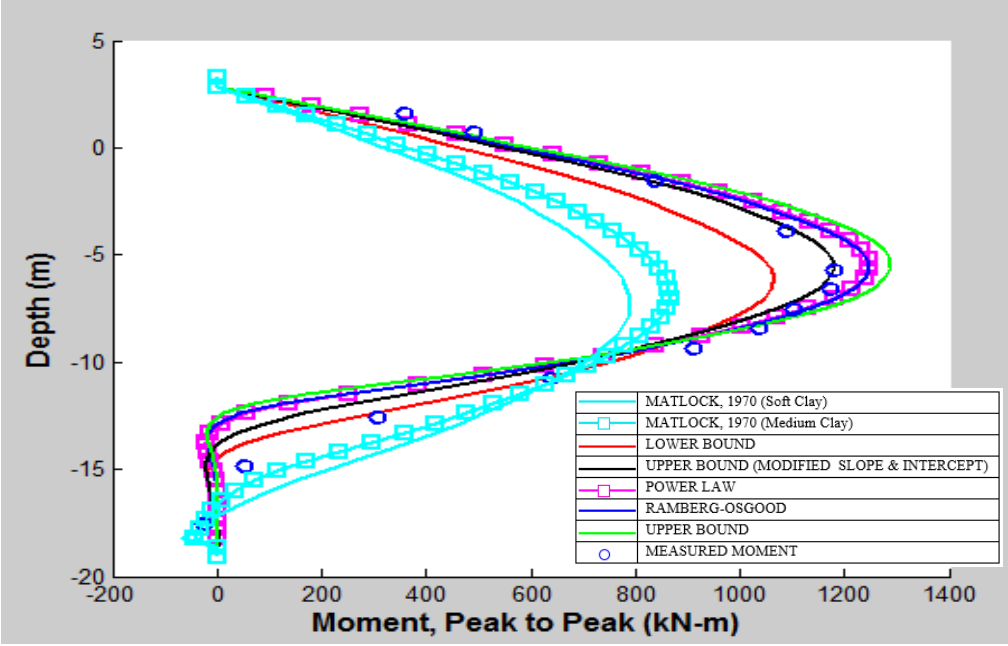

Figure E-3: Calculated Versus Measured Bending Moment Profiles from Centrifuge Test 4, M1 Load - Cycle 400 With Zero Offset.

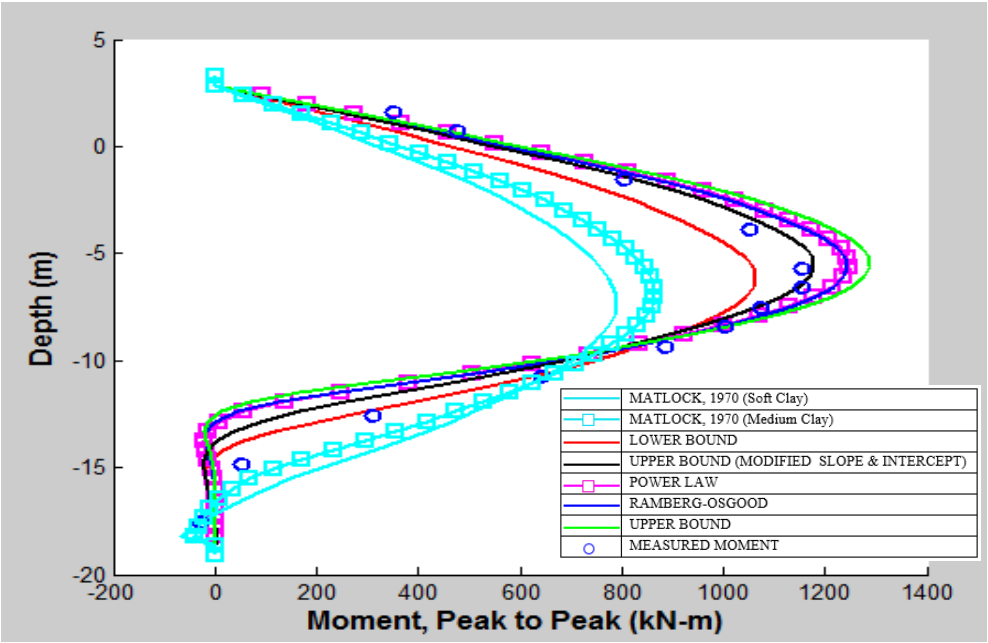

Figure E-4: Calculated Versus Measured Bending Moment Profiles from Centrifuge Test 4, M1 Load - Cycle 500 With Zero Offset.

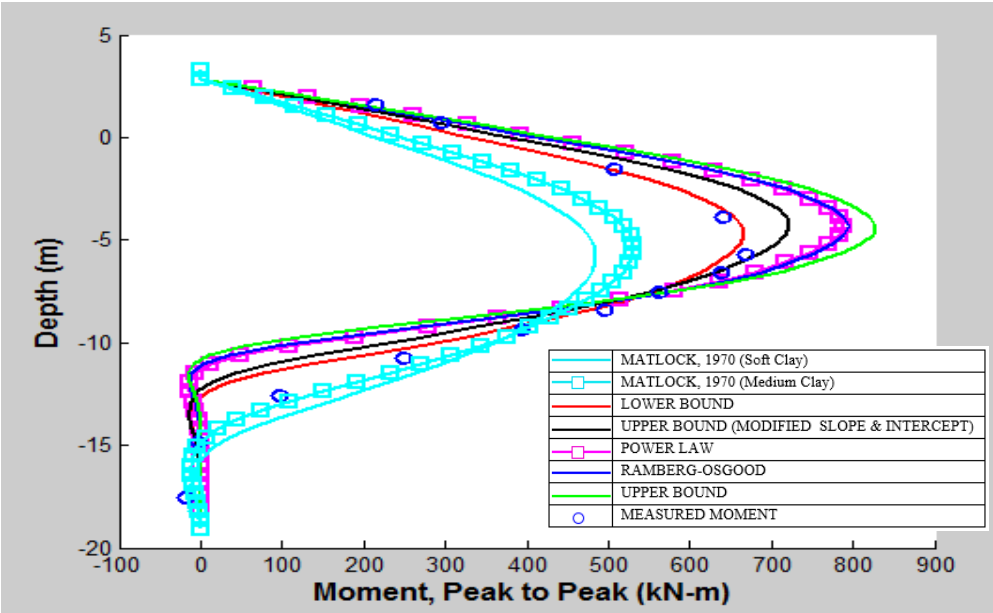

Figure E-5: Calculated Versus Measured Bending Moment Profiles from Centrifuge Test 4, M2 Load - Cycle 200 With 0.05 Offset.

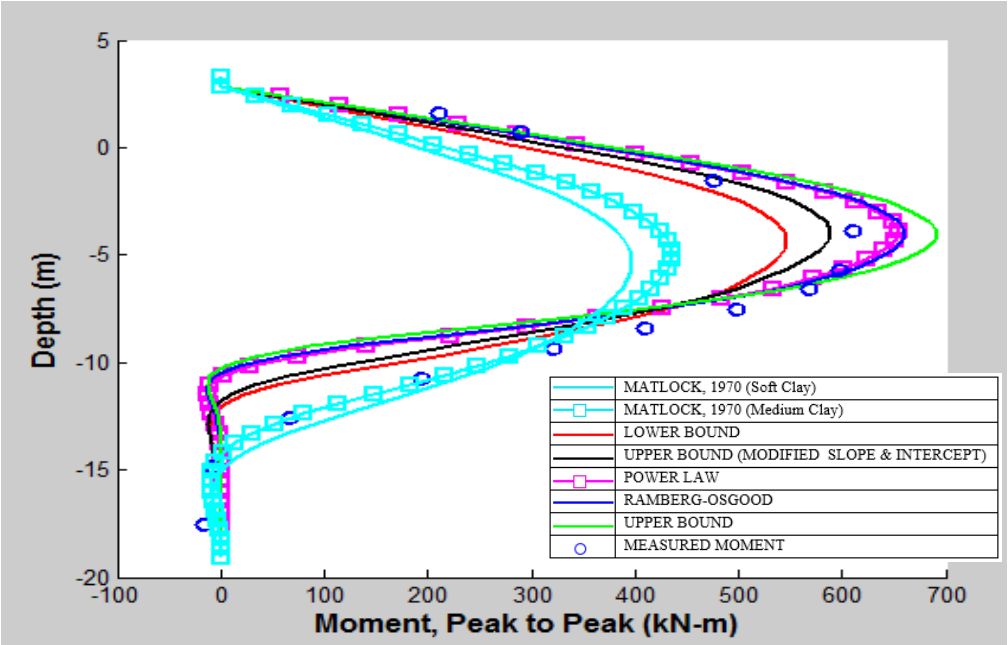

Figure E-6: Calculated Versus Measured Bending Moment Profiles from Centrifuge Test 4, M2 Load - Cycle 300 With 0.05 Offset.

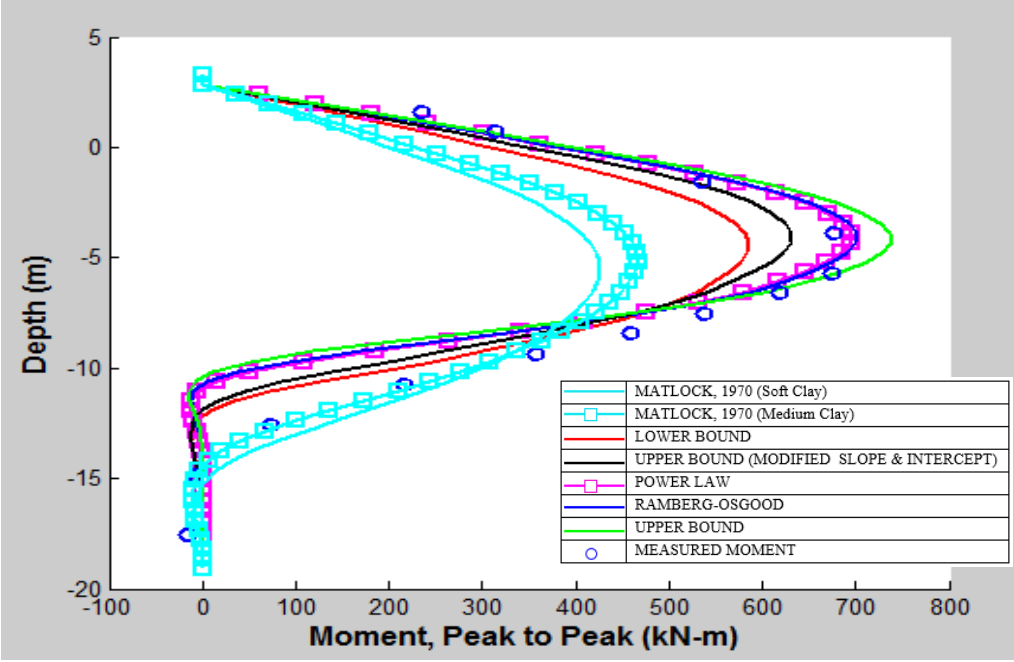

Figure E-7: Calculated Versus Measured Bending Moment Profiles from Centrifuge Test 4, M2 Load - Cycle 400 With 0.05 Offset.

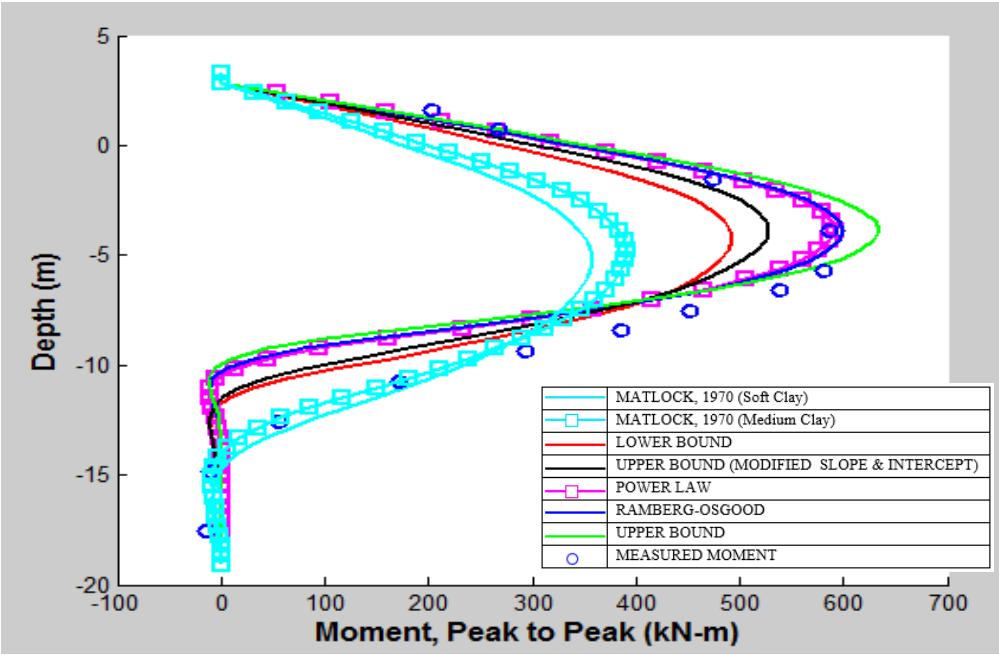

Figure E-8: Calculated Versus Measured Bending Moment Profiles from Centrifuge Test 4, M2 Load - Cycle 500 With 0.05 Offset.

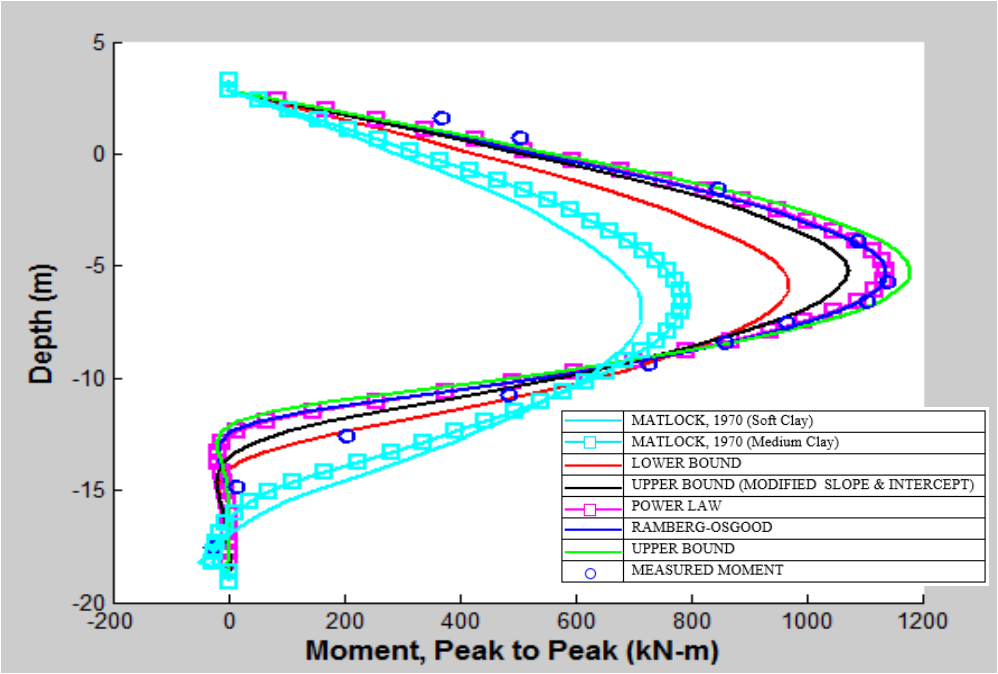

Figure E-9: Calculated Versus Measured Bending Moment Profiles from Centrifuge Test 4, M3 Load - Cycle 200 With Zero Offset.

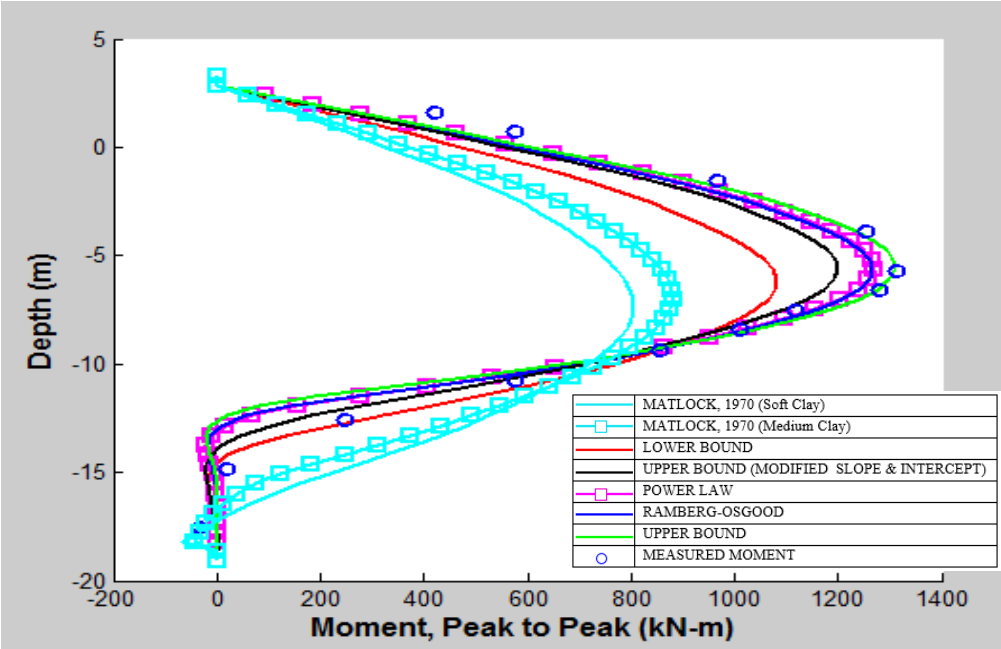

Figure E-10: Calculated Versus Measured Bending Moment Profiles from Centrifuge Test 4, M3 Load - Cycle 300 With Zero Offset.

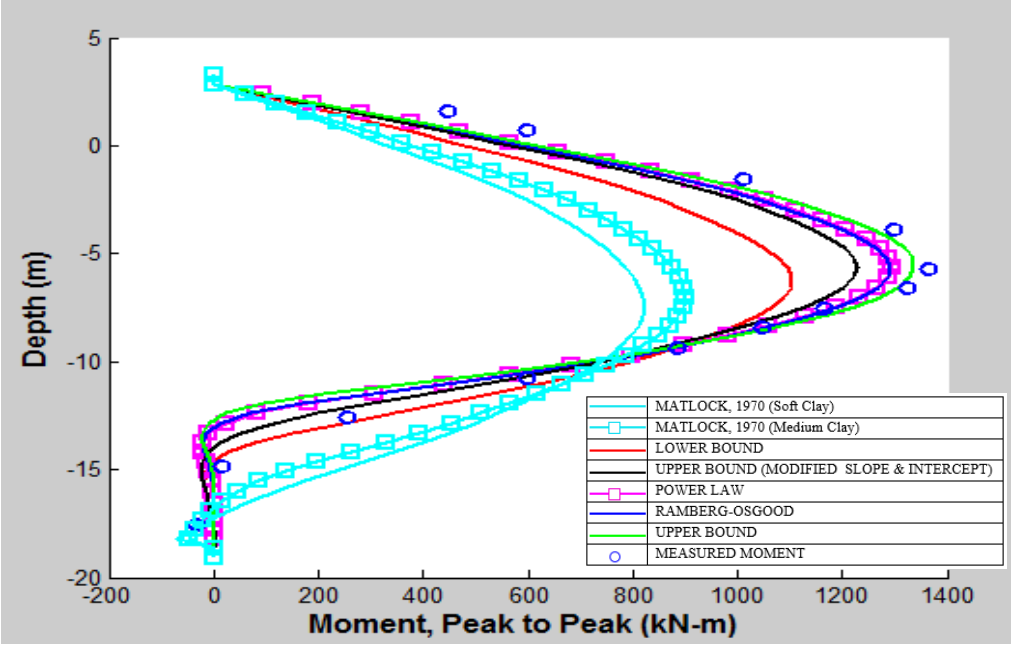

Figure E-11: Calculated Versus Measured Bending Moment Profiles from Centrifuge Test 4, M3 Load - Cycle 400 With Zero Offset.

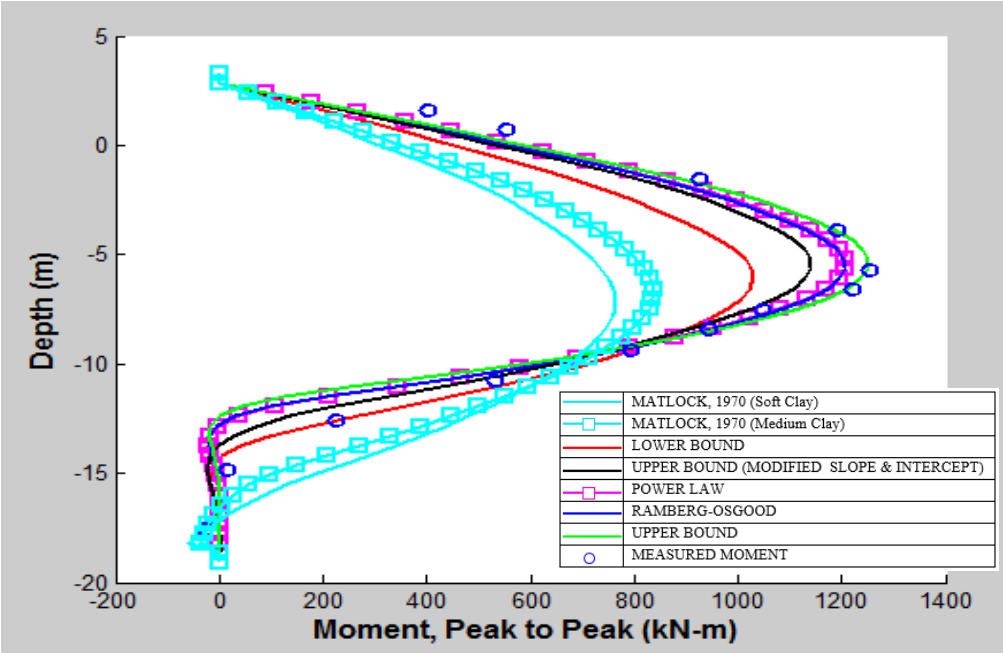

Figure E-12: Calculated Versus Measured Bending Moment Profiles from Centrifuge Test 4, M3 Load - Cycle 500 With Zero Offset.

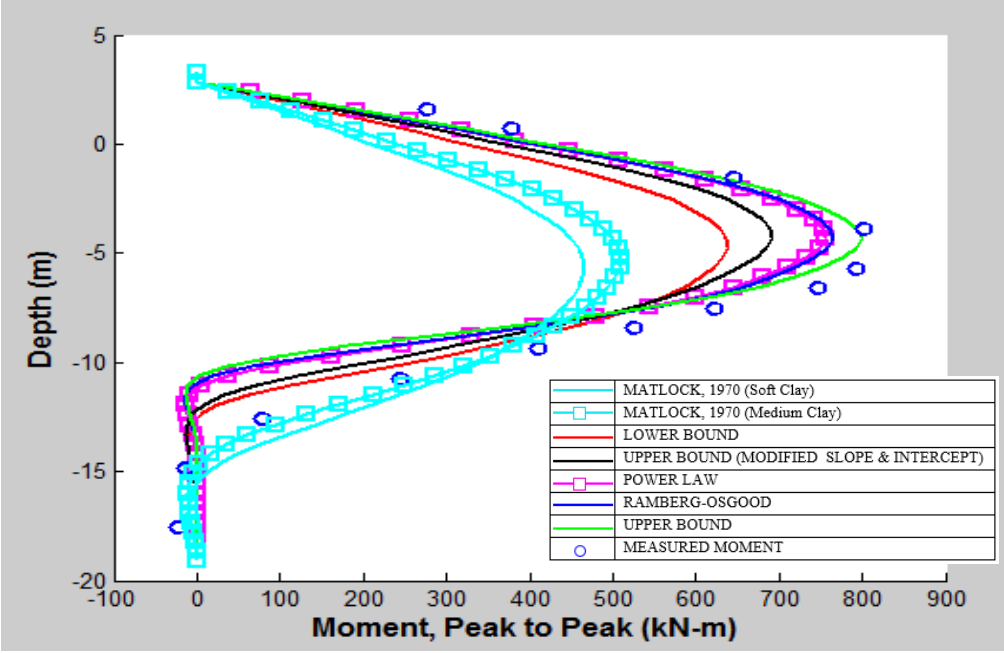

Figure E-13: Calculated Versus Measured Bending Moment Profiles from Centrifuge Test 4, M4 Load - Cycle 200 With 0.05 Offset.

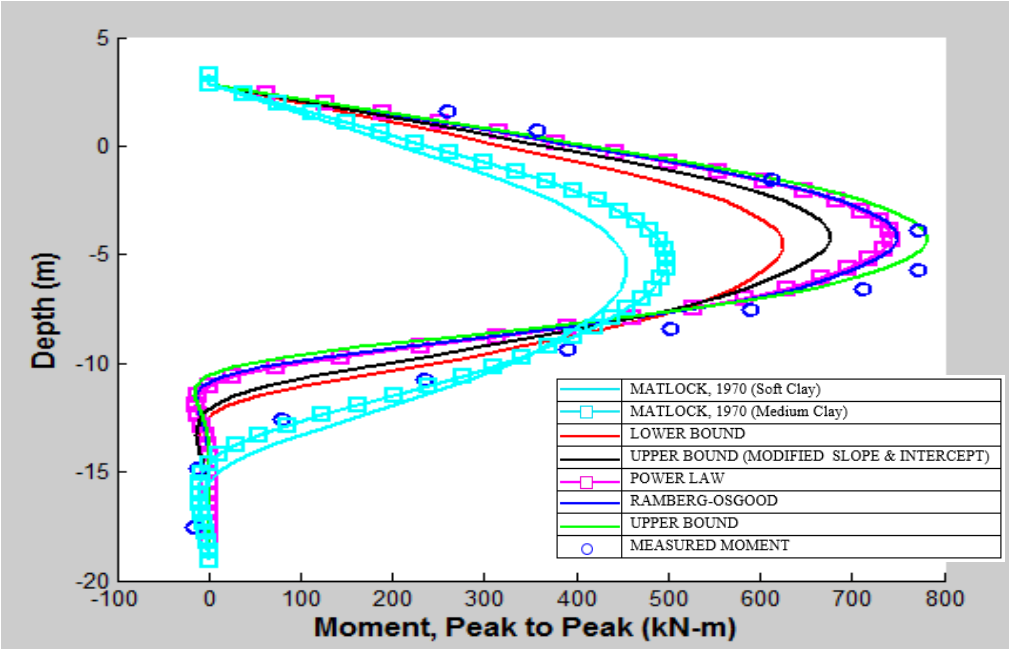

Figure E-14: Calculated Versus Measured Bending Moment Profiles from Centrifuge Test 4, M4 Load - Cycle 300 With 0.05 Offset.

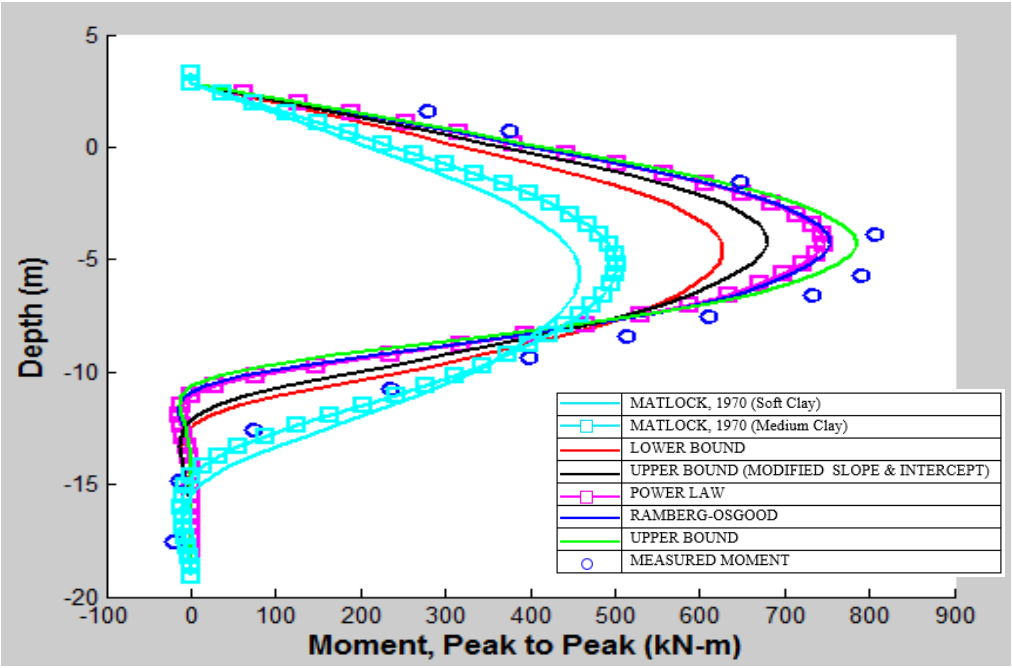

Figure E-15: Calculated Versus Measured Bending Moment Profiles from Centrifuge Test 4, M4 Load - Cycle 400 With 0.05 Offset.

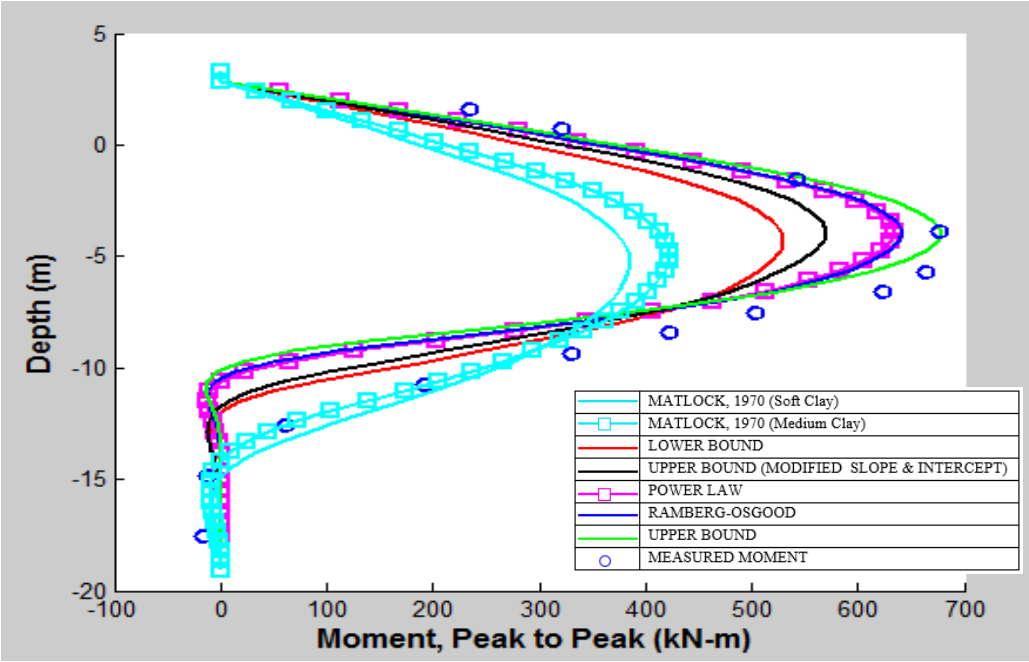

Figure E-16: Calculated Versus Measured Bending Moment Profiles from Centrifuge Test 4, M4 Load - Cycle 500 With 0.05 Offset.

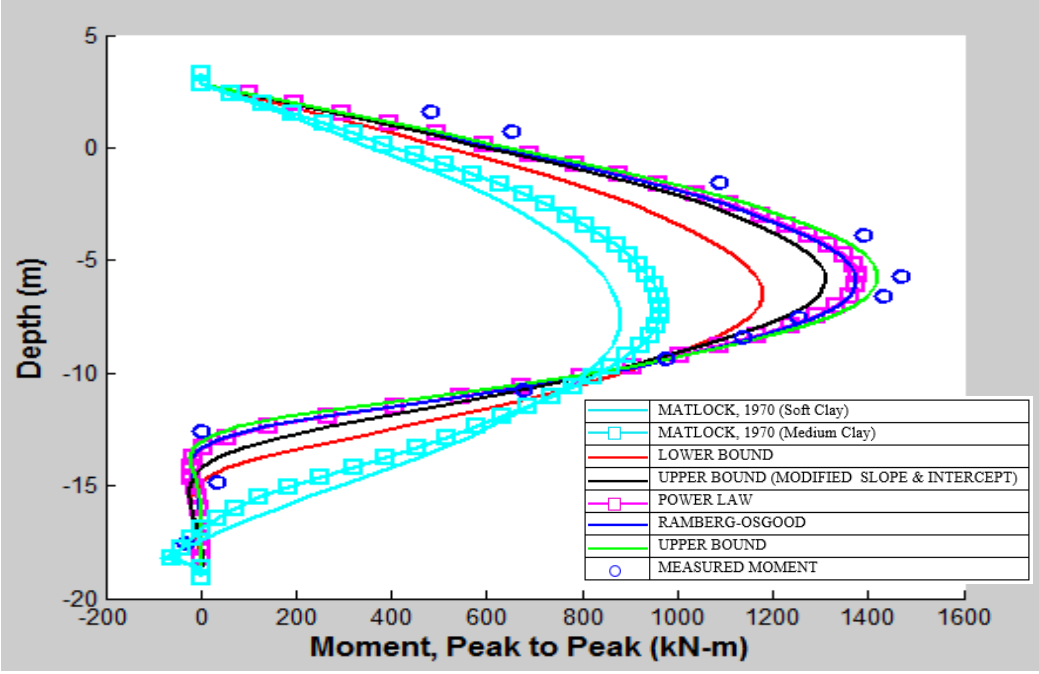

Figure E-17: Calculated Versus Measured Bending Moment Profiles from Centrifuge Test 4, M5 Load - Cycle 200 With Zero Offset.

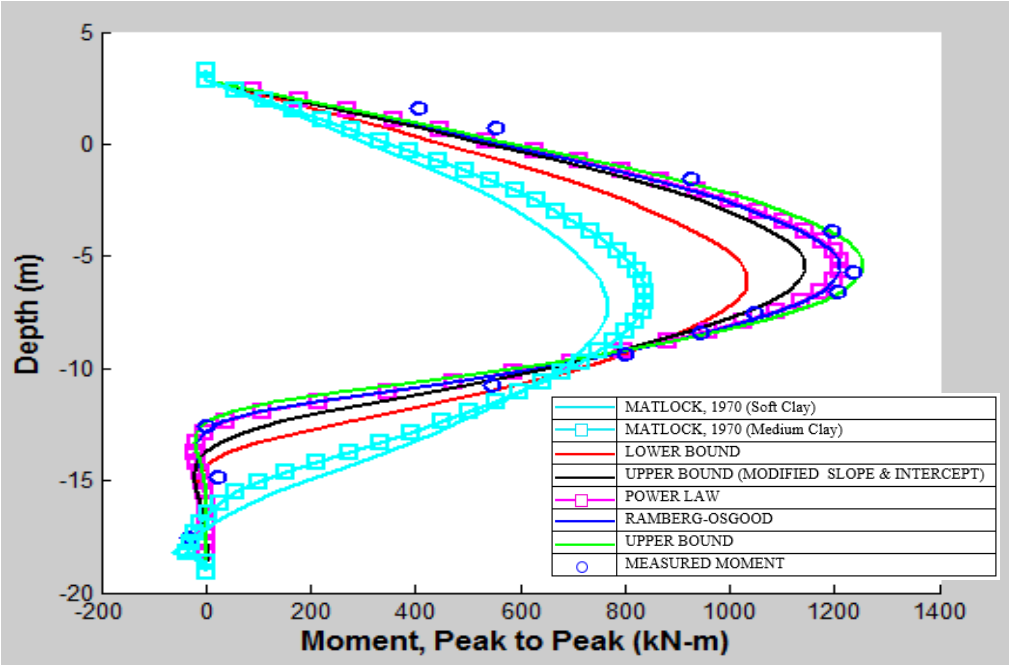

Figure E-18: Calculated Versus Measured Bending Moment Profiles from Centrifuge Test 4, M5 Load - Cycle 300 With Zero Offset.

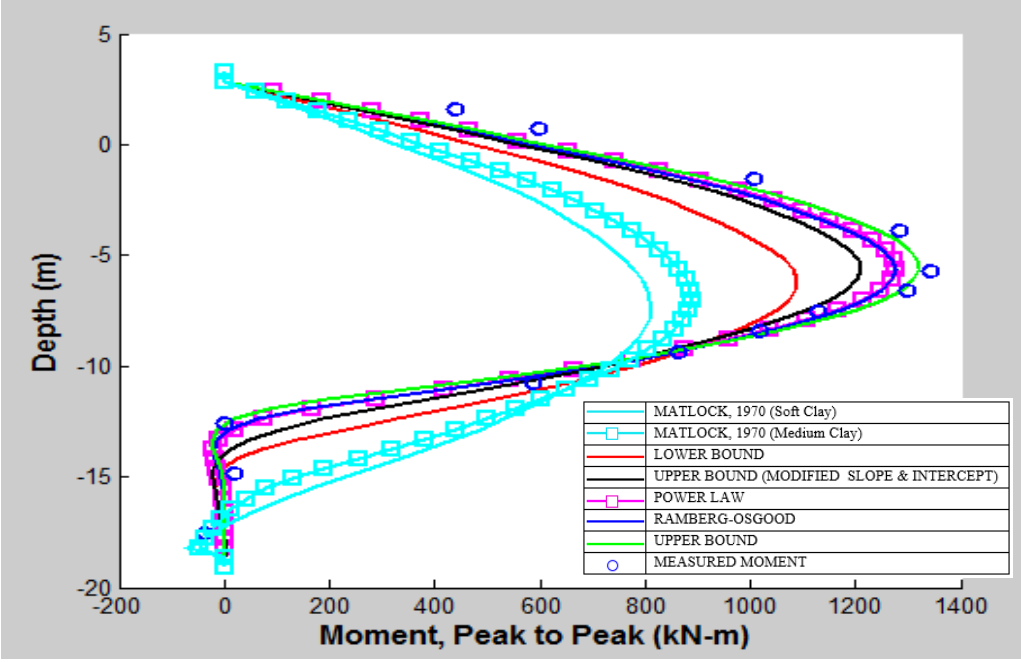

Figure E-19: Calculated Versus Measured Bending Moment Profiles from Centrifuge Test 4, M5 Load - Cycle 400 With Zero Offset.

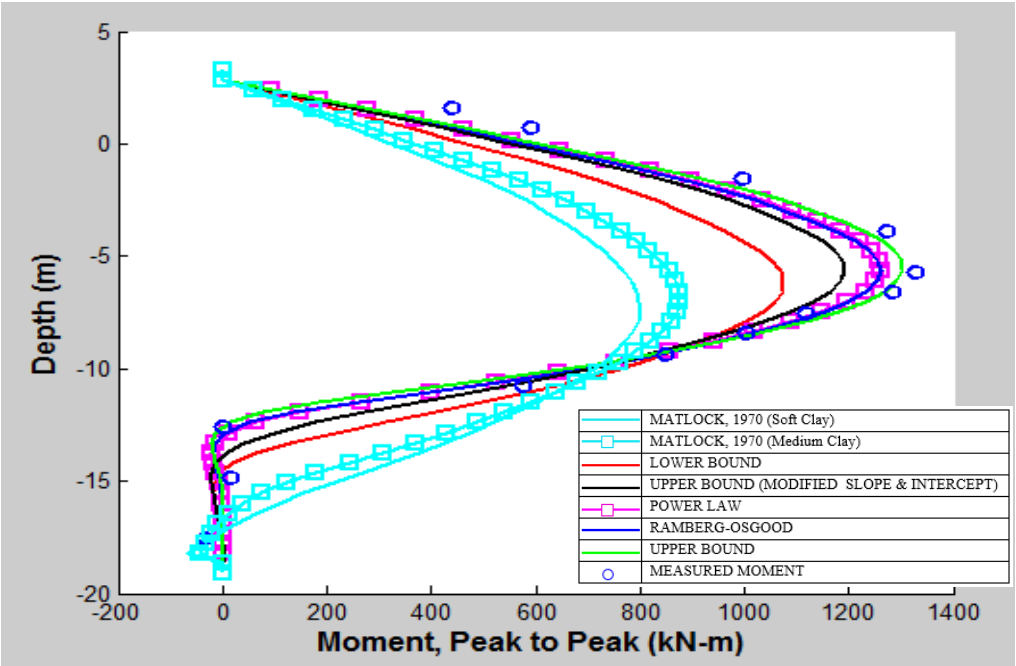

Figure E-20: Calculated Versus Measured Bending Moment Profiles from Centrifuge Test 4, M5 Load - Cycle 500 With Zero Offset.